

University of Rhode Island

DigitalCommons@URI

Open Access Master's Theses

2001

Hafnium Isotope Ratio in Mid-Ocean Ridge Basalts: a Global Survey and a Focus on the Southern Mid-Atlantic Ridge (40°S - 55°S)

Magdalena Andres

University of Rhode Island

Follow this and additional works at: <https://digitalcommons.uri.edu/theses>

Terms of Use

All rights reserved under copyright.

Recommended Citation

Andres, Magdalena, "Hafnium Isotope Ratio in Mid-Ocean Ridge Basalts: a Global Survey and a Focus on the Southern Mid-Atlantic Ridge (40°S - 55°S)" (2001). *Open Access Master's Theses*. Paper 1337. <https://digitalcommons.uri.edu/theses/1337>

This Thesis is brought to you by the University of Rhode Island. It has been accepted for inclusion in Open Access Master's Theses by an authorized administrator of DigitalCommons@URI. For more information, please contact digitalcommons-group@uri.edu. For permission to reuse copyrighted content, contact the author directly.

HAFNIUM ISOTOPE RATIO IN MID-OCEAN RIDGE BASALTS:
A GLOBAL SURVEY AND
A FOCUS ON THE SOUTHERN MID-ATLANTIC RIDGE (40°S - 55°S)
BY
MAGDALENA ANDRES

A THESIS SUBMITTED IN PARTIAL FULFILLMENT OF THE
REQUIREMENTS FOR THE DEGREE OF
MASTER OF SCIENCE
IN
OCEANOGRAPHY

UNIVERSITY OF RHODE ISLAND

2001

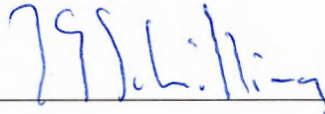
MASTER OF SCIENCE THESIS

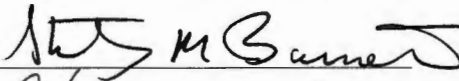
OF

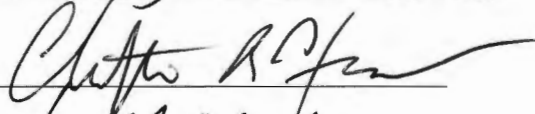
MAGDALENA ANDRES

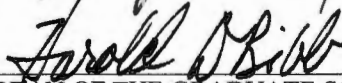
APPROVED:

Thesis Committee
Major Professor

_____

_____

_____

_____

DEAN OF THE GRADUATE SCHOOL

UNIVERSITY OF RHODE ISLAND

2001

ABSTRACT

Using high-precision MC-ICP-MS, $^{176}\text{Hf}/^{177}\text{Hf}$ was measured in 28 MORB as part of a global survey. The goal of the survey is to establish the full range ϵHf in EMORB and NMORB from sections of the mid-ocean ridges which are within or immediately adjacent to areas of mantle plume influence. In addition, $^{176}\text{Hf}/^{177}\text{Hf}$ was measured in 64 MORB from the Mid-Atlantic Ridge between 40°S and 55°S and in 1 basalt from the Discovery Tablemount in order to study mantle mixing processes beneath the southern South Atlantic Ocean.

ϵHf ranges from -2.8 to +11.5 in EMORB included in the global survey and from +12.6 to 24.2 in NMORB from the global survey. This range of ϵHf in MORB completely overlaps the range that is observed in OIB. Most of the basalts from the global survey fall on the well-established ϵHf - ϵNd mantle array. Only the depleted basalt from the Mohns Ridge falls above this array to higher ϵHf (+24.2) for a given ϵNd (9.1). ϵHf versus $^{206}\text{Pb}/^{204}\text{Pb}$ and ϵHf versus $^{87}\text{Sr}/^{86}\text{Sr}$ of basalts from the Mid-Atlantic Ridge (MAR) confirm the existence of the "HIMU province" from 24°S - 34°N which is likely due to the pollution of the upper mantle by plume-head restites from a family of HIMU-type plumes. In addition to this broad upper mantle pollution roughly centered beneath the equator, there is a long-wavelength gradient in ϵHf along the MAR from +24.2 in the Arctic down to +14.7 in the southern South Atlantic. This ϵHf gradient, which correlates positively with ϵNd and negatively with $^{207}\text{Pb}/^{204}\text{Pb}$ and $\Delta^{207}\text{Pb}/^{204}\text{Pb}$, may be due to a lower average, time-weighted mean degree of melting, $\langle F \rangle$, of the Atlantic upper mantle towards the south. It is also possible that the observed isotope gradients are due to a gradient in the onset of melting, T , in the Atlantic upper mantle. This model requires that T decreases to the south. Alternatively, the gradients may be due to pollution of the upper mantle by a Dupal-type component. In this case, the concentration of pollutant must increase to the south.

ϵHf measured in basalts from the southern South Atlantic (40°S to 55°S) range from -2.8 to +16.6. Large-scale pollution of the mantle beneath the southern South Atlantic Ocean can be modeled by a three component mixture of "normal" upper mantle (DM) with recycled ancient oceanic crust (OC) and recycled ancient pelagic sediment (SED). This pollution model requires that less than 5% recycled

oceanic crust and less than 1% recycled pelagic sediment mix with normal depleted upper mantle to produce ambient upper mantle (ADM). In addition to this large-scale pollution, the South Atlantic is a region of localized plume-ridge interactions. The $^{176}\text{Hf}/^{177}\text{Hf}$ from this study confirms the interaction of the Discovery and Shona plumes with the MAR as has been previously proposed based on the Pb, Sr and Nd isotope ratios in these basalts. $^{176}\text{Hf}/^{177}\text{Hf}$ versus $^{206}\text{Pb}/^{204}\text{Pb}$ for basalts from the Shona anomaly indicate that a heterogeneous plume is mixing with a homogeneous ambient upper mantle. The Shona anomaly basalts are successfully modeled as three component mixtures of ambient upper mantle (ADM) with a recycled component consisting of oceanic crust and pelagic sediment. The proportion of sediment in the recycled component mixing with ambient upper mantle in the basalts increases from 0.7% to 1.1% to 1.6% indicating that the plume is not well-mixed. While pelagic sediment is probably not a component in the Discovery plume, delaminated subcontinental lithosphere or lower crust may be.

ACKNOWLEDGEMENTS

I appreciate the guidance and good advice of Dr. Jean-Guy Schilling. I could not have asked for a more dedicated and helpful major professor. I also am indebted to Dr. Janne Blichert-Toft for her hard work running the P54, for helping me learn about the Lu/Hf isotope system and for her enthusiasm and encouragement.

Many thanks to Richard Kinglsey for patiently teaching me the Hf separation chemistry method. Thanks to Urzula Tomza for her help in the lab. Many thanks to my committee members, Dr. Chris Kincaid, Dr. Stanley Barnett and Dr. Scott Rutherford. I also appreciate the help of Dean John Merrill and Meridith Clark from the academic affairs office for their help wading through University regulations.

I am grateful to the NDSEG organization, which supported my work through a fellowship. I owe particular thanks to Michael Moore and Jeff Jarose from ASEE who administered the fellowship. Finally, I would like to thank Della Rogers from the University of Washington and Dr. Stanley Barnett for encouraging me to apply for this fellowship.

PREFACE

The University of Rhode Island has an extensive collection of basalts dredged from the global mid-ocean ridge system. These basalts come primarily from those sections of the mid-ocean ridges which are within or adjacent to areas influenced by material from upwelling mantle plumes. Thus, this collection of basalts provides a unique opportunity to study the interaction between the upper mantle and mantle plumes. These basalts have been well characterized in terms of major element chemistry, trace element chemistry and Sr, Nd and Pb isotope ratios. With the recent advent of more simple technology to measure $^{176}\text{Hf}/^{177}\text{Hf}$, Hf isotopes can provide another source of information about dynamics in the upper mantle. This thesis focuses on the measurement and interpretation of $^{176}\text{Hf}/^{177}\text{Hf}$ in a subset of mid-ocean ridge basalts from the URI collection.

CONTENTS

	Page
ABSTRACT.....	ii
ACKNOWLEDGEMENTS	iv
PREFACE.....	v
LIST OF TABLES.....	viii
LIST OF FIGURES.....	ix
Chapter	
1. INTRODUCTION.....	1
Goals of Research.....	1
Lu-Hf Isotope System.....	1
Geochemistry of Lu.....	1
Geochemistry of Hf.....	2
Lu-Hf in the mantle.....	3
Zircon effect.....	3
Garnet effect.....	4
Methods Used.....	4
Chemical separation of Hf.....	5
Hf isotope ratio measurement with MC-IC-PMS.....	5
Previous data collection on thesis samples.....	6
2. GLOBAL SURVEY.....	8
Introduction.....	8
End-member mixing components.....	9
ϵ Hf in mantle reservoirs.....	10
Global Survey Samples.....	12
Results.....	15

Discussion.....	16
Mohns Ridge.....	16
ϵ_{Hf} of DMM.....	17
MORB from the MAR between 34°N and 24°S The "HIMU province".....	18
Long- and medium- wavelength signals in Atlantic NMORB.....	19
Conclusions.....	24
3. MANTLE MIXING IN THE SOUTH ATLANTIC FROM 40°S - 55°S.....	26
Introduction.....	26
South Atlantic plume-ridge interactions.....	26
Large-scale pollution of South Atlantic MORB source (Dupal, plume-heads, LOMU).....	27
Results.....	29
Mixing Relationships.....	31
Upper mantle - plume mixing between 40°S - 55°S.....	31
Ambient depleted verses "normal" depleted mantle.....	32
Mixing lines within the Shona anomaly.....	35
Discovery and LOMU anomalies.....	39
Conclusions.....	42
4. SUMMARY.....	44
TABLES	46
FIGURES	54
APPENDIX	85
BIBLIOGRAPHY	89

LIST OF TABLES

Table		Page
2.1	$^{176}\text{Hf}/^{177}\text{Hf}$ for the global survey.....	47
3.1	$^{176}\text{Hf}/^{177}\text{Hf}$ for the South Atlantic study.....	48
3.2	Ambient and normal upper mantle compositions.....	50
3.3	DM, OC, SED isotope and trace element compositions.....	51
3.4	ADM isotope and trace element compositions.....	52
3.5	Isotope ratios for lower crust xenoliths compared to MORB.....	53
A.1	Errors in the calculated composition of ADM.....	87

LIST OF FIGURES

Figure	Page
1.1 Procedure to separate Hf from bulk rock.....	55
2.1 Global survey map.....	56
2.2 $\epsilon\text{Nd}-^{206}\text{Pb}/^{204}\text{Pb}$ and $\epsilon\text{Nd}-^{87}\text{Sr}/^{86}\text{Sr}$ for global survey MORB.....	57
2.3 $\epsilon\text{Hf} - \epsilon\text{Nd}$ for global survey MORB.....	58
2.4 $\epsilon\text{Hf} - ^{206}\text{Pb}/^{204}\text{Pb}$ and $\epsilon\text{Nd} - ^{87}\text{Sr}/^{86}\text{Sr}$ for global survey MORB.....	59
2.5 Estimate of ϵHf for DMM.....	60
2.6 Atlantic MORB populations from 24S° to 79°N.....	61
2.7 Atlantic MORB isotope profiles.....	62
2.8 Two stage $^{176}\text{Hf}/^{177}\text{Hf}$ evolution of upper mantle.....	64
2.9 Model 1a: decrease in $\langle F \rangle$ from north to south.....	65
2.10 Model 1b: decrease in age of melting, T, from north to south.....	66
3.1 South Atlantic map.....	67
3.2 Dredge station locations in the South Atlantic.....	68
3.3 Isotope profiles for South Atlantic basalts.....	69
3.4 $\epsilon\text{Hf} - ^{206}\text{Pb}/^{204}\text{Pb}$ for South Atlantic basalts.....	70
3.5 $\epsilon\text{Hf} - \epsilon\text{Nd}$ for South Atlantic basalts.....	71
3.6 $\epsilon\text{Hf} - ^{87}\text{Sr}/^{86}\text{Sr}$ for South Atlantic.....	72
3.7 ϵHf of South Atlantic ambient upper mantle.....	73
3.8 DM-OC-SED mixtures to generate ADM.....	74
3.9 Plume-upper mantle mixing models.....	76
3.10 ϵHf and $\text{Ba}/\text{Nb} - ^{206}\text{Pb}/^{204}\text{Pb}$ for Shona segmentation.....	77
3.11 Map of Shona anomaly segmentation.....	78
3.12 Isotope - isotope plots for Shona segmentation.....	79
3.13 ADM-OC-SED mixtures.....	80

3.14	Modeling Shona segmentation with ADM-OC-SED mixtures.....	82
3.15	Discovery and LOMU anomalies relative to ADM-OC-SED.....	84
A.1	Anomalous Shona basalt.....	88

CHAPTER 1

INTRODUCTION

Goals of Research

In this thesis, lutetium-hafnium isotope systematics of mid-ocean ridge basalts (MORB) are used to study mantle mixing and melting processes. The study is split into two parts. In the first part, which is presented in chapter 2, the global variation of $^{176}\text{Hf}/^{177}\text{Hf}$ in normal and hotspot-influenced mid-ocean ridge basalts is documented. The second part of the study, presented in chapter 3, focuses in more detail on the mantle beneath the southern South Atlantic Ocean. $^{176}\text{Hf}/^{177}\text{Hf}$ is measured in basalts from the Mid-Atlantic Ridge between 40°S-55°S.

Lu-Hf isotope system

^{176}Lu decays by beta decay to ^{176}Hf with a half-life of 36.9 Ga. (Dalmaso et al. 1992, Nir-EI and Lavi 1998). Since Lu and Hf are refractory lithophile elements, their concentrations in the Bulk Silicate Earth can be estimated fairly accurately from their concentrations in carbonaceous chondrites. Their concentrations in the Bulk Silicate Earth are about 2.7 times their concentrations in C1 chondrites (McDonough and Sun 1995). The modern day Bulk Silicate Earth values for isotope ratio and parent-daughter ratio for the Lu-Hf isotope system also have been determined from chondrites (C, O and E classes). These values are $^{176}\text{Hf}/^{177}\text{Hf} = 0.282772 \pm 29$ and $^{176}\text{Lu}/^{177}\text{Hf} = 0.0332 \pm 2$ (Blichert-Toft and Albarède 1997).

Geochemistry of Lu

Lu is the heaviest of the rare earth elements (REE). REE are generally in the 3⁺ valence state. The ionic radii of REE decrease from La (Z = 57, 1.06 Å) to Lu (Z = 71, 0.85 Å) (Wedepohl 1978). This decrease in size is due to the "lanthanide contraction" (Goldschmidt 1958) which results from the

successive addition of electrons to the internal f orbital. Because of this regular decrease in size, the heavier REE are accommodated more readily in the crystal structure of many mantle minerals (Wedepohl 1978). This is reflected in the REE crystal/melt partition coefficients for silicate melts which increase with increasing REE atomic number. Therefore, REE concentrations normalized to chondritic abundances are smooth functions of atomic number in basic to intermediate igneous rocks derived from the mantle (Wedepohl 1978, Bau 1995).

In aqueous fluids and evolved (highly siliceous) magmas, however, the behavior of REE is no longer controlled only by charge and ionic radius. Chemical complexation, which depends on electron configuration and the nature of the chemical bond (covalent versus electrostatic), becomes important (Bau 1995). Therefore REE patterns in rocks crystallized from siliceous magmas or affected by aqueous fluids are often not smooth functions of atomic number (e.g. Bau 1996).

Geochemistry of Hf

Hf is a high field strength element (HFSE). It is in the 4^+ valence state and has an ionic radius of 0.79 Å. HFSE are less soluble than REE in aqueous fluids. In those magmatic processes where charge and ionic radius control the partitioning behavior of elements, Hf behaves similarly to REE. For mantle-mineral/ silicate-melt systems, the compatibility of Hf generally falls between that of Nd ($Z = 60$) and Sm ($Z = 62$) which are REE (Sun and McDonough 1989).

In magmatic processes, Hf also behaves similarly to Zr (also a HFSE) because the valence state of these elements is the same (4^+) and their ionic radii are very similar, again due to the "lanthanide contraction". Zr ($Z = 40$) has an ionic radius of 0.80 Å (Wedepohl 1978).

An interesting exception to this close behavior of Hf and Zr is in clinopyroxene (CPX) (Hart and Dunn 1993). According to experimental data collected on CPX crystallized from an alkali basalt, the CPX-melt partition coefficient for Zr is ~ 0.12 while that for Hf is ~ 0.26 . Thus, MORB produced during melting in the presence of CPX should have a negative Zr anomaly ($Zr_{\text{normalized}} < Hf_{\text{normalized}}$). Hart and Dunn (1993) note that this negative anomaly is not commonly observed in MORB, possibly because the presence of garnet in the bulk rock will reduce the effect of CPX on the bulk partition coefficient.

Lu-Hf in the mantle

During mantle melting, the parent element (Lu) is more compatible than the daughter element (Hf). Therefore, solid residues have high $^{176}\text{Lu}/^{177}\text{Hf}$ in comparison to melts. Over time the upper mantle, which is a residue of melt extraction to form the continents, has developed relatively high $^{176}\text{Hf}/^{177}\text{Hf}$ by radiogenic decay of ^{176}Lu . The continents on the other hand have developed relatively low $^{176}\text{Hf}/^{177}\text{Hf}$.

The melting behavior of the Lu-Hf system is in many ways analogous to that of the Sm-Nd isotope system. As in the Lu-Hf system, the parent (Sm) is more compatible than the daughter (Nd). In general, terrestrial samples fall on a well-defined correlation line in Hf-Nd isotope space (Patchett et al. 1984 and Blichert-Toft and Albarède 1997, Vervoort et al. 1999). Continental material lies toward the unradiogenic end of this correlation line (low $^{176}\text{Hf}/^{177}\text{Hf}$ and $^{143}\text{Nd}/^{144}\text{Nd}$; negative ϵ^1 values) and oceanic material lies towards the radiogenic end (high $^{176}\text{Hf}/^{177}\text{Hf}$ and $^{143}\text{Nd}/^{144}\text{Nd}$; positive ϵ values).

Zircon effect

Several aspects of the Lu-Hf isotope system make it particularly useful in studying mantle processes. One application of the Lu-Hf isotope system is to help distinguish different reservoirs of recycled sediments in the mantle. Pelagic sediments have relatively radiogenic Hf (high $^{176}\text{Hf}/^{177}\text{Hf}$) while the isotope ratio in terrigenous sediments is unradiogenic (low $^{176}\text{Hf}/^{177}\text{Hf}$) (Patchett et al. 1984). The reason for this fractionation in the Hf isotope system is the zircon effect. Hafnium is a minor element, as opposed to a trace element, in the mineral zircon since it can replace zirconium. Zircons are resistant to chemical and mechanical weathering. Therefore, zircon grains tend to be large and stay close to continental margins. Since the hafnium is sequestered in zircons at continental margins, pelagic clays in the deep sea have low Hf concentrations resulting in high Lu/Hf. Over time, these

¹ $\epsilon\text{Hf} = [(^{176}\text{Hf}/^{177}\text{Hf})_{\text{measured}} / (^{176}\text{Hf}/^{177}\text{Hf})_{\text{BulkEarth}} - 1] \times 10,000$, where $^{176}\text{Hf}/^{177}\text{Hf}_{\text{BulkEarth}} = 0.282772$ (Blichert-Toft and Albarède 1997).

$\epsilon\text{Nd} = [(^{143}\text{Nd}/^{144}\text{Nd})_{\text{measured}} / (^{143}\text{Nd}/^{144}\text{Nd})_{\text{BulkEarth}} - 1] \times 10,000$, where $^{143}\text{Nd}/^{144}\text{Nd}_{\text{BulkEarth}} = 0.512638$. Negative ϵ values indicate the samples have experienced time-integrated enrichment in incompatible elements relative to Bulk Earth. Samples with positive ϵ have experienced time-integrated depletion in incompatible elements relative to Bulk Earth.

pelagic clays develop high $^{176}\text{Hf}/^{177}\text{Hf}$ (Patchett et al. 1984). Because of this characteristic hafnium behavior, it may be possible to detect recycled pelagic sediments in the source of MORB.

Garnet effect

The Lu-Hf system is a powerful tool for studying mantle melting processes when used in conjunction with the Sm-Nd isotope system. Combined Lu-Hf and Sm-Nd data can be used to constrain the degree of melting and the amount of melting which occurs in the presence of garnet (Salters and Hart 1989, Salters 1996). In the presence of most mantle minerals, Sm, Nd, Lu and Hf are all incompatible during partial melting. In the presence of garnet, however, Lu is compatible since Lu^{3+} can replace the major element Al^{3+} . When garnet is present in the mantle lithology, the difference in compatibility is much greater for Lu versus Hf than for Sm versus Nd. Thus, melting in the presence of garnet fractionates Lu more from Hf than it fractionates Sm from Nd.

The major element composition of garnet can vary greatly. Peridotitic garnet is Ca poor in comparison to eclogitic garnet. van Westrenen et al. (2001) report that the partition coefficient of Hf is sensitive to garnet major element composition. Hf is more incompatible in peridotitic garnet than in eclogitic garnet. Lu, on the other hand, is equally compatible in both. Thus, Lu/Hf is fractionated more by melting peridotite than eclogite. This results in a more pronounced garnet effect from melting garnet peridotite than from melting eclogite.

Methods Used

In order to measure $^{176}\text{Hf}/^{177}\text{Hf}$ in MORB samples, Hf must be separated from the bulk rock. For this thesis, the chemical separation used to isolate Hf was carried out at the University of Rhode Island. The isotope measurements were carried out on these separated samples by Janne Blichert-Toft at Ecole Normale Supérieure de Lyon in France. The measurements were made on a magnetic sector-multiple collector Inductively Coupled Plasma Mass Spectrometer MC-ICP-MS (also called the Plasma 54 or P54).

Chemical Separation of Hf

The separation method used to isolate Hf from basalt samples is described in detail in Blichert-Toft et al. (1997). A brief summary is given here. A flow diagram of the procedure is presented in figure 1.1. In order to avoid isobaric interference in the measurement of ^{176}Hf (HFSE), Yb and Lu (both REE) must be removed from the sample. In addition, Ti (also a HFSE) must be removed from the sample because its presence reduces the transmission of Hf during mass spectrometry. It is not necessary to remove Zr (HFSE) from the sample.

In order to remove the bulk matrix, the basalt samples are leached in hydrochloric acid and then dissolved for 2 days in a 3:1 mixture of concentrated hydrofluoric and nitric acid. This solution is then dried. The remaining residue is dissolved for 1 day in concentrated hydrofluoric acid creating a milky solution. The precipitate (containing insoluble Ca, Mg, Al and REE fluorides) is separated from the liquid (containing Hf, Zr, Cr, Ti and U) by centrifuging. The precipitate is then treated with hydrofluoric acid and centrifuged two more times to ensure complete dissolution of the hafnium. The combined supernatants are evaporated leaving a residue containing the HFSE (and other elements) and no REE. This is re-dissolved in dilute HCl-HF. This solution is loaded onto an anion exchange chromatographic column (AG1 x 8 100-200 mesh). Washing with dilute HCl-HF pushes the other constituents through the column while the HFSE (Zr, Hf and Ti) remain on the resin as fluoride complexes. These are eluted from the column with 6N HCl. This is then evaporated with perchloric acid to drive off any fluorides. Next, the Ti is removed from the sample using a cation exchange column (AG50W x 8 200-400 mesh). First H_2O_2 is added to reduce the HFSE to negative complexes. The Ti complex moves through the column more quickly than the Hf and Zr complexes. Once the Ti has been eluted from the column, the Hf (and Zr) is eluted with 2.5N HCl-0.3N HF. This is evaporated. Since it is not necessary to separate the Zr from the Hf the sample is ready for Hf isotope measurement.

Hf Isotope ratio measurement with MC-IC-PMS

$^{176}\text{Hf}/^{177}\text{Hf}$ is measured on the Plasma 54 MC-ICP-MS in Lyon, France. The dried sample containing the $^{176}\text{Hf}/^{177}\text{Hf}$ is dissolved in dilute nitric acid and aspirated into a chamber containing argon plasma. The plasma, which is at very high temperatures, ionizes the Hf. The ions are accelerated

and extracted from the plasma chamber through sample and skimmer cones with 6000V applied to them. The sample passes through openings in the cones and is accelerated by ion optics through an electrostatic sector. Here the ion beam is focused, reducing the energy dispersion so the beam is monoenergetic. This beam then passes into the mass spectrometer where the ions are separated through a magnetic field and collected in one of 9 Faraday cups. Because of the mass difference of isotopes, each isotope travels along a different path and is collected in a different cup. The ratio of the signals from 2 cups gives the ratio of the isotopes collected in those cups. A bias factor must be applied to the signals in order to correct for different cup efficiencies. In order to determine the bias factor for each cup, JMC-475 standard solution is measured. Since isotope ratios in this standard are known, the bias factor for each cup can be determined. The standard solution is run at the start of machine operation, as well as throughout the day to correct for possible machine drift (changes in cup bias factor). The suggested value for the JMC-475 standard is $^{176}\text{Hf}/^{177}\text{Hf} = 0.282160 \pm 0.000010$ (Blichert-Toft et al. 1997). The internal precision of the P54 is better than 20 ppm and the external precision is better than 40 ppm (Blichert-Toft et al. 1997).

$^{176}\text{Hf}/^{177}\text{Hf}$ measurement by MC-ICP-MS replaces the thermal ionization (TIMS) method of Patchett and Tatsumoto (1980a). In TIMS the sample is loaded onto a metal filament and heated by passing a current through the filament. Since the first ionization potential of Hf is very high, the sample must be heated to very high temperatures. The yield of Hf ions in the TIMS method is poor (Blichert-Toft et al. 1997). Therefore, this method requires large sample sizes and long measurement times for each sample. MC-ICP-MS on the other hand, requires only 50 ng of Hf and run times are on the order of 15 minutes (Blichert-Toft et al. 1997).

Previous data collection on thesis samples

The samples included in this study have previously been analyzed for major and trace element concentrations and Pb, Sr and Nd isotope ratios. Trace element concentrations, including Lu, Hf, Sm and Nd were measured on dissolved samples at the University of Rhode Island using ICP-MS (Douglass 2000 and unpublished data). Trace element concentrations on glasses from 40°S - 55°S were

also performed on solid glass samples at the University of Cape Town using ICP-MS with laser ablation (le Roux et al. in preparation). Methods for Sr, Nd and Pb isotope measurements are described in Schilling et al. (1994). Rare gas concentrations and isotope ratios of a subset of the South Atlantic basalts have been studied by Sarda et al. (2000) and Moreira et al. (1996). Osmium (Schiano et al. 1997) and oxygen (Eiler et al. 2000) isotope ratios are available for three of the South Atlantic samples.

CHAPTER 2

GLOBAL MORB SURVEY

Introduction

The earth's mantle is heterogeneous. Reservoirs of geochemically distinct material are continually formed and remixed in the mantle as a result of plate tectonics and mantle convection. These reservoirs form primarily along mid-ocean ridges and subduction zones through differentiation processes such as partial melting, fractional crystallization and metasomatism. Through these processes, reservoirs develop different parent/daughter trace element ratios and thus, over time also different radiogenic isotope ratios. A goal of geochemistry is to identify these reservoirs and to determine how they form as well as how they remix in the mantle.

Mantle reservoirs contain one or more end-member components. These end-member components are defined based on their Pb, Sr and Nd isotope characteristics. While reservoirs are real and exist as distinct entities in the earth's mantle (e.g. anchored on the bottom of continents, piled up at the core-mantle boundary, floating as chunks or stretched schlieren in the mantle), end-members are hypothetical isotope compositions which are used to classify reservoir material. End-member isotope compositions may coincide with the actual composition of a real reservoir as in the case of DMM (end-member) and the depleted upper mantle (reservoir). Since heavy isotope ratios (e.g. Pb, Nd, Sr and Hf isotope ratios) are not fractionated by partial melting, the isotope ratios measured in oceanic basalts are representative of the isotope ratios in their mantle source. Thus, basalts can be used to help determine which end-members are involved in mantle mixing and the characteristics of the mantle reservoirs which contain these end-members.

As the technology for measuring $^{176}\text{Hf}/^{177}\text{Hf}$ has improved (Salters and Zindler 1995, Blichert-Toft et al. 1997), the body of data for the range of $^{176}\text{Hf}/^{177}\text{Hf}$ in the earth's reservoirs has increased. To date most ϵHf reported for oceanic samples are for ocean island basalts (OIB) and normal mid-ocean

ridge basalts (NMORB) (e.g. Patchett and Tasumoto 1980b, Patchett 1983, Stille et al. 1983, Stille et al. 1986, Salters and White 1998, Salters and Hart 1991, Blichert-Toft et al. 1999, Blichert-Toft and Albarède 1999, Blichert-Toft and White submitted). In order to fully document the range of ϵ_{Hf} in MORB, the present study includes NMORB as well as enriched mid-ocean ridge basalts (EMORB) from sections of the mid-ocean ridges which are affected by mantle plumes. (Here MORB with $\text{La}/\text{Sm}_n < 0.75$ are classified as NMORB.)

End-member mixing components

The number of mantle end-members and their isotopic compositions is controversial since basalts typically sample mixtures of more than one reservoir and these reservoirs may themselves contain more than one end-member. There is disagreement on how many end-members are necessary to produce the observed variation in basalt isotope ratios. In addition, there is disagreement about the evolution of the reservoirs in which these end-members reside.

Those mantle end-members, which enclose most of the observed basalt compositions in isotope space (Hart et al. 1992), were identified by White (1985) and named by Zindler and Hart (1986). These are "depleted MORB mantle" (DMM), "high time integrated U/Pb" (HIMU, $\mu = \text{U}/\text{Pb}$), "enriched mantle 1" (EM1), and "enriched mantle 2" (EM2). A fifth end-member, "low time integrated U/Pb" (LOMU), was introduced by Douglass et al. (1999). In addition to these five end-members, which each have extreme isotope characteristics, isotopically intermediate end-members have been defined as well. It is not clear whether reservoirs containing intermediate end-members are mixtures of reservoirs that contain the extreme end-members or whether they have evolved independently, isolated from mantle mixing. Names given to the intermediate end-members are "bulk silicate earth" (BSE), "common plume component" (C) (Hanan and Graham 1996), "focus zone" (FOZO) (Hart et al. 1992), "primitive helium mantle" (PHEM) (Farley et al. 1992) and "primitive mantle" (PRIMA) (Zindler and Hart 1986).

ϵ Hf in mantle reservoirs

The **DMM** end-member is contained in the convecting upper mantle. The upper mantle is tapped at mid-ocean ridges and is the source of MORB. NMORB generally arise from pure DMM² while EMORB arise from mixtures of DMM with one or more of the other end-members (EM1, EM2, HIMU and LOMU). It is commonly held that the upper mantle is the residue of the melting events that formed the continents from the primitive mantle. The residue (upper mantle) is depleted in incompatible elements (depleted in Hf relative to Lu) and therefore over time has developed radiogenic ¹⁷⁶Hf/¹⁷⁷Hf (positive ϵ Hf) because of its high Lu/Hf. In NMORB, ϵ Hf ranges from about +11 to +25 (Salters and White 1998 and references therein). This is a large range, so ϵ Hf of DMM is not well-constrained (Salters and Hart 1991). ϵ Hf in NMORB is not well correlated with ϵ Nd (Patchett and Tatsumoto 1980b).

The continents are the complement to the upper mantle. Since continents are enriched in incompatible elements (enriched in Hf relative to Lu), continental material as a whole has unradiogenic ¹⁷⁶Hf/¹⁷⁷Hf (negative ϵ Hf). After formation from the mantle, the continents themselves have undergone differentiation processes (weathering, partial melting, metasomatism etc.). Thus, the range of ϵ Hf in continental samples is large (about -30 to +20) (Vervoort et al. 1999 and references therein). In contrast to NMORB, ϵ Hf in crustal samples (sediments, continental basalts, granitoids, juvenile crustal rocks) is well correlated with ϵ Nd (Vervoort et al. 1999). This correlation line in ϵ Hf- ϵ Nd isotope space is called the crustal array (Vervoort et al. 1999).

The end-members **EM1** and **EM2** have enriched isotope signatures (high ⁸⁷Sr/⁸⁶Sr coupled with low ϵ Hf and ϵ Nd) which is characteristic of continental rather than mantle material. EM2 has significantly higher ⁸⁷Sr/⁸⁶Sr than EM1. Which mantle reservoirs contain the EM end-members is controversial. Oceanic crust that has been subducted together with sediment is a possible EM reservoir.

² NMORB and EMORB are defined based on a trace element concentration ratio (La/Sm) while end-members like DMM are defined by isotope ratios. Thus, it is possible to have an NMORB, which does not have isotope characteristics of DMM. In this case, the NMORB must have been recently depleted in incompatible elements resulting in decoupling of trace element ratios and isotope ratios. It is also possible that a basalt has isotope characteristics of DMM, but is enriched in incompatible elements (i.e. (La/Sm)_n > 1). In this case, the basalt source has been recently enriched in incompatible elements.

In this case, the continental material in reservoirs with EM1 characteristics may be small amounts of ancient pelagic sediment while reservoirs with EM2 characteristics likely contain terrigenous sediment (Weaver et al. 1986, Weaver 1991, Chauvel et al. 1992). An alternate model suggests that the reservoir containing each of the EM end-members is metasomatized subcontinental lithosphere (Tatsumoto et al. 1992). Finally, a third model for the EM1 end-member is that it resides in recycled subducted plateau basalts (Gasperini et al. 2000). The most enriched basalts from Pitcairn, which is a typical EM1 ocean island, have ϵ_{Hf} of about -4 (Salters and White 1998). In the EM2 end-member, which is present most clearly in the Society Islands, ϵ_{Hf} is about -1 (Salters and White 1998). In EM1 and EM2-type OIB ϵ_{Hf} is strongly correlated with ϵ_{Nd} and forms the mantle array (Patchett and Tatsumoto 1980b, Patchett et al. 1984, Salters and Hart 1991, Blichert-Toft and Albarède 1997, Salters and White 1998). The mantle array is essentially collinear with the crustal array. The crustal array and mantle array together form the terrestrial array (Vervoort et al. 1999). NMORB lie in a cluster at the high (radiogenic) end of this array. Figure 2.3 shows the different end-members relative to this array.

The HIMU end-member is characterized by high $^{206}\text{Pb}/^{204}\text{Pb}$. The reservoir containing HIMU is most likely pure subducted oceanic crust (Hofmann and White 1981, Weaver et al. 1986, Weaver 1991, Chauvel et al. 1992). In the most extreme HIMU ocean islands (St. Helena, Rurutu and Tubaii), ϵ_{Hf} is around 2 (Salters and White 1998). HIMU-type basalts fall slightly below the mantle array (Salters and White 1998).

Recently another end-member was proposed by Douglass et al. (1999). This is the LOMU end-member. Like EM1, it is characterized by low $^{206}\text{Pb}/^{204}\text{Pb}$. However, LOMU has higher $^{87}\text{Sr}/^{86}\text{Sr}$ and $^{207}\text{Pb}/^{204}\text{Pb}$ than EM1. There are no clear examples of OIB containing this end-member. It seems to be present (together with DMM) in MORB from a short segment of the MAR between 48.5°S and 49°S (Douglass et al. 1999) and in several basalts from the Afanasy-Nikitin Rise (Mahoney et al. 1996). In addition, an individual fresh MORB glass (S60-18/1) from just north of the Bouvet triple junction seems to be tapping relatively pure LOMU material (Kamenetsky et al. 2001). It is not clear where in the mantle LOMU resides though it may be in the upper mantle since it has been found in MORB but not in OIB. Possible LOMU reservoirs include delaminated subcontinental lithosphere or lower crust.

Regardless of where the reservoir resides, it is clear that this reservoir must have been isolated for a long time because of its high $^{207}\text{Pb}/^{204}\text{Pb}$. If Kamenetsky's MORB is representative of LOMU, ϵHf in the LOMU end-member is about -25.6 (V.S. Kamenetsky personal communication) and ϵNd is -18 (Kamenetsky et al. 2001). This falls on the mantle array, but at values much less radiogenic than any other oceanic basalts (figure 2.3, inset).

As mentioned earlier, the evolution of the intermediate reservoir, which has **C, FOZO, PHEM** or **PRIMA**-type composition, is not certain. The material may represent pure primitive mantle material that has not yet undergone any differentiation or mixing processes. Alternately, the intermediate reservoir may be a mixture of depleted upper mantle (DMM) with reservoirs containing the more enriched end-members (EM1, EM2, HIMU or LOMU). Of course, there may be several processes occurring which each lead to slightly different intermediate reservoirs. Many mantle plumes have an intermediate composition. ϵHf in these intermediate-composition plumes is roughly 8 and these basalts fall on the mantle array.

Global Survey Samples

Basalts included in this global survey come from sections of the mid-ocean ridge system which are near mantle plumes. In some cases, the plumes are ridge-centered. In other cases, the plumes are off-axis and the plume material flows from the plume to the ridge (e.g. Schilling 1985). From each region, those basalts with the strongest plume signal and the strongest DMM signal are included in the survey. These were chosen based on previously collected Pb-Sr-Nd isotope ratios. Generally, the basalts with the strongest plume signal lie closest to the plumes. The basalts with the lowest plume signals (with the strongest DMM signals) lie far enough away from the plumes so that they are outside of the regions of plume influence (i.e. outside of the plume anomaly). The basalts that lie between these isotopic extremes exhibit a systematic isotopic gradient indicating that as one moves along the ridge away from a plume, the proportion of plume material mixing with DMM decreases. Sometimes this gradient along the ridge is as long as 1000 km. For those regions where basalts have been dredged from both sides of the gradient, two DMM basalts are included in the survey. Basalts locations are listed in

table 2.1. Figure 2.1 shows a map of these basalts. The caption lists the references for the Nd-Sr-Pb data used to select them. The plumes influencing MORB included in this study are the Jan Mayen plume in the Arctic, the Azores and Great Meteor plumes in the North Atlantic, the Sierra Leone plume in the Equatorial Atlantic, the St. Helena, Tristan, Discovery and Shona plumes in the South Atlantic, the Afar plume in the Gulf of Aden and the Galapagos and Sala y Gomez plumes in the Pacific. The following paragraphs briefly describe the tectonic setting of the basalts and the isotope characteristics of the plumes from these areas. $\epsilon_{\text{Nd}} - ^{87}\text{Sr}/^{86}\text{Sr}$ and $\epsilon_{\text{Nd}} - ^{206}\text{Pb}/^{204}\text{Pb}$ for the MORB are plotted in figure 2.2.

Three basalts from the Greenland Sea are included in the survey. Two are from the Mohns ridge which lies just northeast of the ridge-centered **Jan Mayen** mantle plume. ENO26 16D-2g from the northern end of the Mohns ridge is isotopically similar to DMM. ENO26 2D-1 from the southern end of the Mohns ridge exhibits mildly-HIMU or C-type isotope characteristics similar to basalts from the Jan Mayen platform (Schilling et al. 1999). The third basalt from this region is from the center of the Kolbeinsey ridge near the Spar Fracture Zone. This depleted (DMM-like) basalt is TR139 25D-3g.

Isotope profiles from the **Azores** plume anomaly along the Mid-Atlantic Ridge (MAR) show two distinct peaks (Yu et al. 1997) possibly because the Azores anomaly is caused by two plumes or by blobs detaching and rising from a single bending plume. The Azores plume is essentially ridge-centered and mildly-HIMU/C-type except for some basalts from Sao Miguel Island, which are EM2 type (Hawkesworth et al. 1979). The samples representing DMM are TR 138 6D-1Bg from north of the Azores anomaly and TR123 5D-3g from south of the Azores anomaly. The enriched sample, TR 31D-1, is from the Azores Plateau and lies at the maximum of the northern peak of the isotope profiles on the MAR.

One basalt from the **Great Meteor** plume anomaly is also included. This anomaly is superimposed on the southern end of the Azores anomaly and straddles the Oceanographer Fracture Zone. The basalt from this region, which contains an EM1 or EM2 component, is TR119 7D-1 (e.g. Shirey et al. 1987).

The **Sierra Leone** plume is probably HIMU-type and affects the MAR just north of the equator (Schilling et al. 1994). The DMM-like basalt, which lies north of the anomaly, is RC2806 49D-1g. The enriched basalt included from this area is RC2806 40D-3g.

A group of basalts that have very depleted Pb, Sr and Nd isotope characteristics lies south of the Sierra Leone plume anomaly. These basalts are from the MAR between 2°S and 7°S. Their depleted nature lead Schilling et al. (1994) to suggest that the upper mantle being tapped by the basalts here is a good example of pure unpolluted DMM end-member since these basalts approach the composition of the depleted mantle calculated through inversion of global basalt data by Allègre and coworkers (Allègre et al. 1983, Allègre et al. 1988, Allègre and Levin 1989). One basalt from this region, ENO61 4D-1g, is included in this survey to try to establish ϵ_{Hf} of DMM.

St. Helena, which is a HIMU plume, lies ~800 km from the Mid-Atlantic Ridge. The MORB showing the strongest St. Helena plume influence is ENO61 18D-1g. RC16 3D-1 is a DMM-like basalt north of this and ENO 63 2D-5g is a DMM basalt south of this.

The EM1-type **Tristan** plume lies about 400 km from the MAR. The depleted sample from north of the Tristan anomaly is ENO63 24D-5g. The most plume-like basalt is AII 107-7 14-77. The depleted basalt, which lies between the Tristan plume anomaly and the Discovery anomaly to the south, is EW9309 40D-1g.

The most enriched sample from the **Discovery** anomaly is EW9309 25D-5g. This basalt has a strong EM1+EM2 signal as does the Discovery plume, which lies about 425 km east of the MAR (Douglass et al. 1999). Basalt EW9309 7D-6g is from the short **LOMU** anomaly just south of the main Discovery anomaly. Whether this enriched basalt arises from the influence of a heterogeneous Discovery plume or from a mixture of DMM with LOMU material that is separate from the Discovery plume (Douglass et al. 1999) is uncertain (see chapter 3). The depleted basalt which lies between the Discovery/ LOMU anomaly and the Shona anomaly to the south is EW9309 10D-3g.

The enriched basalt from the **Shona** anomaly is EW9309 19D-1g. The Shona plume is ridge-centered and mildly-HIMU or C-type (Douglass et al. 1999).

In contrast to the Atlantic, the Gulf of Aden is a region where the continent is breaking apart to form a young ocean. Whether the **Afar** plume, which is rising beneath this area, initiated the breakup of the continent or not is controversial although Schilling et al. (1992) suggest that continental breakup began before plume impingement. Basalts from this region are mixtures of continental material, depleted upper mantle and the mildly-HIMU/ C-type Afar plume. Samples included in the global survey are from opposite ends of the West Sheba Ridge. Sample V33-07 58D-1 is from the eastern end and is representative of the ambient depleted upper mantle. The upper mantle in this region does not seem to be pure DMM but rather more Dupal-like (see chapter 3). The plume-like sample from this region is from the western end of the Sheba Ridge. It is V33-07 49D-1.

Two regions in the Pacific Ocean are included in the global survey. The mildly-HIMU **Sala Y Gomez** plume, which lies about 1000 km from the ridge, influences basalts from both margins of the Easter microplate (EMP) (Kingsley and Schilling 1998). Three basalts from this region are included in the survey. They are EN113 36D-1g (DMM-like) from the East Pacific Rise north of the Sala y Gomez anomaly and EN113 46D-2g from the East Pacific Rise south of the anomaly. EN113 6D-1Ag from the East rift of the microplate is the most plume-like basalt from the ridge.

The second region included from the Pacific Ocean is the Galapagos Spreading Center which is influenced by the mildly-HIMU or C-type **Galapagos** plume. There is evidence that the Galapagos plume is heterogeneous (White et al. 1993, Blichert-Toft and White submitted). Samples included from this region are TR164 22D-1g from west of the anomaly, STD 7D-1 from east of the anomaly and TR164 26D-3g from the peak of the anomaly.

Results

$^{176}\text{Hf}/^{177}\text{Hf}$ results together with two sigma errors are listed in table 2.1. Measurements are corrected to JMC-475 standard $^{176}\text{Hf}/^{177}\text{Hf} = 0.282160 \pm 0.000010$. Replicate analyses were performed on two samples and are in good agreement with one another. These are also listed in the table. ϵHf variation with ϵNd , $^{87}\text{Sr}/^{86}\text{Sr}$ and $^{206}\text{Pb}/^{204}\text{Pb}$ is plotted in figures 2.3 and 2.4.

The total range of ϵHf measured in basalts from this global MORB survey is -2.8 to +24.2. As expected, within a given region, the MORB influenced by the local plume always have lower ϵHf than the regional basalts that are outside of the area of plume influence. In MORB influenced by plumes, ϵHf ranges from -2.8 to +11.5. In MORB outside of the plume anomalies (i.e. in the NMORB), ϵHf ranges from +12.6 to +24.2 which is comparable to the previously reported range of ϵHf in Pacific and Atlantic NMORB (+9.5 to +24.9) (Salters 1996, Salters and White 1998).

While NMORB from this study show a limited range of ϵHf , NMORB and EMORB taken together cover a range of ϵHf which is as large as the range found in OIB. Most of the plume-influenced basalts from this study (EMORB) have ϵHf close to 9 which is typical of the intermediate-composition plumes. However the two enriched basalts from the Discovery and LOMU anomalies have very low ϵHf (-2.8 and -1.0, respectively) indicating a large continental contribution in these basalts. In ϵHf - ϵNd space, these two enriched basalts lie well below the field for EM2-type basalts and in the field for EM1-type basalts (figure 2.3).

Most NMORB and EMORB from the survey fall close to the mantle array in ϵHf - ϵNd isotope space with NMORB at the radiogenic end (open symbols) and EMORB towards the unradiogenic end (closed symbols) (figure 2.3). Since the compositions of the different end-members (HIMU, EM1 etc.) are nearly linear in ϵHf - ϵNd space, the global survey EMORB influenced by different plume-types are not distinct from each other. In plots of ϵHf versus $^{206}\text{Pb}/^{204}\text{Pb}$ and ϵHf versus $^{87}\text{Sr}/^{86}\text{Sr}$ however, the influence of the different plume-types on these basalts is more apparent (figure 2.4).

Discussion

Mohns Ridge

While most of the ϵHf - ϵNd data for basalts from this global MORB survey do fall along the ϵHf - ϵNd mantle array (figure 2.3), there is one region that deviates from this correlation. This is the northern Mohns Ridge in the Arctic. The NMORB measured from this ridge, ENO26 16D-2g, has a very high ϵHf for its ϵNd . The reason for this requires a more in depth study of the area, but there are several possible mechanisms that can lead to high ϵHf for a given ϵNd in an NMORB. The first

possibility is that the source of this basalt contains a small amount of ancient pelagic sediment. Pelagic sediment has high ϵ_{Hf} for a given ϵ_{Nd} due to the zircon effect (Patchett et al. 1984) as described in chapter 1. However, the amount of pelagic sediment mixing with DMM to produce EN026 16D-2g must be very small for two reasons. First pelagic sediment is enriched in incompatible elements and this basalt is depleted in incompatible elements. Second pelagic sediment has low ϵ_{Nd} and the Mohs Ridge basalt does not have particularly low ϵ_{Nd} in comparison to other NMORB.

Another possibility is that the source of this Mohs Ridge NMORB is the residue of an ancient melting event, during which the upper mantle melted in the garnet stability field rather than in the spinel stability field (Johnson and Beard 1993). The residue of garnet peridotite melting has very high Lu/Hf compared to the residue of spinel peridotite melting because Lu is compatible in garnet. Over time, this high Lu/Hf leads to radiogenic $^{176}\text{Hf}/^{177}\text{Hf}$. The presence of garnet will not have a big effect on Sm/Nd of this ancient residue. Therefore, $^{143}\text{Nd}/^{144}\text{Nd}$ in the residue will be similar to that in upper mantle, which has undergone previous melting events in the spinel stability field. Thus, the result of melting ancient garnet peridotite residue is a basalt with "normal" ϵ_{Nd} and high ϵ_{Hf} . This is an example of the garnet effect described in chapter 1. Since the Mohs Ridge is close to the continents, it is quite possible that fragments of the sub-continental mantle which have experienced an ancient garnet effect are present in the upper mantle beneath the ridge and contribute to the source of MORB here.

ϵ_{Hf} of DMM

As noted by Salters and White (1998), the range of ϵ_{Hf} documented for NMORB is +11 to +25. This large range in ϵ_{Hf} is accompanied by a smaller range in ϵ_{Nd} (+7 to +13) (Salters and White 1998, Atlantic and Pacific MORB field in their figure 1). Because of the large range of ϵ_{Hf} in NMORB, defining ϵ_{Hf} of the DMM end-member is difficult. The basalt from the depleted 2°S - 7°S region along the equatorial MAR (ENO61 4D-1g) has $\epsilon_{\text{Hf}} = 17.6$ which is a little higher than the average of the fifteen NMORB from this study (17.1). If 2°S - 7°S really is representative of pure unpolluted DMM, as suggested by Schilling et al. (1994), then 17.6 may be a reasonable value for ϵ_{Hf} of DMM. An alternative method to determine ϵ_{Hf} of DMM is to calculate it from ϵ_{Nd} of DMM (from Hart et al.

1992) and the equation for the mantle array. This results in ϵ_{Hf} of DMM = 20.8 (see caption of figure 2.3 for equation of mantle array).

There is evidence from the St. Helena plume anomaly that 20.8 is a better estimate of ϵ_{Hf} in DMM than 17.6. Since St. Helena is a HIMU plume, OIB from this island fall noticeably below the mantle array (figure 2.3) (e.g. Salters and White 1998). Thus, the most enriched basalt from the MAR affected by this plume (ENO61 18D-1g) should fall below the mantle array as well. Figure 2.3 shows that ENO61 18D-1g does fall slightly below the mantle array, but not nearly as much as typical HIMU-type OIB do. Presumably, this is because ENO61 18D-1g is not pure HIMU material, but a mixture of St. Helena plume material (HIMU) and the upper mantle (DMM). If ϵ_{Hf} of DMM is calculated from ϵ_{Nd} and the mantle array ($\epsilon_{\text{Nd}} = 12.9$, $\epsilon_{\text{Hf}} = 20.8$) then ENO61 18D-1g falls on the mixing line which connects DMM to HIMU (figure 2.5, red line). This is consistent with the idea that this MORB is a plume-upper mantle mixture. On the other hand, if DMM is estimated from the basalt from 2°S - 7°S ($\epsilon_{\text{Nd}} = 12.6$, $\epsilon_{\text{Hf}} = 17.6$), the mixing line which passes from DMM through 18D-1g does not intersect the HIMU-type basalts from St. Helena (figure 2.5, green line). Thus, while arguments can be made in favor of either method of estimating ϵ_{Hf} of DMM, 20.8 is probably more accurate value for DMM. (This argument assumes that mixtures between HIMU and DMM fall along straight lines. In order for this to be true, Hf/Nd in HIMU must be the same as Hf/Nd in the upper mantle. This is a reasonable assumption since Hf behaves similarly to Nd and Sm in most mantle melting processes.)

MORB from the MAR between 34°N and 24°S - the "HIMU province"

Based on ϵ_{Nd} versus $^{87}\text{Sr}/^{86}\text{Sr}$ for a large set of Atlantic MORB, Schilling et al. (1994) divided Atlantic MORB from 6°S to 79°N into two isotopic groups. The northern group includes basalts from 79°N to 34°N and the southern group includes basalts from 34°N to 6°S. The southern group can be extended to 24°S if the subsequent data of Fontignie and Schilling (1996) from the MAR near Ascension and St. Helena are included. The isotopic distinction between these two groups is evident both in EMORB and in NMORB. The southern group has a lower ϵ_{Nd} for a given $^{87}\text{Sr}/^{86}\text{Sr}$ than MORB from the northern group (figure 2.6a). Since low ϵ_{Nd} for a given $^{87}\text{Sr}/^{86}\text{Sr}$ is a characteristic of the

HIMU end-member, Schilling et al. (1994) call this 24°S - 34°N group the "HIMU province". (This province includes basalts from the 14°N MAR anomaly documented by Dosso et al. (1991).)

ϵ_{Hf} versus $^{87}\text{Sr}/^{86}\text{Sr}$ for the basalts from the current global survey confirms the existence of these two distinct MORB populations between 24°S and 79°N. Figure 2.6b shows that for a given $^{87}\text{Sr}/^{86}\text{Sr}$, the southern population has lower ϵ_{Hf} than the northern population, both for MORB influenced by plumes (solid symbols) and for normal MORB (open symbols). In contrast to the population originally considered by Schilling et al. (1994), figure 2.6 includes only a small basalt population. However, work in progress at URI indicates that ϵ_{Hf} of the other basalts from these regions are consistent with the trends reported here.

The isotopic differences between these two regions are likely caused by the different plume-types which are upwelling in the two regions. Schilling et al. (1994) noted that the "HIMU province" (24°S - 34°N) is influenced by strongly HIMU-type plumes (14°N, Sierra Leone, Circe (or Ascension) and St. Helena). The northern region, on the other hand, is influenced by mildly-HIMU/ C-type and EM2-type plumes (Jan Mayen, Iceland, Azores and Great Meteor). Since the plume-types in these two regions are distinct, EMORB, which are mixtures of upper mantle and plume material, fall into distinct groups. Since NMORB also fall into these groups, NMORB from the "HIMU province" likely are affected by plume material as well. However, NMORB are incompatible element depleted by definition. Thus, this plume material influencing the upper mantle in the "HIMU province" must have been depleted in incompatible elements relatively recently. This can be achieved by melting HIMU plume-heads (which depletes the plume-head residue in incompatible elements without changing isotope ratios) followed by dispersal of the plume-head residue into the upper mantle (e.g. Hanan et al. 1986).

Long- and medium-wavelength signals in Atlantic NMORB

To further investigate the cause for the two isotopic provinces discussed in the previous section, and to investigate the nature of the entire upper mantle beneath the Atlantic, it is helpful to consider isotope profiles for the Atlantic NMORB. ϵ_{Hf} collected in this global survey show that Atlantic NMORB, rather than falling into two groups, actually exhibit a remarkable 15,000 km long

gradient along the entire MAR from 79°N to 55°S. For this MAR basalt population there is a clear decrease in ϵ_{Hf} from north to south from +24.2 down to +14.7 (figure 2.7a, red line). A similar gradient is also visible in ϵ_{Nd} versus latitude for NMORB (figure 2.7b, red line), although this is not as pronounced. The opposite trend is visible for these NMORB in $^{207}\text{Pb}/^{204}\text{Pb}$ and $\Delta^{207}\text{Pb}/^{204}\text{Pb}^3$ versus latitude which both increase from north to south (figure 2.7c and 2.7d, red lines). These four trends contrast with $^{206}\text{Pb}/^{204}\text{Pb}$ and $^{87}\text{Sr}/^{86}\text{Sr}$ versus latitude. The $^{206}\text{Pb}/^{204}\text{Pb}$ profile has a broad maximum roughly centered on the equator (figure 2.7e, red line) and $^{87}\text{Sr}/^{86}\text{Sr}$ has a broad minimum over the equator (figure 2.7f, red line).

From the NMORB profiles in figure 2.7, it is apparent that the isotopic trends can be divided into two categories. The first category is a long-wavelength trend represented by the 15,000 km gradient along the entire MAR (apparent in ϵ_{Hf} , ϵ_{Nd} , $^{207}\text{Pb}/^{204}\text{Pb}$ and $\Delta^{207}\text{Pb}/^{204}\text{Pb}$). The second category is a medium-wavelength trend which is manifested in a broad maximum or minimum at the equator (apparent in $^{206}\text{Pb}/^{204}\text{Pb}$ and $^{87}\text{Sr}/^{86}\text{Sr}$). This indicates that there are at least two processes affecting the Atlantic NMORB population and by inference, the Atlantic upper mantle. One process produces long-wavelength signals and the other produces medium-wavelength signals.

The isotope signals from these two processes are superimposed on each other. The isotope profile observed along the MAR is a function of the magnitudes of the isotope signals from the two processes. For example, ϵ_{Hf} is relatively unaffected by the medium-wavelength process and therefore increases linearly to the south without any increase or decrease near the equator due to the medium-wavelength process. $^{206}\text{Pb}/^{204}\text{Pb}$ on the other hand is much more affected by the medium-wavelength process and therefore exhibits a maximum over the equator. There is however, a very slight effect on $^{206}\text{Pb}/^{204}\text{Pb}$ from the long-wavelength process as well since NMORB from the south have slightly higher $^{206}\text{Pb}/^{204}\text{Pb}$ than NMORB from the north (figure 2.7e, red line, $^{206}\text{Pb}/^{204}\text{Pb} = 17.6$ the Arctic NMORB and 17.9 in the southern South Atlantic NMORB).⁴

³ $\Delta^{207}\text{Pb}/^{204}\text{Pb}$ represents the deviation from the Northern Hemisphere Reference Line in $^{206}\text{Pb}/^{204}\text{Pb}$ - $^{207}\text{Pb}/^{204}\text{Pb}$ space (Hart 1984). $\Delta^{207}\text{Pb}/^{204}\text{Pb} = [^{207}\text{Pb}/^{204}\text{Pb} - (0.1084 \times ^{206}\text{Pb}/^{204}\text{Pb} - 13.491)] \times 100$.

⁴ There are, of course, also short wavelength interactions between plumes and the ridge, which punctuate the long- and medium-wavelength isotope trends along the MAR. However, these short-

The medium-wavelength process affects the $^{206}\text{Pb}/^{204}\text{Pb}$ and $^{87}\text{Sr}/^{86}\text{Sr}$ profiles along the MAR which have a broad maximum and a broad minimum respectively near the equator. This process likely is the dispersal of HIMU plume-head residue, discussed in the previous section, which results in the "HIMU province" from 34°S - 24°N . $^{206}\text{Pb}/^{204}\text{Pb}$ of HIMU is significantly higher than that of DMM (figure 2.2a or 2.4a). In comparison, ϵHf and ϵNd of HIMU and DMM, while certainly not equal, are much closer in value (fig 2.2a and 2.4b). In addition, since HIMU material is old but not ancient (perhaps $\sim 2\text{Ga}$ rather than $\sim 3\text{Ga}$), it does not have particularly high $^{207}\text{Pb}/^{204}\text{Pb}$ for its $^{206}\text{Pb}/^{204}\text{Pb}$. Thus, the dispersal of HIMU plume-head restites into the upper mantle does not affect ϵHf , ϵNd , or $^{207}\text{Pb}/^{204}\text{Pb}$ nearly as much as $^{206}\text{Pb}/^{204}\text{Pb}$. ϵHf , ϵNd and $^{207}\text{Pb}/^{204}\text{Pb}$ are essentially "immune" to the dispersal of HIMU plume-head restite. Therefore, these three isotope signals do not exhibit a maximum (or minimum) near the equator.

The long-wavelength process affecting the upper mantle beneath the entire MAR causes the nearly linear 15,000 km long decrease of ϵHf and ϵNd and increase of $^{207}\text{Pb}/^{204}\text{Pb}$ and $\Delta^{207}\text{Pb}/^{204}\text{Pb}$ from north to south⁵. This process can be explained by various models. The first model relates the observed gradients to ancient melting events. The second model explains the gradients through pollution of the upper mantle.

Model 1: ancient melting events

If the linear gradients in ϵHf , ϵNd and $^{207}\text{Pb}/^{204}\text{Pb}$ are caused by melting events, it is helpful to consider the equations for radiogenic growth for a two-stage model (figure 2.8). For $^{176}\text{Hf}/^{177}\text{Hf}$ (ϵHf) this is:

$$(^{176}\text{Hf}/^{177}\text{Hf})_{\text{today}} = (^{176}\text{Hf}/^{177}\text{Hf})_{\text{BSE, T}} + \langle ^{176}\text{Lu}/^{177}\text{Hf} \rangle (e^{\lambda T} - 1) \quad (1)$$

wavelength plume-ridge interactions affect EMORB much more strongly than NMORB. Thus, by considering just the NMORB, it is possible to analyze just the large-scale and medium-scale processes affecting the upper mantle.

⁵ The effect of this long-wavelength process on $^{206}\text{Pb}/^{204}\text{Pb}$ and $^{87}\text{Sr}/^{86}\text{Sr}$ is difficult to discern because these two isotope ratios are affected so strongly by the medium-wavelength HIMU plume-head dispersal. In order to include $^{206}\text{Pb}/^{204}\text{Pb}$ and $^{87}\text{Sr}/^{86}\text{Sr}$ in an analysis of long-wavelength processes, it would be necessary to filter out the effect of the medium-wavelength process. In the absence of such filtering, neither of these isotope ratios is a good tool for determining what process causes the long-wavelength isotope trends.

where:

λ

is the decay constant for ^{176}Lu ($1.876 \times 10^{-11} \text{ yr}^{-1}$).

T

is the age of the melting event which changed the upper mantle's parent-daughter ratio from the Bulk Earth value to a new value. In the case of continuous melting, T is the age when the melting begins. T may vary with latitude (model 1b, below).

$\langle ^{176}\text{Lu}/^{177}\text{Hf} \rangle$

is the average time-weighted, parent-daughter ratio in the upper mantle since time T:

$$\langle ^{176}\text{Lu}/^{177}\text{Hf} \rangle = \frac{\int_T^0 ^{176}\text{Lu}/^{177}\text{Hf}(t) dt}{\int_T^0 dt} \quad (2)$$

where $^{176}\text{Lu}/^{177}\text{Hf}(t)$ is the upper mantle's parent-daughter ratio at a given latitude at time, t. $\langle ^{176}\text{Lu}/^{177}\text{Hf} \rangle$ may vary with latitude (model 1a, below).

$(^{176}\text{Hf}/^{177}\text{Hf})_{\text{today}}$

is the isotope ratio of the upper mantle (and NMORB) observed today. This varies with latitude in the Atlantic.

$(^{176}\text{Hf}/^{177}\text{Hf})_{\text{BSE, T}}$

is the isotope ratio of the upper mantle T years ago, assuming a bulk silicate earth evolution for the upper mantle prior to time T. While $(^{176}\text{Hf}/^{177}\text{Hf})_{\text{BSE, T}}$ is a function of T, it is assumed to be constant for all latitudes prior to the melting which began T years ago (figure 2.8).

From equation (1), it is apparent that the gradient in $(^{176}\text{Hf}/^{177}\text{Hf})_{\text{today}}$ (i.e. in ϵHf) observed in Atlantic NMORB can be caused either by a gradient in $\langle ^{176}\text{Lu}/^{177}\text{Hf} \rangle$ with constant T (model 1a) or a gradient in T with constant $\langle ^{176}\text{Lu}/^{177}\text{Hf} \rangle$ (model 1b), or gradients in both $\langle ^{176}\text{Lu}/^{177}\text{Hf} \rangle$ and T. (Analogous equations can be written for $^{143}\text{Nd}/^{144}\text{Nd}$ and $^{207}\text{Pb}/^{204}\text{Pb}$.)

Model 1a: long-wavelength gradient in the average, time-weighted, mean degree of melting, $\langle F \rangle$ (constant T)

The observed decrease in ϵHf from north to south can be caused by a decrease in $\langle ^{176}\text{Lu}/^{177}\text{Hf} \rangle$ from north to south at constant T (figure 2.9). Such a gradient can be caused by a decrease in the average, time-weighted mean degree of melting, $\langle F \rangle$, experienced by the upper mantle from north to south.

$$\langle F \rangle = \frac{\int_0^T F(t) dt}{\int_0^T dt} \quad (3)$$

where $F(t)$ is the mean degree of melting experienced by the upper mantle at a given latitude T years ago.

This gradient in $\langle F \rangle$ leaves behind an upper mantle restite that is progressively less depleted in incompatible elements towards the south. This gradient in $\langle F \rangle$ also leads to a decrease in time-integrated Sm/Nd and increase in time-integrated U/Pb towards the south (because Hf , Nd and U are more incompatible than Lu , Sm and Pb respectively). Over time, T , this leads to gradients in ϵHf and ϵNd (both decreasing to the south) and $^{207}Pb/^{204}Pb$ (increasing to the south) in the Atlantic upper mantle.⁶

Such a gradient in $\langle F \rangle$ is consistent with the observation that the ϵHf gradient is much more pronounced than the ϵNd gradient. Since Lu/Hf is fractionated by melting much more than Sm/Nd is, a given degree of ancient melting will result in a more pronounced signal in ϵHf than in ϵNd . In addition, since the half-life of ^{176}Lu is shorter than that of ^{147}Nd , ϵHf increases more quickly than ϵNd . Since the gradient is apparent in $^{207}Pb/^{204}Pb$, it is also necessary that the melting event is ancient because $^{207}Pb/^{204}Pb$ is produced by the almost extinct ^{235}U .

Model 1b: long wavelength gradient in the age of melting, T (constant $\langle ^{176}Lu/^{177}Hf \rangle$)

The observed decrease of ϵHf and ϵNd from north to south is also consistent with a model where $\langle ^{176}Lu/^{177}Hf \rangle$ is constant with latitude, but the age of upper mantle melting, T , decreases to the south (figure 2.10). This model of earlier melting in the north than in the south will cause an increase in $^{207}Pb/^{204}Pb$ from north to south. This is because the parent element (U) is more incompatible than the daughter element (Pb) for melt extraction at mid-ocean ridges.

⁶ The increased U/Pb also should lead to increased $^{206}Pb/^{204}Pb$ towards the south. However, this is not observed. It is likely that this is because the observed $^{206}Pb/^{204}Pb$ profile is obscured by the overwhelming effect on $^{206}Pb/^{204}Pb$ of the medium-wavelength dispersal of HIMU plume-heads.

Models 1a and 1b indicate that ancient melt processes may indeed be the cause of the long-wavelength isotope gradients observed along the MAR. This is either via a gradient in the average, time-weighted mean degree of melting, $\langle F \rangle$ or via a gradient in the age of melting, T (or both). Either $\langle F \rangle$ decreases to the south or T decreases to the south (or both).

Model 2: large-scale pollution

Another possible model for the process controlling the long-wavelength isotope gradients in the NMORB population is that the Atlantic upper mantle has been polluted on a large-scale by a Dupal component (Hart 1984, Dupré and Allègre 1983, Hamelin and Allègre 1985, Hamelin et al. 1985). (The Dupal component is discussed in more detail in chapter 3.) In this case, the pollutant may be material with low ϵNd and ϵHf and high $^{207}Pb/^{204}Pb$ and $\Delta^{207}Pb/^{204}Pb$, which was introduced to the upper mantle relatively *recently*. The concentration of this pollutant in the upper mantle increases to the south.

Alternately, the same gradient can be caused by *ancient* pollution by material with low Lu/Hf and Sm/Nd. Again, in this case the concentration of the pollutant increases to the south. Over time, this pollutant has led to low ϵNd and ϵHf towards the south. In this model, the polluted upper mantle must originally have had higher U/Pb towards the south while ^{235}U was still fairly abundant to enable the buildup of $^{207}Pb/^{204}Pb$ and $\Delta^{207}Pb/^{204}Pb$ from decay of ^{235}U . Subsequently, the polluted upper mantle in the south may have experienced a decrease in U/Pb since $^{206}Pb/^{204}Pb$ of the Dupal signal is rather low.

Conclusions

The Hf isotope system in MORB was largely ignored for many years because of its similarity to the Nd isotope system and difficulty in $^{176}Hf/^{177}Hf$ measurement. This global MORB survey shows that the two systems are in fact not redundant. There are important differences between them that make ϵHf a valuable additional source of information about mantle processes.

In the Arctic, high ϵHf for a given ϵNd indicates that the two isotope systems have become decoupled in the local upper mantle. This mantle may have been polluted locally by ancient pelagic sediment. Alternatively, this upper mantle may contain material which has undergone ancient melt extraction in the garnet stability field rather than in the spinel stability field. This ancient garnet restite

may come from the sub-continental mantle which is fairly close to the Mohns Ridge. Either of these processes lead to high ϵ_{Hf} for a given ϵ_{Nd} .

ϵ_{Hf} of DMM is difficult to define because of the relatively large range of ϵ_{Hf} in NMORB. ϵ_{Hf} from this global survey provides a reasonable estimate for ϵ_{Hf} of DMM. Based on the $\epsilon_{\text{Hf}}-\epsilon_{\text{Nd}}$ composition of the EMORB from the St. Helena plume anomaly and the composition of HIMU-type ocean island basalts, ϵ_{Hf} of DMM is estimated as 20.8.

ϵ_{Hf} for MORB from the Mid-Atlantic Ridge confirms the existence of a "HIMU province" from 24°N to 34°S. This province is formed by a medium-wavelength process, namely, the pollution of the upper mantle around the equator by HIMU plume-head restites. Low $^{87}\text{Sr}/^{86}\text{Sr}$ for a given ϵ_{Hf} and ϵ_{Nd} distinguishes this "HIMU province" from the rest of the Atlantic. The isotopic signal of this process is most clear in profiles of $^{206}\text{Pb}/^{204}\text{Pb}$ and $^{87}\text{Sr}/^{86}\text{Sr}$ versus latitude, which exhibit a broad maximum and minimum respectively over the "HIMU province".

The 15,000 km long decrease of ϵ_{Hf} in NMORB southwards along the Mid-Atlantic Ridge clearly shows that there is a long-wavelength process, which affects the entire Atlantic upper mantle. This process also produces the decrease in ϵ_{Nd} and increase in $\Delta^{207}\text{Pb}/^{204}\text{Pb}$ and $^{207}\text{Pb}/^{204}\text{Pb}$ southwards. It is possible that these gradients are due to an ancient gradient in the average, time-weighted mean degree of melting, $\langle F \rangle$, experienced by the upper mantle. This model is supported by the stronger gradient in ϵ_{Hf} compared to ϵ_{Nd} . In this model, $\langle F \rangle$ decreases to the south. The gradients can also be explained by a gradient in the age, T , when melting began in the Atlantic upper mantle. In this case, melting in the north must have started earlier than in the south. A final possibility is that these isotope gradients are due to pollution (either ancient or recent) and that the proportion of the Dupal-type pollutant present in the upper mantle increases to the south.

CHAPTER 3

MANTLE MIXING IN THE SOUTH ATLANTIC FROM 40°S TO 55°S

Introduction

Mixing relationships in the southern South Atlantic mantle are complex. This work is an attempt to constrain mantle mixing processes beneath the southern South Atlantic Ocean on two different scales: the localized interaction between plumes and the upper mantle and the large-scale pollution of the upper mantle. Proposed mechanisms of large-scale upper mantle pollution include plume-head dispersal, delamination of continental material from thermal erosion by plumes, dispersal of continental material during the breakup of Gondwana and metasomatism of the mantle by subduction zone melts or fluids. In addition, localized plume-upper mantle mixing relationships may be complex because plumes themselves may be heterogeneous. The Hf isotope data presented here build on previous major element, trace element, rare gas and isotope data for the same sample set (Douglass et al. 1995, Douglass et al. 1999, Douglass 2000, le Roux et al. a in press, le Roux et al. b submitted, le Roux et al. c in preparation, Sarda et al. 2000, Moreira et al. 1995, Schiano et al. 1997, and Eiler et al. 2000).

South Atlantic plume-ridge interactions

Numerous mantle plumes are upwelling beneath the South Atlantic Ocean. According to the plume-source/ridge-sink model (Schilling 1985), material can travel from an upwelling mantle plume along the base of the lithosphere to a ridge where it mixes with upper mantle material and is incorporated in mid ocean ridge basalts (MORB) (Morgan 1978, Schilling 1985, Kincaid et al. 1996). Plume-ridge interactions have been documented between the Mid-Atlantic Ridge (MAR) and the Circe (or Ascension), St. Helena, Tristan da Cunha, Gough, Discovery, and Shona mantle plumes (Hanan et

al. 1986, Graham et al. 1992, Fontignie and Schilling 1996, Humphris et al. 1985, Schilling et al. 1985, Douglass et al. 1995, Douglass et al. 1999).

Previously collected Pb, Sr and Nd isotope data indicate that compositions of some MORB from the present study area (40°S-55°S) are influenced by the Discovery and Shona plumes (figures 3.1 and 3.2) (Douglass et al. 1995, Douglass et al. 1999). The Discovery plume is located about 425 km east of the ridge at 44.45°S, 6.45°W (Douglass et al. 1995). MORB influenced by the Discovery plume lie along the MAR between 40°S and 48.2°S. Since the Discovery plume is EM-type, the Discovery anomaly is most apparent in a $^{87}\text{Sr}/^{86}\text{Sr}$ profile (figure 3.3c). The Shona plume is ridge centered at 51.5°S (Small 1995, Douglass et al. 1995). The Shona plume is mildly-HIMU or C-type and influences MORB compositions from 49.2°S - 52.65°S. This HIMU influence is most clearly seen on a $^{206}\text{Pb}/^{204}\text{Pb}$ profile (figure 3.3d).

The location of the mildly-HIMU or C-type Bouvet plume, which may also influence the compositions of the southernmost basalts in this study area (le Roex et al. 1987, Douglass et al. 1999), is uncertain. It may be located beneath Bouvet Island on the Antarctic Plate (Kurz et al. 1998, le Roex et al. 1983). Another suggestion by H.J.B. Dick (personal communication) is that the plume is currently located at the Bouvet triple junction (intersection of the MAR, South West Indian Ridge and American Antarctic Ridge) and that it oscillates back and forth between this location and Bouvet Island.

Large-scale pollution of South Atlantic MORB source (Dupal, plume-heads, LOMU)

In addition to the localized influences of plumes on the MORB source, the southern South Atlantic may represent a transition region from a MORB source that is normal Pacific/North Atlantic-type upper mantle to a source that is Dupal-type upper mantle. The Dupal anomaly was originally defined as a longitudinal band of ocean island basalts (OIB) and MORB stretching from about 0° - 60°S (centered around 30°S - 40°S) (Dupré and Allègre 1983, Hart 1984, Hamelin and Allègre 1985, Hamelin et al. 1986). In comparison to basalts which lie outside of this band, these Dupal anomaly basalts have high $^{208}\text{Pb}/^{204}\text{Pb}$ and $^{207}\text{Pb}/^{204}\text{Pb}$ for a given $^{206}\text{Pb}/^{204}\text{Pb}$ as well as high $^{87}\text{Sr}/^{86}\text{Sr}$. There is disagreement about the area influenced by the Dupal anomaly. Mahoney et al. (1992) find evidence of a transition region from Dupal to North Atlantic/ Pacific mantle along the South West Indian Ridge

between 17°E - 26°E. However, Dupal material may extend further to the west into the South Atlantic region from 24°S to 50°S along the MAR (Hanan et al. 1986, Castillo 1988, Fontignie and Schilling 1996, Douglass and Schilling 2000).

The cause of the anomalous Dupal basalts must be a reservoir with high time integrated Rb/Sr, Th/Pb, and Th/U, which has been isolated for a long time since it also has high $^{207}\text{Pb}/^{204}\text{Pb}$. (^{207}Pb is produced by the now almost extinct ^{235}U .) The source of this anomalous reservoir may be mantle contaminated by recycled continental sediments or delaminated subcontinental lithosphere (Hart 1984). In the model supported by Hart (1984) and Dupré and Allègre (1983), the Dupal source is deep in the mantle and is brought up by plumes thereby producing the Dupal OIB. Then these plumes contaminate the upper mantle and this imparts a Dupal signature on MORB as well. In contrast, the Dupal source may reside in the subcontinental lithosphere (Hawkesworth et al. 1986). In this case, the Dupal signature in basalts may be due to erosion and dispersal of this shallow Dupal reservoir into the upper mantle by upwelling plumes (e.g. Storey et al. 1989) or by remobilization of the subcontinental lithosphere during continental breakup (Fontignie and Schilling 1996).

A synthesis of these models has been suggested for large-scale contamination of the South Atlantic upper mantle. The region has been polluted by dispersal of the St. Helena plume-head (which is not Dupal-type) from ~2°S - 47°S and the Tristan plume-head (which is Dupal-type) from ~24°S - 47°S (Hanan et al. 1986). In addition to this upper mantle pollution by plume-heads, delaminated subcontinental lithosphere may be present as passive heterogeneities in the upper mantle (Douglass et al. 1999, Mahoney et al. 1992). In the view of these authors, these heterogeneities, which Douglass et al. (1999) call LOMU material, were delaminated during the breakup of Gondwana. The heterogeneities may be widely dispersed throughout the region, but since they are refractory, large heterogeneities are only melted and incorporated in MORB when plumes are available to provide excess heat (Douglass et al. 1999, Mahoney et al. 1992). According to Douglass et al. (1999) MORB from 48.5°S to 49.1°S arise from mixing of such a LOMU rafter with the ambient depleted mantle. However, since this segment of the ridge is adjacent to the Discovery anomaly, it is not clear whether or not the Discovery and LOMU anomaly basalts do in fact arise from two distinct enriched sources (i.e. one plume and one upper mantle heterogeneity). It is possible that the Discovery plume is heterogeneous and that the

Discovery and LOMU anomalies arise from mixing of the upper mantle with a single, heterogeneous plume.

Results

The MORB included in this part of the study come from three cruises. Fifty-two samples were collected during cruise 93-09 aboard the R/V *Maurice Ewing* (EW9309) (Douglass et al. 1995). Four samples between 40°S and 46°S are from cruise 107-07 aboard the R/V *Atlantis II* (AII 107-7) (Humphris et al. 1985). Eight of the southernmost samples are from cruise 32 aboard the R/V *Agulhas* (AG32) (le Roex et al. 1987). The MORB are all glass rims, except for six of the AG32 basalts, which are pillow interiors. In addition to the 64 MORB, one basalt from the Discovery Tablemount is included in the study (Kempe and Schilling 1974, le Roux et al. in preparation). This sample is a crushed whole rock powder.

$^{176}\text{Hf}/^{177}\text{Hf}$ results with 2 sigma errors are listed in table 3.1. Standards were run numerous times during machine operation to correct for machine drift. During the analyses (March 2000- May 2001), the JMC-475 Hf standard gave $^{176}\text{Hf}/^{177}\text{Hf} = 0.282160$ with an external reproducibility of ± 0.000010 . Replicate analyses performed on three of the South Atlantic MORB are in good agreement with one another (table 3.1). Measured ϵHf in the South Atlantic data set range from -2.75 ($^{176}\text{Hf}/^{177}\text{Hf} = 0.282694$) to +16.62 ($^{176}\text{Hf}/^{177}\text{Hf} = 0.283242$). This range covers about 60% of the range documented for OIB which fall approximately between -8 and +24 (Salters 1996, figure 1, corrected to JMC-475 = 0.282160).

As expected, the $^{176}\text{Hf}/^{177}\text{Hf}$ profile along the MAR between 40°S and 55°S resembles that of $^{143}\text{Nd}/^{144}\text{Nd}$ (figure 3.3 *a* and *b*). In regions of plume-ridge interaction, both $^{176}\text{Hf}/^{177}\text{Hf}$ and $^{143}\text{Nd}/^{144}\text{Nd}$ are lower (less radiogenic) than in the surrounding NMORB population. This indicates that these plume-influenced basalts arise from a source that has time integrated enrichment in incompatible elements (i.e. low Sm/Nd and low Lu/Hf) which is typical of mantle plumes.

Basalts from 40°S to 45.2°S are largely NMORB with relatively high (non plume-like) $^{176}\text{Hf}/^{177}\text{Hf}$ (figure 3.3*a*). For the most part, the ridge here is probably not currently being fed by plume

material. ϵ_{Hf} ranges from +10.9 to +16.6 which is a little lower than the estimates for normal North Atlantic/Pacific type NMORB ($\epsilon_{\text{Hf}} = 20.8$ or $\epsilon_{\text{Hf}} = 17.6$ depending on how ϵ_{Hf} of DMM is defined). (See chapter 2 for a discussion of the methods used to determine ϵ_{Hf} of DMM.) However, one of the two EMORB from this region (EW9309 42D-1g) does have moderately low (moderately plume-like) ϵ_{Hf} of 7.5. This is probably due to mixing of the upper mantle with a small amount of Gough plume material as has been suggested by Douglass et al. (1999) to account for elevated Sr and Pb isotope ratios. Gough Island lies approximately at 40°S, 10°W and a small chain of seamounts extends from the island to the east just south of the Walvis Ridge- Tristan hotspot track (Humphries et al. 1985).

The Hf data collected in this study support the model of Discovery and Shona plume-ridge interactions along the MAR between 45°S and 53°S deduced from Pb-Sr-Nd isotope space (Douglass et al. 1995, Douglass et al. 1999). The $^{176}\text{Hf}/^{177}\text{Hf}$ profile (figure 3.3a) shows two broad regions of low $^{176}\text{Hf}/^{177}\text{Hf}$ due to the influences of the Discovery plume from 45.2°S to 48.2°S ($\epsilon_{\text{Hf}} = -2.8$ to 14.4) and the Shona plume from 49.2°S to 52.6°S ($\epsilon_{\text{Hf}} = 6.6$ to 14.7). In addition to these two broad regions of low $^{176}\text{Hf}/^{177}\text{Hf}$, there is one narrow region of low $^{176}\text{Hf}/^{177}\text{Hf}$ just south of the main Discovery anomaly from 48.5°S to 49.1°S ($\epsilon_{\text{Hf}} = -1.6$ to 7.7). This region is called the LOMU segment by Douglass et al. (1999), although if the Discovery plume is heterogeneous, it may be part of the region of Discovery plume influence.

Establishing the southern end of the Shona anomaly with confidence is difficult because there is a gap in dredging between 53°S and 54°S (Douglass et al. 1995, 1999). Gravity data shows that an axial valley is present in the short region between 52.2°S and 53°S while most of the surrounding regions to the north and south have smooth topography with no axial valley (Douglass et al. 1999). If the Shona anomaly ends at 52.6°S, the low Hf ratios just north of the triple junction are likely due to material from the Bouvet plume. Sorting out these mixing relationships is not unambiguous since both the Bouvet and Shona plumes are mildly-HIMU or C-type and therefore do not have distinctive isotope signals.

It is interesting to note that $^{176}\text{Hf}/^{177}\text{Hf}$ of the two basalts from dredge station EW9309 25D along the MAR are even lower (more plume-like) than $^{176}\text{Hf}/^{177}\text{Hf}$ in the basalt from the Discovery

Tablemount. The Discovery Tablemount (42°S, 0°) is northeast of the present location of the Discovery plume (Douglass et al. 1995). The Discovery Tablemount basalt is 25 Ma and was probably formed by intraplate Discovery plume volcanism (Kempe and Schilling 1974, Douglass et al. 1999, le Roux et al. in preparation).

Mixing relationships

Upper mantle - plume mixing between 40°S - 55°S

In order to help establish whether mixing is occurring and which mantle reservoirs are involved in the mixing process, the data can be plotted on isotope-isotope plots. The three mixing trends of Discovery (45.2°S-48.2°S), LOMU (48.5°S-49.1°S) and Shona (49.2°S-52.6°S) material with upper mantle material are most clear on a plot of $\epsilon_{\text{Hf}} - {}^{206}\text{Pb}/{}^{204}\text{Pb}$ (figure 3.4). The three mixing trends converge on the high ϵ_{Hf} (non plume-like) end but they diverge towards different "enriched" (plume-like) end-members. The Shona anomaly basalts trend towards $\epsilon_{\text{Hf}} = 6.7$, ${}^{206}\text{Pb}/{}^{204}\text{Pb} = 18.9$ and ${}^{208}\text{Pb}/{}^{204}\text{Pb} = 38.8$ (EW9309 19D-1g). This points towards a mildly-HIMU or C-type end-member. The Discovery anomaly basalts trend towards $\epsilon_{\text{Hf}} = -2.8$, ${}^{206}\text{Pb}/{}^{204}\text{Pb} = 18.2$ and ${}^{208}\text{Pb}/{}^{204}\text{Pb} = 38.7$ (EW9309 25D-5g). The LOMU segment basalts trend towards $\epsilon_{\text{Hf}} = -1.6$, ${}^{206}\text{Pb}/{}^{204}\text{Pb} = 17.8$ and ${}^{208}\text{Pb}/{}^{204}\text{Pb} = 38.2$ (EW9309 7D-1g). Basalts from both the Discovery and LOMU segments trend towards EM-type end-members. While basalts from the Discovery and LOMU segments overlap in terms of ϵ_{Hf} values, for a given ϵ_{Hf} the LOMU basalts have lower ${}^{206}\text{Pb}/{}^{204}\text{Pb}$ and ${}^{208}\text{Pb}/{}^{204}\text{Pb}$ than the Discovery basalts.

$\epsilon_{\text{Hf}} - {}^{207}\text{Pb}/{}^{204}\text{Pb}$ shows no clear mixing trends because basalts from all three trends have overlapping ϵ_{Hf} and ${}^{207}\text{Pb}/{}^{204}\text{Pb}$ values.

The Discovery, LOMU and Shona mixing vectors are not distinguishable in $\epsilon_{\text{Hf}}-\epsilon_{\text{Nd}}$ space (figure 3.5). All of these basalts fall on the Hf-Nd mantle array (Patchett and Tatsumoto 1984, Blichert-Toft and Albarède 1997). However, basalts from the Discovery and LOMU anomalies extend to much lower ϵ_{Hf} and ϵ_{Nd} values than the Shona anomaly basalts. This indicates there is a continental component in the sources of the Discovery and LOMU basalts. This is supported by the $\epsilon_{\text{Hf}} - {}^{87}\text{Sr}/{}^{86}\text{Sr}$

plot (figure 3.6), which shows that Discovery and LOMU basalts extend to much higher $^{87}\text{Sr}/^{86}\text{Sr}$ than Shona anomaly basalts. It is also noteworthy that for a given $^{87}\text{Sr}/^{86}\text{Sr}$ value, ϵ_{Hf} is lower for Shona anomaly basalts than for Discovery or LOMU basalts.

Ambient depleted mantle versus "normal" depleted mantle

Each of the three mixing trends identified in the previous section is a mixture between an enriched source (i.e. the Shona plume, Discovery plume or LOMU rafters) and a depleted source (i.e. the ambient upper mantle). Douglass et al. (1999) found that the upper mantle with which the Discovery and Shona plumes are mixing is not the normal North Atlantic/Pacific -type upper mantle. They defined the likely isotopic composition of this ambient upper mantle from the intersection of the Discovery and Shona mixing trends on isotope-isotope plots. They found that the ambient upper mantle is radiogenic relative to the North Atlantic and Pacific in terms of Pb and Sr isotopes and unradiogenic in terms of Nd isotopes. This indicates that in comparison to normal upper mantle, the South Atlantic ambient upper mantle may have experienced a slight long term enrichment in incompatible elements (i.e. model 2 of chapter 2) or less long term depletion in incompatible elements (i.e. model 1a of chapter 2) leading to high Rb/Sr, U/Pb, Th/Pb and low Sm/Nd parent-daughter ratios. Alternately, the mantle may have been polluted relatively recently with a component with radiogenic Pb and Sr and unradiogenic Nd. The isotopic composition of this ambient upper mantle is compared to normal upper mantle in table 3.2. (There is much controversy surrounding the "real" composition of the normal upper mantle. Some workers advocate a composition like that of Hart et al. (1992) which is based on the mean isotopic composition of NMORB rather than the most depleted NMORB. Other workers support a more extreme end-member type composition for the normal upper mantle which is either based on the most depleted NMORB documented from 2°S-7°S in the Equatorial Atlantic (Schilling et al. 1994) or on inversion of global NMORB isotope data (Allègre et al. 1983, Allègre et al. 1988, Allègre and Lewin 1989).)

The data collected in this study now allow characterization of the $^{176}\text{Hf}/^{177}\text{Hf}$ of the South Atlantic ambient upper mantle (figure 3.7). Following the method of Douglass et al. (1999), the

intersection of the Shona and Discovery trends is roughly $^{176}\text{Hf}/^{177}\text{Hf} = 0.28324$ ($\epsilon\text{Hf} = 16.6$). This ambient mantle value compares to $\epsilon\text{Hf} = 20.8$ for normal upper mantle (see caption of table 3.2 for calculation). Thus, the South Atlantic ambient upper mantle is relatively unradiogenic in comparison to the North Atlantic and Pacific in terms of Hf as one would expect based on Nd isotopes. This indicates that the ambient upper mantle (or a pollutant present in the ambient upper mantle) has experienced long-term depletion of Lu relative to Hf. This is consistent with a slightly incompatible element enriched (or slightly less depleted) ambient upper mantle (compared to normal upper mantle) since Hf is more incompatible than Lu.

In order to investigate the source of the South Atlantic upper mantle "pollution" which causes this time integrated incompatible element enrichment, a three-component mixing model is applied to try to reproduce the observed ambient upper mantle isotopic composition. This model is based on the work of Rehkämper and Hofmann (1997) who successfully modeled the pollution of the Indian Ocean MORB source as a mixture of normal North Atlantic/ Pacific upper mantle with a recycled component. This recycled component is ancient altered oceanic crust that has been subducted together with variable amounts of ancient pelagic sediment. Their model, with some modifications, is applied to the South Atlantic MORB source to test whether the South Atlantic ambient upper mantle can result from pollution of normal upper mantle with such a recycled component.

The model presented here uses the three mixing end-members suggested by Rehkämper and Hofmann (1997): unpolluted upper mantle (DM), 1.5 Ga. subducted oceanic crust (OC) and 1.5 Ga. subducted pelagic sediment (SED). The trace element concentrations and isotope compositions of these end-members are listed in table 3.3.

There are some differences between the values used in the present model and those used in the original Rehkämper and Hofmann (R&H) model. First of all, in the present model the isotopic composition of the unpolluted upper mantle is taken from S.R. Hart (personal communication) and Hart et al. (1992). (For comparison, the original R&H DM values are also shown in table 3.3.) In addition, Lu and Hf data, which were not considered in the original R&H model, are included in the present model.

Isotopic compositions of DM-OC-SED mixtures are plotted in figure 3.8. Ancient pelagic sediment (SED) has very different Sr/Pb, Nd/Pb and Hf/Pb from ancient oceanic crust (OC) or upper mantle (DM) (e.g. $Sr/Pb_{SED} = 5$, $Sr/Pb_{OC} = 360$, $Sr/Pb_{DM} = 230$). Therefore, DM-SED and OC-SED binary mixtures have high degrees of curvature in isotope-isotope space. The three binary mixtures in figure 3.8 define the allowable area for isotopic compositions of three component DM-OC-SED mixtures.

From figure 3.8, it is apparent that the ambient upper mantle's isotope composition does not fall on the DM-SED binary. Therefore, pelagic sediment alone cannot be the source of upper mantle pollution. The isotope characteristics of the ambient upper mantle require the presence of oceanic crust as well. The ambient upper mantle can be reproduced by a mixture of 96% DM + 3.94% OC + 0.06% SED. (See the appendix for an explanation of the calculations.)

Pollution of DM with a small amount of OC and SED also can explain trace element characteristics of the ambient upper mantle. While Ba and Nb concentrations individually change during melting and fractional crystallization, the ratio of the two in the melt (i.e. in the basalt) is representative of the ratio in the source (i.e. the upper mantle). Ba/Nb for typical North Atlantic/Pacific MORB (and by inference the "unpolluted" upper mantle) is ~ 2.8 (Hofmann 1988). MORB from the Discovery and Shona anomalies, however, converge to an ambient upper mantle composition with Ba/Nb ~ 5 . Figure 3.8f shows that pollution of DM by OC + SED can cause this unusually high Ba/Nb. Thus both the unusual trace element ratios and isotope ratios observed in the South Atlantic upper mantle can be achieved through pollution by very little recycled component.

In an OC-SED binary mixture, even very small amounts of pelagic sediment have a very big effect on $^{206}Pb/^{204}Pb$ of the mixture. This effect on $^{206}Pb/^{204}Pb$ is much bigger than the effect of sediment on Sr, Hf or Nd isotope ratios. Generally, pure recycled oceanic crust (with no sediments) is considered the source of HIMU basalts (Hofmann and White 1982). True HIMU plumes are rare (St. Helena, Tubaii, Mangaia (e.g. White 1985)). It is much more common to find mildly-HIMU or C-type plumes (Shona, Bouvet, Iceland, Azores (e.g. Hanan and Graham 1996)). This is probably because subduction of oceanic crust that is completely free of sediments is unlikely and even a small amount of sediment quickly erases the high $^{206}Pb/^{204}Pb$ associated with pure HIMU plumes.

Many sources of upper mantle pollution have been proposed (i.e. subcontinental lithosphere, subduction zone fluids, garnet granulites from the lower crust). The calculations described above do not rule out these other sources of pollution, but the calculations do suggest that if pelagic sediments are involved in the pollution of the upper mantle, they must be present together with recycled oceanic crust. The mixing calculations also do not constrain *how* the pollutants were dispersed in the upper mantle.

Mixing lines within the Shona anomaly

In isotope-isotope space, the Shona anomaly (49.25°S-52.65°S) is quite broad in comparison to the Discovery and LOMU anomalies. $^{176}\text{Hf}/^{177}\text{Hf}$ for these basalts reveal systematic structure within the Shona anomaly that has not been recognized previously based only on Pb-Sr-Nd isotope space. This structure indicates that the Shona anomaly cannot be caused by simple binary mixing of a homogeneous plume with a homogeneous ambient upper mantle. At least three mixing end-members are needed to describe the observed isotopic structure of the Shona anomaly. Two different physical models can be used to describe mixing of these three end-members.

Model 1: homogeneous plume

In the first model (figure 3.9a), a homogeneous plume is mixing with a heterogeneous upper mantle. In this case, the ambient upper mantle has passive heterogeneities embedded in it. The plume, ambient mantle and passive heterogeneities mix in varying proportions to produce the MORB.

Model 2: heterogeneous plume

In a second possible model, the local upper mantle is homogeneous but the upwelling Shona plume is heterogeneous (figure 3.9b). In this case, the mixing of the three end-members is sequential binary mixing. In stage 1, two end-members mix to produce the heterogeneous Shona plume. Then in stage 2 this heterogeneous plume mixes with the homogeneous ambient mantle.

The isotopic structure within the Shona anomaly basalts is evident on plots of $^{206}\text{Pb}/^{204}\text{Pb}$ - $^{176}\text{Hf}/^{177}\text{Hf}$ and $^{206}\text{Pb}/^{204}\text{Pb}$ - Ba/Nb (figure 3.10). Basalts from the Shona anomaly fall along distinct mixing vectors. The basalts within each of these geochemical groups are also distinct spatially. The Shona anomaly can be subdivided into 4 segments along the MAR (figure 3.11):

segment 1 - (49.25°S - 49.99°S)
segment 2 - (50.27°S - 51.06°S)
segment 3 - (51.05°S - 52.16°S)
segment 4 - (52.27°S - 52.65°S)

There is some overlap at the ends of the segments. For example, basalt EW9309 18D-1g lies within the southern end of *segment 2* but is geochemically like the basalts immediately to the south in *segment 3*. (One basalt from the Shona anomaly, EW9309 14D-4g, is excluded from this discussion. Justification is given in the appendix.)

While Ba/Nb - $^{206}\text{Pb}/^{204}\text{Pb}$ (figure 3.10b) clearly shows that *segments 1* and *2* fall on different mixing trends, in isotope-isotope space these two segments appear to lie along the same trend. This may indicate a recent decoupling of trace elements and isotopes as has been suggested by Douglass et al. (1999). The segmentation of the Shona anomaly is evident from the three mixing vectors in plots of $^{206}\text{Pb}/^{204}\text{Pb}$ - ϵNd , $^{206}\text{Pb}/^{204}\text{Pb}$ - $^{87}\text{Sr}/^{86}\text{Sr}$ and $^{206}\text{Pb}/^{204}\text{Pb}$ - $^{208}\text{Pb}/^{204}\text{Pb}$ (figure 3.12). It is not possible to discern separate mixing trends in $^{206}\text{Pb}/^{204}\text{Pb}$ - $^{207}\text{Pb}/^{204}\text{Pb}$ space, possibly because of the lower precision of $^{207}\text{Pb}/^{204}\text{Pb}$ measurements.

The "depleted" ends of these mixing vectors converge to the ambient upper mantle composition discussed in the previous section. The mixing vectors trend towards different enriched compositions. Since binary mixing of two homogeneous end-members must form a single mixing line in Pb isotope-isotope space, basalts within the Shona anomaly must arise from a more complicated mixing process.

It is possible that three component DM-OC-SED mixtures, which are used in the previous section to model the ambient upper mantle, also give rise to basalts from the Shona anomaly. In order to test this hypothesis, the model of Rehkämper and Hofmann (1997) is applied to Shona anomaly basalts. In this case, however, rather than using pure upper mantle (DM) as a mixing end-member, the polluted ambient mantle (ADM) is used. The isotope composition of ADM is taken from the intersection of the Shona and Discovery anomalies in isotope-isotope space (Douglass et al. 1999 and this study). The trace element concentrations in this polluted upper mantle are taken from the calculations in the previous section where it was shown that ADM can be modeled from a mixture of 96% DM + 3.94% OC + 0.06% SED. The isotope ratios and trace element concentrations used in the

calculations are listed in table 4. The other two end-members used in the mixing calculations (OC and SED) are the same as in the modeling of the ambient mantle.

Figure 3.13 shows three component mixtures of ADM-OC-SED. The figure shows dashed lines representing mixtures in which the oceanic crust to sediment ratio is constant. If one considers oceanic crust plus sediment a single recycled component (REC), then these lines each represent mixing of ADM with a different recycled component. Mixtures that fall along these lines can be considered binary mixtures of ambient upper mantle with different recycled components (i.e. model 2: heterogeneous plume).

In general, these binary ADM-REC trends are not linear (except for on Pb-Pb plots) because the ambient upper mantle (ADM) and the recycled component (OC+SED) often have very different trace element ratios (i.e. Sr/Pb, Nd/Pb, Hf/Nd). Over a restricted range of recycled component compositions, however, the ADM + REC mixing trends are virtually linear. When the recycled component contains less than 2% sediment, the trace element ratios in the recycled component are almost equal to the trace element ratios in the ambient upper mantle (e.g. $(\text{Sr/Pb})_{\text{Recycled}} \sim (\text{Sr/Pb})_{\text{ADM}}$). Therefore, if the sediment fraction is less than 2% and the ratio of sediments to oceanic crust is constant, SED-ADM-OC mixing trends are linear in isotope-isotope space and point from ADM to the composition of the recycled component.

It is evident that *segments 2, 3 and 4* from the Shona anomaly each fall along a trend of constant sediment-oceanic crust ratio (figure 3.14). Thus, each segment can be considered a binary mixture. The depleted end-member in all three cases is the ambient upper mantle (ADM). In *segment 2* the recycled end-member is a mixture of approximately 0.7% sediment with 97.3% oceanic crust. (The best-fit in Sr-Pb isotope space is 0.4% sediment while in Nd-Pb, Hf-Pb and $^{207}\text{Pb}/^{204}\text{Pb}$ - $^{206}\text{Pb}/^{204}\text{Pb}$ space the best fit is for a recycled component with 0.7% sediment.) In *segment 3* the recycled end-member contains about 1.1% sediment and in *segment 4* this increases to about 1.6% sediment. These results show that very small amounts of pelagic sediment have a very large effect on the composition of the resulting mixture. Mixtures of these three recycled components (0.7%, 1.1% and 1.6% sediment) with ADM also successfully reproduce the observed Ba/Nb trends of *segments 2, 3 and 4* (figure 3.14f).

The above results imply that the Shona plume consists of recycled material, namely anciently subducted oceanic crust with pelagic sediment. In this model, the Shona plume is not well mixed since there seem to be three different "flavors" of recycled component (i.e. three different crust/sediment ratios) mixing with a locally homogeneous ambient upper mantle. This ambient upper mantle was likely polluted with oceanic crust and pelagic sediment in an event prior to (and likely unrelated to) the present-day mixing with the Shona plume.

It is of course possible that the Shona plume is in fact homogeneous (i.e. model 1), either with a HIMU composition (pure oceanic crust with no sediment present) or C composition (some small, but constant fraction of sediments present). In this case, the ambient upper mantle with which the plume is mixing must be heterogeneous with the sediment fraction in the ambient upper mantle increasing to the south. In such a scenario, however, it is difficult to explain how the sediment-oceanic crust fraction remains constant over a given ridge segment since the oceanic crust resides in the plume and the sediment resides in the ambient upper mantle. There is evidence for heterogeneous plumes in other areas such as Hawaii (Hauri 1996), Iceland (Chauvel and Hémond 2000) and the Galapagos (Blichert-Toft and White submitted). It is likely that the Shona plume is also an example of a heterogeneous plume rather than a homogeneous plume mixing with a locally heterogeneous ambient upper mantle.

A final point can be made regarding ADM-OC-SED mixtures and Hf-Nd isotope systematics. Patchett et al. (1984) suggested that ϵ_{Hf} can be used to evaluate whether pelagic sediment is included in the source of a basalt because ϵ_{Hf} for basalts which include pelagic sediment will fall above the Hf-Nd mantle array. This is because, for a given ϵ_{Nd} , ϵ_{Hf} is high in pelagic sediment due to the high time integrated Lu/Hf (the zircon effect). In fact, Blichert-Toft et al. (1999) used ϵ_{Hf} with ϵ_{Nd} and $^{206}\text{Pb}/^{204}\text{Pb}$ to identify pelagic sediment in the source of Hawaiian basalts. From figure 3.13e, it is clear that ϵ_{Hf} is a sensitive indicator of pelagic sediment only when the sediment component of the basalt source is greater than about 2%. If smaller sediment fractions are involved, the $\epsilon_{\text{Hf}}-\epsilon_{\text{Nd}}$ of the mixture falls very close to the mantle array, especially if oceanic crust is also present in the basalt source. This seems to be the case for the Shona anomaly data (figure 3.14e). While the Shona anomaly data falls

within the Hf-Nd isotope space defined by ADM-OC-SED, since the sediment component is so small, the data is clustered near the ADM-OC binary.

Discovery and LOMU anomalies

ADM-OC-SED mixing used to model the compositions of basalts from the Shona anomaly does not successfully reproduce compositions of basalts from the Discovery or LOMU anomalies (figure 3.15). Isotope compositions of some basalts from these two regions fall outside of the range of possible isotope compositions of ADM-OC-SED mixtures for two reasons. The first reason is that the $^{207}\text{Pb}/^{204}\text{Pb}$ of the pelagic sediment component (SED) is too low to encompass all of the Discovery and LOMU anomaly basalt compositions on a $^{207}\text{Pb}/^{204}\text{Pb}$ - $^{206}\text{Pb}/^{204}\text{Pb}$ plot (figure 3.15b). (Note that on Pb-Pb diagrams, the binaries connecting the three end-members are always straight lines. These binaries bound the area of allowable compositions of mixtures.) The second problem with application of the ADM-OC-SED model to the Discovery and LOMU anomalies is the difference in Sr/Pb, Nd/Pb and Hf/Pb in the SED and the OC end-members. These large differences in trace element concentration ratios cause high degrees of curvature in the OC-SED binaries in Pb-Sr, Pb-Nd and Pb-Hf isotope space. Because of this curvature, many Discovery and LOMU anomaly basalt compositions fall outside of the possible range of ADM-OC-SED mixtures (figure 3.15 a, c and d). Different end-member(s) must be involved. Several possibilities for alternatives to the SED end-member can be investigated qualitatively.

One possibility is that pelagic sediment is in fact mixing with ambient depleted mantle and oceanic crust to produce Discovery and LOMU anomaly basalts but that SED is an inaccurate representation of pelagic sediment. If this is true, $^{207}\text{Pb}/^{204}\text{Pb}$ of SED is too low and Pb concentration is too high to accurately represent ancient pelagic sediment. The SED end-member used in the previous ADM-OC-SED model is from Rehkämper and Hofmann (1997). These authors estimate the $^{206}\text{Pb}/^{204}\text{Pb}$, $^{207}\text{Pb}/^{204}\text{Pb}$ and $^{208}\text{Pb}/^{204}\text{Pb}$ of 1.5 Ga. pelagic sediment from a two-stage Stacey-Kramers Pb evolution model (Stacey and Kramers 1975). There is some evidence that the Stacey-Kramers model underestimates the U/Pb in the first stage of Pb evolution. If one uses stage 1 U/Pb ratios suggested by Tatsumoto (1978) or Allègre et al. (1988) then pelagic sediment does have the appropriate Pb isotope

ratios (i.e. high enough $^{207}\text{Pb}/^{204}\text{Pb}$ for a relatively low $^{206}\text{Pb}/^{204}\text{Pb}$) to encompass all the data on Pb-Pb plots.

While the Pb isotope evolution of 1.5 Ga. pelagic sediment may be modeled such that it is an appropriate mixing component for Discovery and LOMU anomaly basalts, the Pb concentration of pelagic sediment is more problematic. The SED Pb concentration of Rehkämper and Hofmann (1997) is 55ppm. While this value is in the range of pelagic sediment concentrations reported in the literature, it falls on the high end of the range of pelagic sediment data from Plank and Langmuir (1998) or Ben Othman et al. (1989). The average of Pb concentrations in pelagic sediment samples from these two sources is about 35 ppm (the range is 16 ppm - 64 ppm). However, neither 35ppm nor 16 ppm (the lowest value reported in Ben Othman et al. (1989)) is low enough to reduce the curvature in the SED-OC mixing binaries enough to encompass the Discovery and LOMU anomaly data completely. Thus, because of the relatively high Pb concentration in pelagic sediment, it is not likely that pelagic sediment is involved in the mixtures that give rise to Discovery anomaly and LOMU section basalts.

A final argument against ancient pelagic sediment in the source of Discovery and LOMU anomaly basalts is based in the Hf-Nd isotope systematics of ADM-OC-SED mixtures. Figure 3.15e shows that many of the Discovery and LOMU anomaly basalts fall outside of the range of possible compositions for ADM-OC-SED mixtures. (This is in contrast to Shona anomaly data in figure 3.14e.) The Discovery and LOMU anomaly basalts that fall outside of the possible $\epsilon\text{Hf}-\epsilon\text{Nd}$ range have ϵHf values that are too low for a given ϵNd . However, one of the distinguishing features of ancient pelagic sediment is that it has high time integrated Lu/Hf (and therefore high ϵHf) for a given time integrated Sm/Nd due to the zircon effect (Patchett et al. 1984). The trends of Discovery and LOMU data indicate that they arise from such a source with a much lower ϵHf (and therefore lower time integrated Lu/Hf) than pelagic sediment. Thus, pelagic sediment is probably not involved in the source of Discovery and LOMU basalts.

It is possible that material from the lower continental crust rather than pelagic sediment (which arises from the upper continental crust) is involved in mixtures that produce the Discovery and LOMU anomaly basalts. Whether or not lower crust is an appropriate mixing reservoir can be assessed from

the isotopic composition of lower crustal material which is brought to the surface as garnet granulite xenoliths. The isotopic compositions of such xenoliths, which come from depths between about 25 km - 45 km (Rudnick and Fountain 1990)), vary greatly from one region to another depending on their protolithic nature (Rudnick and Goldstein 1990, Rudnick and Fountain 1995). The component which is mixing with the ambient depleted mantle to produce Discovery and LOMU anomaly basalts must have $^{206}\text{Pb}/^{204}\text{Pb}$ significantly lower than 18. Globally, many garnet granulite xenoliths do not have such low $^{206}\text{Pb}/^{204}\text{Pb}$. However, those xenoliths from stable regions (cratons) do have low $^{206}\text{Pb}/^{204}\text{Pb}$ (e.g. Rudnick and Goldstein 1990). The Kaapvaal Craton in southern Africa is one such region where xenoliths with low $^{206}\text{Pb}/^{204}\text{Pb}$ are found (Huang et al. 1995). Of these Kaapvaal Craton xenoliths, however, only those from the northern Lesotho region have a high enough $^{207}\text{Pb}/^{204}\text{Pb}$ for a given $^{206}\text{Pb}/^{204}\text{Pb}$ (Huang et al. 1995) to be appropriate end-members in ADM-granulite binary or ADM-OC-granulite three component mixtures.

While the $^{206}\text{Pb}/^{204}\text{Pb}$ and $^{207}\text{Pb}/^{204}\text{Pb}$ of these Lesotho xenoliths make them appropriate mixing end-members, their $^{87}\text{Sr}/^{86}\text{Sr}$ do not. Of the 13 xenoliths from the Lesotho region reported by Rogers and Hawkesworth (1982) only one (LT2, a felsic xenolith) has high enough $^{87}\text{Sr}/^{86}\text{Sr}$ to be an appropriate mixing end-member in the source of Discovery and LOMU anomaly basalts. Xenoliths from regions in South Africa other than Lesotho do have high enough $^{87}\text{Sr}/^{86}\text{Sr}$ but not high enough $^{207}\text{Pb}/^{204}\text{Pb}$ for a given $^{206}\text{Pb}/^{204}\text{Pb}$. Apparently, only one xenolith from the Kaapvaal Craton region has the combined isotope characteristics that make it a suitable mixing end-member in Discovery and LOMU anomaly basalts. It is possible that some combination of South African lower crustal material is involved in mixing to produce the Discovery and LOMU anomaly basalts, but because of the heterogeneity in recovered xenoliths, this is too open ended to model qualitatively. Table 3.5 lists the average isotope ratios for the Lesotho granulites, granulites from the whole region, LT2 values and the isotope composition of the most plume like samples from the Discovery and LOMU segments.

Finally, material from the subcontinental lithosphere may be considered as a possible component in mixtures that give rise to the Discovery and LOMU anomaly basalts. Walker et al. (1989) report isotope data for peridotite xenoliths from the subcontinental lithosphere (SLC) beneath southern Africa. These SLC xenoliths come from depths of about 180 km. As with the garnet granulite

xenoliths from the southern African lower crust, these SLC xenoliths exhibit great variability in their isotopic compositions. In general, these SLC xenoliths have $^{207}\text{Pb}/^{204}\text{Pb}$ that is too low for a given $^{206}\text{Pb}/^{204}\text{Pb}$ to be a mixing end-member producing the LOMU anomaly basalts. None of the xenoliths reported by Walker et al. (1989) is an appropriate end-member for Discovery or LOMU anomaly basalts.

Neither the SLC nor the lower crust can be ruled out definitively as reservoirs involved in producing Discovery and LOMU anomaly basalts since xenoliths from both reservoirs exhibit isotopic variability and the recovered xenoliths may not be completely representative of SLC or lower crust compositions. Although there is no overwhelming evidence in favor of a lower crustal granulite source in the Discovery and LOMU anomaly basalts from xenolith compositions, there is some evidence from the trace element characteristics of the S18-60/1 basaltic glass described by Kamenetsky et al. (2001). This basalt, collected from just north of the Bouvet triple junction, represents relatively pure LOMU end-member material (see chapter 2). It has high $^{87}\text{Sr}/^{86}\text{Sr}$, $^{207}\text{Pb}/^{204}\text{Pb}$ and low ϵHf and ϵNd , even more extreme than any Discovery or LOMU anomaly basalts. Kamenetsky et al. (2001) feel that mafic granulite from the lower crust is a reasonable source for this basalt. In their view, based on rare earth elements, CaO, Sc, and V, the source of this basalt could have a mineralogy that is consistent with the mineralogy of lower crustal mafic granulites (i.e. the source contains olivine, orthopyroxene and garnet). Thus, although a mafic xenolith with the appropriate Sr and Pb isotope characteristics has not yet been recovered, it is still possible that the lower crust is indeed the reservoir that contains the end-member involved in generating the unusual isotope characteristics of Discovery and LOMU basalts.

Conclusions

The large-scale pollution of the upper mantle beneath the southern South Atlantic is apparent from the $^{176}\text{Hf}/^{177}\text{Hf}$ data collected in this study. ϵHf for normal upper mantle is 20.8 while that for the ambient upper mantle is 16.6. This pollution can be modeled with a three component mixture of "unpolluted" upper mantle with a very small amount of oceanic crust and pelagic sediment (DM-OC-

SED). Pollution with pelagic sediment alone cannot reproduce the observed isotope and trace element characteristics of the ambient upper mantle.

$^{176}\text{Hf}/^{177}\text{Hf}$ of basalts from the Shona anomaly indicate that the Shona plume is heterogeneous. Mixing of this heterogeneous plume with the homogeneous ambient upper mantle can be modeled by a three component mixture of ambient upper mantle with recycled oceanic crust and pelagic sediment (ADM-OC-SED). According to this model, the Shona plume contains recycled components with three different oceanic crust-sediment ratios. Each of these three recycled components (oceanic crust + sediment) contains less than 2% sediment.

$^{176}\text{Hf}/^{177}\text{Hf}$ data indicates that pelagic sediment is not involved in mixtures that produce Discovery or LOMU basalts. The question about which reservoirs are mixing with the ambient upper mantle to produce Discovery and LOMU anomaly basalts remains unresolved. Douglass et al. (1999) provide an isotope composition for this end-member which they call the LOMU end-member. It is a source with low $^{206}\text{Pb}/^{204}\text{Pb}$ and $^{143}\text{Nd}/^{144}\text{Nd}$ and high $^{207}\text{Pb}/^{204}\text{Pb}$ and $^{87}\text{Sr}/^{86}\text{Sr}$. While lower crustal or lithospheric xenoliths exhibiting this isotopic composition are elusive, there is some indication that the reservoir containing this end-member is lower crustal granulites (Kamenetsky et al. 2001).

CHAPTER 4

SUMMARY

This study demonstrates that hafnium isotope systematics in MORB can be used to study mantle mixing processes. Despite the similarity between the Lu-Hf and Sm-Nd isotope systems, ϵHf data often reveal information about mixing processes that is less apparent in ϵNd isotope space. This is because the range of ϵHf (-3 to +24) in MORB is larger than the range of ϵNd (-4 to +12). There are two causes for this larger range. First, Lu-Hf is fractionated more than Sm-Nd in mantle melting processes. This results in a larger range of Lu/Hf than Sm/Nd in the earth's reservoirs. Second, the half-life of ^{176}Lu is about $1/3$ that of ^{146}Sm . Thus, radiogenic ^{176}Hf is built up more rapidly than ^{143}Nd .

The present study of ϵHf in MORB shows that, despite the continual convective stirring experienced by the upper mantle, material in the earth's upper mantle is not well-mixed. Heterogeneities in the mantle are preserved on many length scales and in some cases, for long time periods. The 15,000 km long gradient of ϵHf in Atlantic NMORB clearly demonstrates that the Atlantic upper mantle is heterogeneous on a massive scale. Possible causes for this heterogeneity include ancient melting events or large-scale pollution of the Atlantic upper mantle. On the other end of the length scale spectrum, ϵHf - $^{206}\text{Pb}/^{204}\text{Pb}$ indicates that the Shona plume is internally heterogeneous.

ϵHf data from this study, together with previously collected isotope data, are incorporated into mixing models, which identify possible mixing components in the mantle. The upper mantle beneath the South Atlantic can be modeled as a three component mixture of unpolluted mantle with ancient pelagic sediment and ancient oceanic crust. The Shona plume can be modeled as a mixture of ancient oceanic crust with varying concentrations of ancient pelagic sediment. This heterogeneous plume is currently mixing with the ambient (polluted) South Atlantic mantle to produce Shona anomaly basalts. Further, ϵHf data indicate that pelagic sediment is not a component of the Discovery plume.

The mixing models developed in this study show that despite the zircon effect, when the concentration of pelagic sediment in a mixture is very low, ϵ_{Hf} cannot be used to confirm its presence. In these cases, other isotope ratios (like $^{206}\text{Pb}/^{204}\text{Pb}$) are better indicators of the presence of pelagic sediment. However, when the concentration of pelagic sediment in a mixture is larger than a few percent, $\epsilon_{\text{Hf}}-\epsilon_{\text{Nd}}$ systematics can be used to confirm the presence of pelagic sediment and to estimate its concentration.

The main focus of the present study is identification of heterogeneities in the mantle and assessment of the components, which mix to produce these heterogeneities. Thus, the conclusions are static; they indicate *what* is mixing, not *how* it is mixing. The next step in analysis of mantle mixing processes is to relate the observed isotope data to dynamic physical mixing models. In addition, it may be possible to determine the ages of heterogeneities using Pb isotope data.

TABLES

Table 2.1

Table 2.2

Table 2.3

Table 2.4

Table 2.5

Table 2.6

Table 2.7

Table 2.8

Table 2.9

Table 2.10

Table 2.11

Table 2.12

Table 2.13

Table 2.14

Table 2.15

Table 2.16

Table 2.1. $^{176}\text{Hf}/^{177}\text{Hf}$ for the global survey MORB

	Sample ID***		Lat. °N	Lon. °W	Depth (m)	$^{176}\text{Hf}/^{177}\text{Hf}^{\dagger}$	Error**	ϵHf	$(\text{La}/\text{Sm})_n$
Mayen	1 [†] EN026 16D-1g	d [‡]	73.41	-7.39	2623	0.283454	7	24.1	0.62
	EN026 16D-1g (repl)					0.283458	8	24.3	
	2 EN026 2D-1	e	71.41	7.49	890	0.283058	7	10.1	4.41
	3 TR139 25D-3g	d	69.15	16.22	1145	0.283317	8	19.3	0.45
Azores	4 TR138 6D-1Bg	d	50.04	28.93	3370	0.283429	9	23.2	0.65
	5 TR89 31D-1	e	39.63	29.71	1750	0.283097	9	11.5	
	6 TR123 5D-3g	d	32.62	39.87	2700	0.283342	8	20.2	0.50
Great Meteor	7 TR119 7D-1	e	35.33	34.90	2250	0.283022	9	8.8	3.42
Sierra Leone	8 RC2806 49D-1g	d	3.70	31.51	3737	0.283254	7	17.0	0.43
	9 RC2806 40D-3g	e	1.70	30.64	3515	0.283089	10	11.2	3.18
Depleted MAR 2S-7S	10 EN061 4D-1g	d	-4.27	12.20	2300	0.283269	8	17.6	0.50
St. Helena	11 RC16 3D-1	d	-12.90	14.73	2303	0.283235	9	16.4	0.61
	12 EN061 18D-1g	e	-15.46	13.26	2860	0.283032	6	9.2	3.49
	13 EN063 2D-5g	d	-21.50	11.82	3460	0.283188	11	14.7	0.44
Tristan	14 EN063 24D-5g	d	-30.98	13.46	3530	0.283137	12	12.9	0.64
	15 AII 107-7 14-77	e	-37.19	17.52	2399	0.283041	8	9.5	1.29
Discovery	16 EW9309 40D-1g	d	-44.41	15.91	3488	0.283242	7	16.6	0.76
	17 EW9309 25D-5g	e	-47.35	10.32	2032	0.282694	7	-2.8	1.01
	18 EW9309 07D-6g	e	-48.76	10.07	3217	0.282743	10	-1.0	3.01
Shona	19 EW9309 10D-3g	d	-49.25	8.14	3860	0.283187	8	14.7	0.64
	20 EW9309 19D-1g	e	-51.06	6.16	1743	0.282962	11	6.7	0.86
	EW9309 19D-1g (repl)					0.282956	8	6.5	
Galapagos	21 TR164 22D-1g	d	2.30	99.56	3215	0.283204	11	15.3	0.62
	22 TR164 26D-3g	e	1.90	90.95	2025	0.283027	8	9.0	2.76
	23 STD 7D-1	d	3.20	83.04	2600	0.283223	7	15.9	
Sala y Gomez	24 EN113 36D-1g	d	-22.68	114.51	2950	0.28324	8	16.6	0.65
	25 EN113 6D-1Ag	e	-26.81	112.64	2362	0.283074	7	10.7	1.92
	26 EN113 46D-2g	d	-28.72	112.73	2750	0.283128	8	12.6	0.66
Afar	27 V3307 58D-1	d	12.90	-49.36	1638	0.283309	12	19.0	0.88
	28 V3307 49D-1	e	12.04	-45.51	795	0.283008	9	8.3	4.37

[†] $^{176}\text{Hf}/^{177}\text{Hf}$ corrected to JMC 475 $^{176}\text{Hf}/^{177}\text{Hf} = 0.282160 \pm 0.000010$.

** Errors are reported as standard error where value listed is \pm the error on the last figure.

*** Samples are glass rims unless sample ID does not end in "g". Replicate analyses are denoted as repl.

[†] Numbers correspond to MORB locations on map in figure 2.1.

[‡] For each region, enriched (plume-like) basalts are denoted as "e" and depleted (DMM-like) basalts are denoted as "d".

Table 3.1. Hafnium isotope data for South Atlantic study

ID**	Latitude °S	Longitude °W	Depth (m)	$^{176}\text{Hf}/^{177}\text{Hf}^*$	Error**	ϵHf
107-7 07-3g	40.44	16.75	2612	0.283181	6	14.5
EW9309 45D-3g	40.59	16.77	3203	0.283104	16	11.7
EW9309 44D-3g	40.86	16.79	3067	0.283122	8	12.4
EW9309 44D-3g (repl.)				0.283118	8	12.4
All 107-7 06-20g	41.25	16.60	2394	0.283081	13	10.9
BM 1954 152	42.07	0.06	.	0.282812	6	1.4
EW9309 43D-1g	42.19	16.08	2925	0.283114	8	12.1
EW9309 43D-2g	42.19	16.08	2925	0.283128	7	12.6
All 107-7 04-4g	42.92	16.10	.	0.283165	7	13.9
EW9309 42D-1g	43.43	16.17	3449	0.282985	6	7.5
EW9309 41D-1g	44.02	16.08	3522	0.283191	8	14.8
EW9309 40D-1g	44.41	15.91	3488	0.283242	7	16.6
EW9309 37D-1g	45.23	15.07	3534	0.283037	6	9.4
EW9309 39D-1g	45.23	15.07	3534	0.283105	10	11.8
EW9309 36D-1g	45.57	14.71	3114	0.283128	7	12.6
EW9309 34D-1g	45.85	14.19	3443	0.283028	9	9.1
EW9309 33D-1g	45.99	14.08	3381	0.282954	7	6.4
All 107-7 02-53g	46.21	13.64	2699	0.283128	7	12.6
EW9309 32D-1g	46.23	13.55	3108	0.283102	9	11.7
EW9309 32D-2g	46.23	13.55	3108	0.283036	6	9.3
EW9309 31D-1g	46.39	13.45	2822	0.283024	8	8.9
EW9309 30D-1g	46.59	13.38	3153	0.283095	8	11.4
EW9309 28D-1g	46.90	13.45	3417	0.283178	7	14.4
EW9309 27D-2g	47.11	13.40	3081	0.283080	8	10.9
EW9309 25D-1g	47.35	10.32	2032	0.282700	7	-2.5
EW9309 25D-5g	47.35	10.32	2032	0.282694	7	-2.8
EW9309 26D-1g	47.35	13.40	3857	0.283114	8	12.1
EW9309 26D-2g	47.35	13.40	3857	0.283159	7	13.7
EW9309 02D-1g	47.55	10.18	2494	0.282891	6	4.2
EW9309 02D-3g	47.55	10.18	2494	0.282913	8	5.0
EW9309 03D-3g	47.80	10.15	2549	0.283038	9	9.4
EW9309 04D-2g	47.97	10.08	2895	0.282965	10	6.8
EW9309 04D-3g	47.97	10.08	2895	0.282994	7	7.9
EW9309 05D-5g	48.24	9.99	3453	0.282909	8	4.8
EW9309 06D-1g	48.55	10.17	3267	0.282811	11	1.4
EW9309 07D-1g	48.76	10.07	3218	0.282728	10	-1.6
EW9309 07D-2g	48.76	10.07	3218	0.282990	8	7.7
EW9309 07D-6g	48.76	10.07	3218	0.282743	10	-1.0
EW9309 08D-1g	48.96	9.97	3894	0.282979	7	7.3
EW9309 09D-1g	49.15	9.91	3892	0.282908	8	4.8
EW9309 09D-3g	49.15	9.91	3892	0.282971	8	7.0
EW9309 10D-3g	49.25	8.14	3860	0.283187	8	14.7
EW9309 10D-5g	49.25	8.14	3860	0.283158	8	13.7

Table 3.1 continued

Sample ID ^{***}	Latitude °S	Longitude °W	Depth (m)	$^{176}\text{Hf}/^{177}\text{Hf}$ [*]	Error ^{**}	ϵHf
EW9309 11D-1g	49.44	7.97	3868	0.283140	7	13.0
EW9309 12D-3g	49.76	8.03	3874	0.283152	7	13.4
EW9309 13D-1g	49.99	7.88	3555	0.283151	11	13.4
EW9309 14D-1g	50.27	7.06	3347	0.283133	6	12.8
EW9309 14D-4g	50.27	7.06	3347	0.283051	14	9.9
EW9309 24D-3g	50.46	6.53	3183	0.283086	6	11.1
EW9309 15D-1g	50.58	6.43	2980	0.283132	7	12.7
<i>EW9309 15D-1g (repl.)</i>				0.283116	8	12.7
EW9309 17D-1g	50.76	6.34	2943	0.283047	10	9.7
EW9309 18D-1g	51.05	6.20	1991	0.283024	8	8.9
EW9309 19D-1g	51.06	6.16	1743	0.282962	9	6.7
<i>EW9309 19D-1g (repl.)</i>				0.282956	9	6.7
EW9309 19D-3g	51.06	6.16	1743	0.283052	9	9.9
AG32-10-1	51.28	5.85	2025	0.282974	8	7.1
EW9309 20D-1g	51.43	5.78	1719	0.282980	7	7.4
AG32-9-1	51.62	5.60	1675	0.282997	7	8.0
EW9309 21D-1g	51.82	5.50	2025	0.282958	9	6.6
EW9309 23D-1g	52.16	5.34	2609	0.283027	7	9.0
AG32-7-1	52.27	4.83	3400	0.282997	7	8.0
EW9309 22D-3g	52.46	4.57	3059	0.283008	10	8.3
AG32-6-2g	52.65	4.38	2325	0.283042	7	9.5
AG32 5-1	52.98	4.33	1700	0.282999	13	8.0
AG32-4-111	54.03	2.30	2500	0.283097	9	11.5
AG32-3-99	54.12	1.97	2250	0.283098	8	11.5
AG32-2-3g	54.37	1.20	2250	0.283067	10	10.4

^{*}Data corrected to JMC-475 standard with $^{176}\text{Hf}/^{177}\text{Hf} = 0.282160 \pm 0.000010$.

^{**}Errors are reported as standard error where value listed is \pm the error on the last significant figure.

^{***}Samples are glass rims, unless the Sample ID does not end in "g". Replicates are denoted as repl.

Table 3.2. Ambient and normal upper mantle compositions

	Ambient Upper Mantle*	Normal Upper Mantle**
$^{206}\text{Pb}/^{204}\text{Pb}$	18	18.00
$^{207}\text{Pb}/^{204}\text{Pb}$	15.5	15.43
$^{208}\text{Pb}/^{204}\text{Pb}$	37.8	37.30
$^{87}\text{Sr}/^{86}\text{Sr}$	0.70250	.7022
$^{143}\text{Nd}/^{144}\text{Nd}$ (ϵNd)	0.51312 (9.4)	0.5133 (12.9)
$^{176}\text{Hf}/^{177}\text{Hf}$ (ϵHf)	0.28324 (16.6)	0.283358 (20.7)

*Ambient upper mantle is from Douglass et al. (1999) except for $^{176}\text{Hf}/^{177}\text{Hf}$, which is from this study.

**Normal upper mantle is from S.R. Hart (personal communication) and Hart et al. (1992) except for $^{176}\text{Hf}/^{177}\text{Hf}$ which is calculated from Hart et al.'s (1992) $^{143}\text{Nd}/^{144}\text{Nd}$ and the equation of the Hf-Nd mantle array (J. Blichert-Toft, personal communication): $\epsilon\text{Hf} = 1.37\epsilon\text{Nd} + 2.72$.

Table 3.3. DM, OC, SED isotope and trace element compositions

	OC 1.5Ga. altered crust	SED 1.5 Ga. pelagic sediment	DM Normal upper mantle	DM from R&H model ^{‡‡}
Rb [*]	1.3	65	0.091	
Ba	10	2000	1	
Th	0.187	11.3	0.0187	
U	0.082	1.85	0.0071	
Nb	3.51	24	0.351	
Pb	0.31	55	0.0489	
Nd	11.2	85	1.12	
Sr	113	300	11.3	
Sm	3.75	18	0.375	
Lu	0.589 ^{***}	1.375 ^{**}	0.0589 [†]	
Hf	2.974 ^{***}	3.8 ^{**}	0.2974 [†]	
⁸⁷ Sr/ ⁸⁶ Sr	0.703	0.7203	0.7022	0.7025
¹⁴³ Nd/ ¹⁴⁴ Nd	0.5129	0.5117	0.5133	.05132
²⁰⁶ Pb/ ²⁰⁴ Pb	22.4	16.7	18	18
²⁰⁷ Pb/ ²⁰⁴ Pb	15.92	15.44	15.43	15.43
²⁰⁸ Pb/ ²⁰⁴ Pb	41.7	36.8	37.3	37.7
¹⁷⁶ Hf/ ¹⁷⁷ Hf	0.28295 ^{††}	0.2826 [‡]	0.283358 ^{†††}	N/A

*Concentration data in ppm. Data from Rehkämper and Hofmann (1997) except the following.

**Lu and Hf concentrations in pelagic sediment are from Ben Othman et al. (1989).

***Lu and Hf concentrations in ancient oceanic crust are from present day NMORB values of Hofmann (1988).

†Lu and Hf concentrations in DM are 10% of these N-MORB values (after Rehkämper and Hofmann 1997).

††¹⁷⁶Hf/¹⁷⁷Hf of pelagic sediment is from a 2 stage model. During stage-1, which lasts until 1.5 Ga., ¹⁷⁶Lu/¹⁷⁷Hf is chondritic (0.0332). During stage-2 ¹⁷⁶Lu/¹⁷⁷Hf = 0.027 which is the average value for modern day pelagic sediments (Patchett et al. 1984).

†††¹⁷⁶Hf/¹⁷⁷Hf of DM is calculated from $\epsilon\text{Nd} = 12.9$ (Hart et al. 1992) and $\epsilon\text{Hf} = 1.37 \epsilon\text{Nd} + 2.72$ (J. Blichert-Toft, personal communication).

‡¹⁷⁶Hf/¹⁷⁷Hf of ancient oceanic crust is estimated from the composition HIMU basalts (Salters 1996, figure 1).

‡‡DM isotope data from R& H model is shown for comparison.

Table 3.4. ADM isotope and trace element compositions

	ADM Ambient upper mantle
Rb*	0.174395
Ba	2.4545
Th	0.031544
U	0.011068
Nb	0.48863
Pb	0.089424
Nd	1.56379
Sr	15.47085
Sm	0.517838
Lu	0.080536
Hf	0.404918
$^{87}\text{Sr}/^{86}\text{Sr}$ **	0.7025
$^{143}\text{Nd}/^{144}\text{Nd}$	0.51312
$^{206}\text{Pb}/^{204}\text{Pb}$	18
$^{207}\text{Pb}/^{204}\text{Pb}$	15.5
$^{208}\text{Pb}/^{204}\text{Pb}$	37.8
$^{176}\text{Hf}/^{177}\text{Hf}$	0.28324

*Trace element concentrations are in ppm and are calculated from a mixture of 96% DM, 3.94% OC and 0.06% SED.

**Isotope values are from Douglass et al. (1999) and this study.

Table 3.5. Isotope ratios for lower crust xenoliths compared to MORB

	Southern Africa- whole region average*	Std. Dev.*	Northern Lesotho region average*	Std. Dev.*	LT2*	Discovery basalt: EW9309 25D-5g**	LOMU basalt: EW9309 7D-1g**
$^{87}\text{Sr}/^{86}\text{Sr}$	0.7057	0.0019	0.70410	0.0005	0.707000	0.705878	0.705093
$^{143}\text{Nd}/^{144}\text{Nd}$	0.51215	0.00061	0.51250	0.00035	0.51176	0.512365	0.512489
$^{206}\text{Pb}/^{204}\text{Pb}$	16.8	1.0	17.1	0.4	17.25	18.187	17.77
$^{207}\text{Pb}/^{204}\text{Pb}$	15.3	0.3	15.6	0.1	15.58	15.6	15.6
$^{208}\text{Pb}/^{204}\text{Pb}$	36.8	1.0	37.1	0.4	37.18	38.7	38.2
$^{176}\text{Hf}/^{177}\text{Hf}$	N/A		N/A		N/A	0.282694	0.282728
No. of	23		10				

*Xenolith data from Huang et al. (1995) and Rogers and Hawkesworth (1982).

**Discovery and LOMU basalts are the most "plume-like" from each region. Data from Douglass et al. (1999) and this study.

FIGURES

Figure 1
[Faint text]

Figure 2
[Faint text]

Figure 3
[Faint text]

Figure 4
[Faint text]

Figure 5
[Faint text]

Figure 6
[Faint text]

Figure 7
[Faint text]

Figure 8
[Faint text]

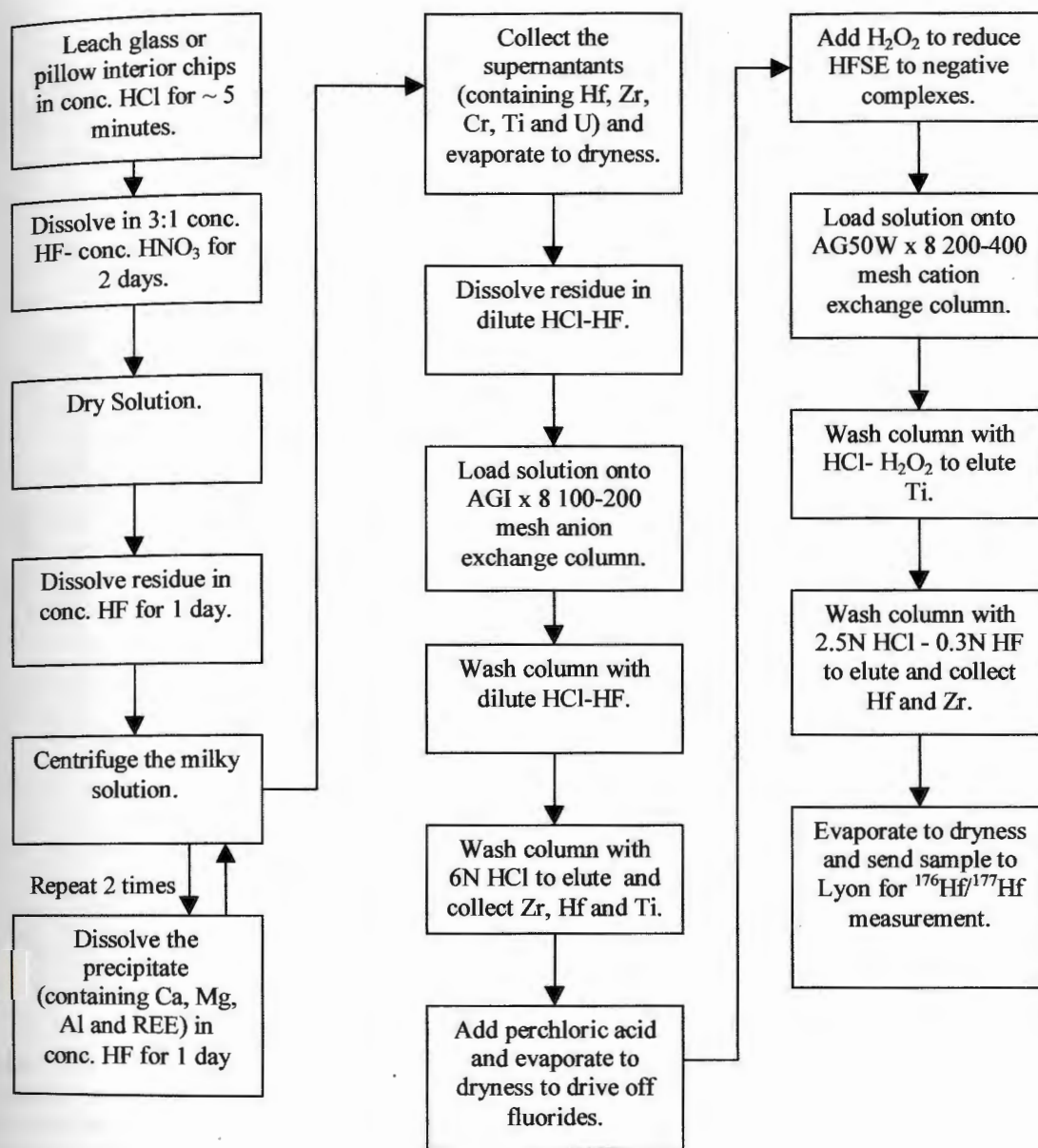


Figure 1.1. Procedure to separate Hf from the bulk rock. For more detailed procedure see Blichert-Toft et al. (1997).

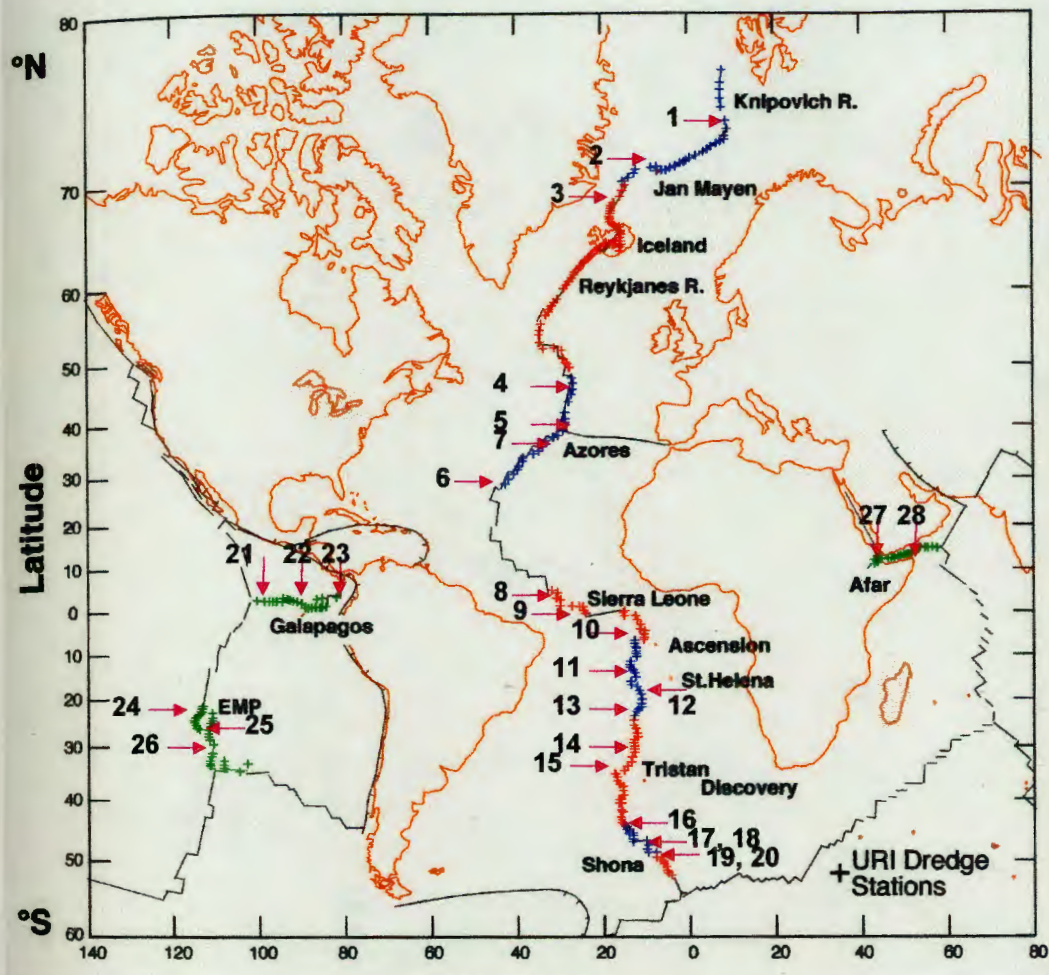


Figure 2.1. Global survey map. Locations of basalts included are indicated by the *pink arrows*. Numbers correspond to basalts listed in table 1. Data used to select basalts for the survey come from the following sources. Jan Mayen plume anomaly: Schilling et al. 1999; Azores plume anomaly: White and Schilling 1978, Yu et al. 1997; Great Meteor plume anomaly: Rideout and Schilling 1985; Sierra Leone plume anomaly and 2°S - 7°S region: Schilling et al. 1994; St. Helena and Tristan plume anomalies: Schilling et al. 1985, Humphris et al. 1985, Hanan et al. 1986, Fontignie and Schilling 1996; Discovery and Shona plume anomalies: Douglass et al. 1999; Galapagos plume anomaly: Schilling et al. 1982, Verma and Schilling 1982, Verma et al. 1983; Sala y Gomez plume anomaly: Kingsley and Schilling 1998; Afar plume anomaly: Schilling et al. 1992. Hf isotope data for Sala y Gomez plume is from a separate study being conducted at URI and by Blichert-Toft.

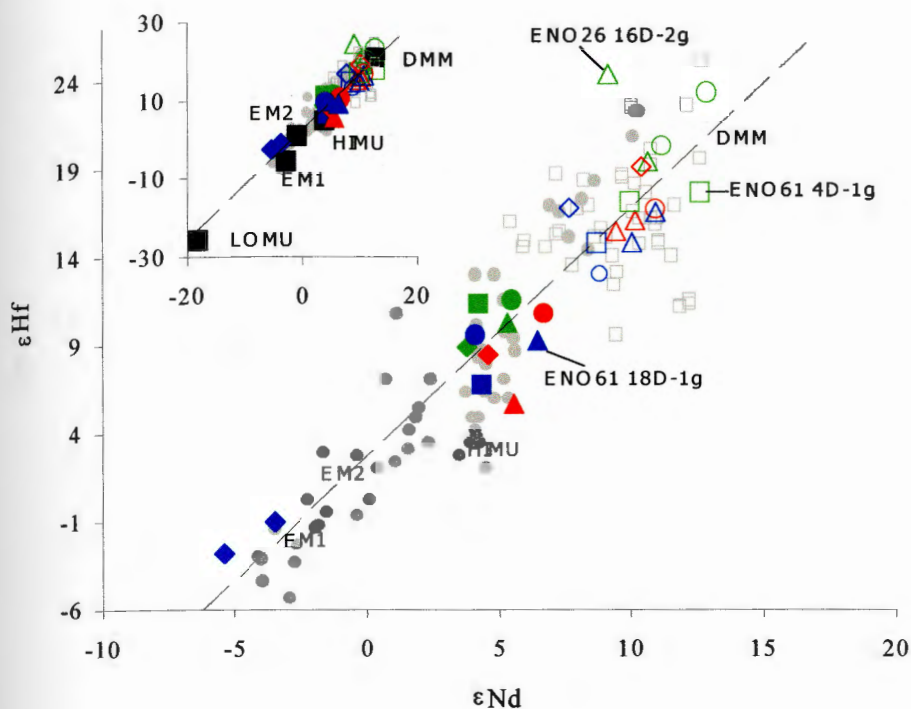


Figure 2.3. $\epsilon_{\text{Hf}}-\epsilon_{\text{Nd}}$ for global survey MORB. Symbols for basalts as in figure 2.2. *Grey filled circles*, published OIB; *grey open squares*, published MORB (Salters and White 1998, Salters 1996, Salters and Hart 1991, and references therein). Mantle end-members of Zindler and Hart (1986) and Hart et al. (1992) are labeled. EM1 is represented by the most enriched Walvis Ridge basalts (Salters and Hart 1991). EM2 is represented by the most enriched basalts from Samoa and Societies (Patchett 1980b, Salters and Hart 1991). HIMU is represented by St. Helena basalts (Hart et al. 1986, Salters and Hart 1991). LOMU is taken from the composition of S18-60/1 (Kamenetsky et al. 2001, Kamenetsky personal communication). DMM taken from ϵ_{Nd} of Hart et al. (1992) (12.9) and the equation for the mantle array. *Dashed line* is $\epsilon_{\text{Nd}}-\epsilon_{\text{Hf}}$ mantle array based on data from 1258 published and unpublished oceanic basalts (Blichert-Toft personal communication): $\epsilon_{\text{Hf}} = 1.4 \epsilon_{\text{Nd}} + 2.7$, $r^2 = 0.81$. (Alternately, DMM could have been taken from ENO61 4D-1g which is from the very depleted region between 2°S-7°S on the MAR with $\epsilon_{\text{Hf}} = 17.6$ and $\epsilon_{\text{Nd}} = 12.6$. (this study, Schilling et al. 1994)). Basalts ENO26 16D-2g and ENO61 18D-1g are discussed in the text. All Hf data is corrected to JMC 475 $^{176}\text{Hf}/^{177}\text{Hf} = 0.282160 \pm 0.000010$.

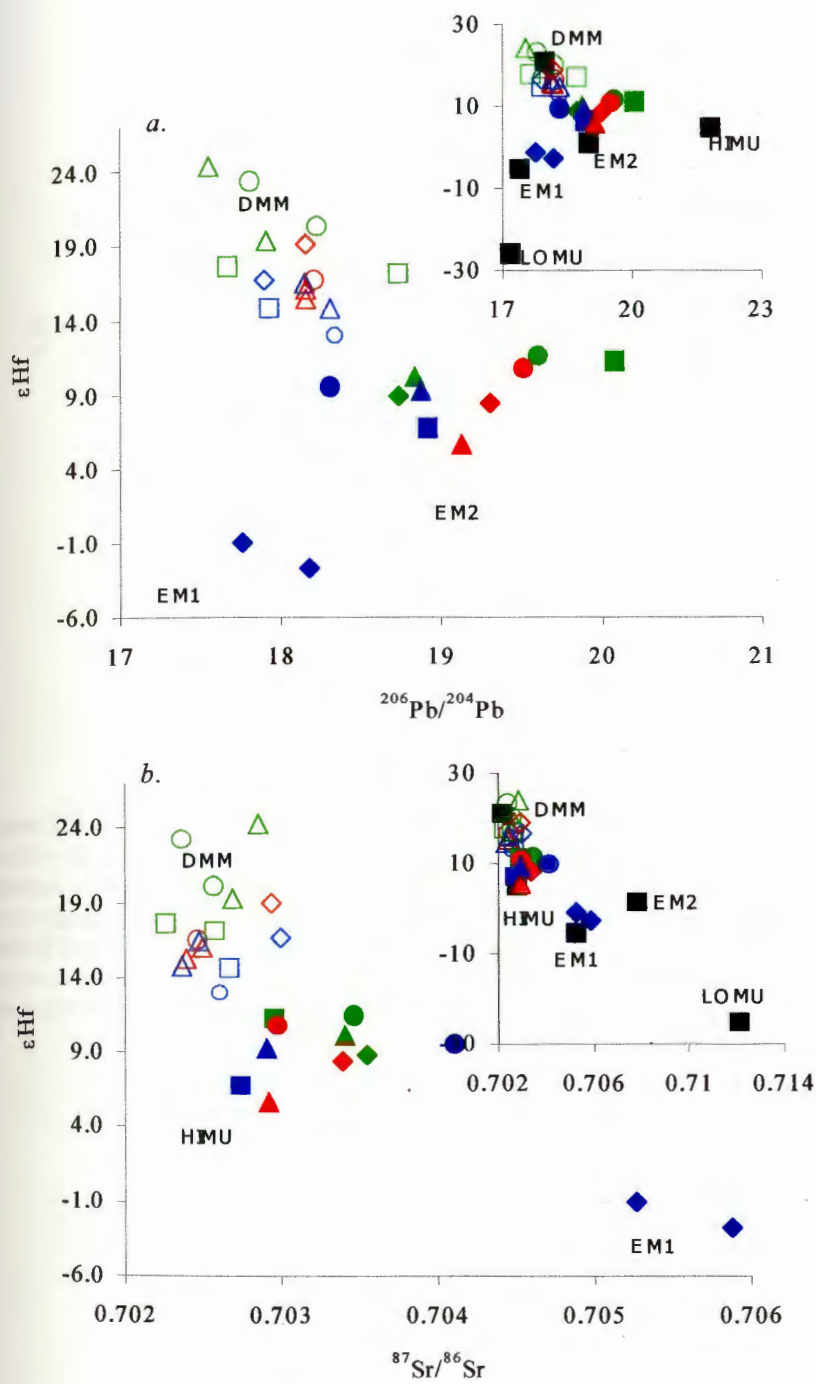


Figure 2.4. ϵ_{Hf} versus $^{206}\text{Pb}/^{204}\text{Pb}$ and $^{87}\text{Sr}/^{86}\text{Sr}$ for global survey MORB. Symbols as in figure 2.2.

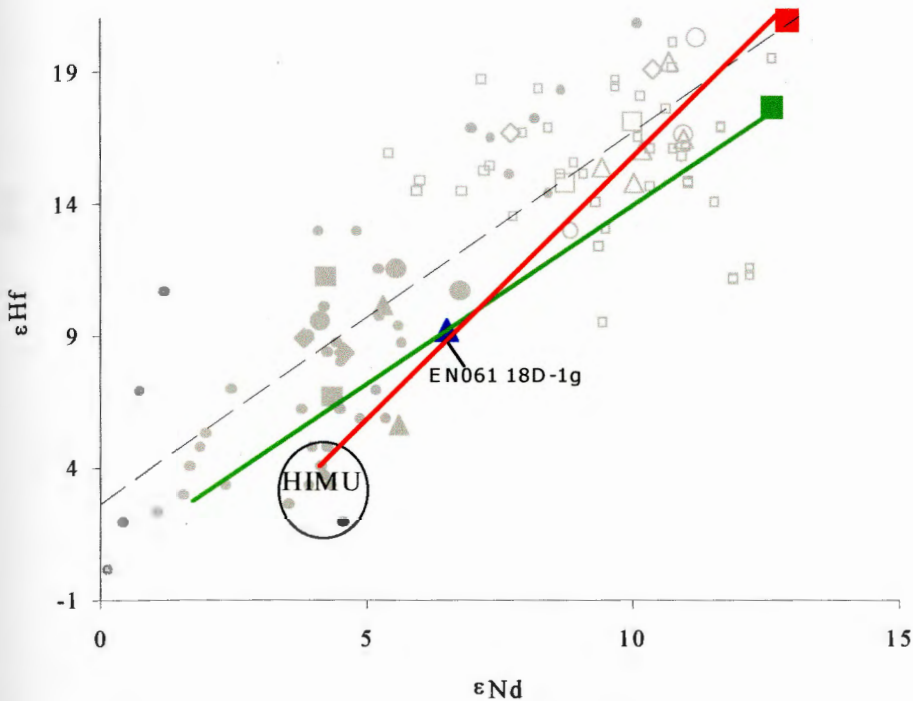


Figure 2.5. Estimate of ϵ_{Hf} for DMM. Two possible DMM compositions are shown. The *red square* is $\epsilon_{\text{Hf}} = 20.8$ and $\epsilon_{\text{Nd}} = 12.9$. This estimates ϵ_{Hf} of DMM by using ϵ_{Nd} of Hart et al. (1992) and the equation of the mantle array. The *green square* is a DMM composition based on EN061 4D-1g from the depleted 2°S - 7°S MAR ($\epsilon_{\text{Hf}} = 17.6$ and $\epsilon_{\text{Nd}} = 12.6$). The *solid lines* represent mixing lines from each of these DMM compositions through EN061 18D-1g which is from the St. Helena anomaly. The red point is a better estimate of DMM since its mixing line intersects the HIMU OIB field. The *dashed line* is the mantle array.

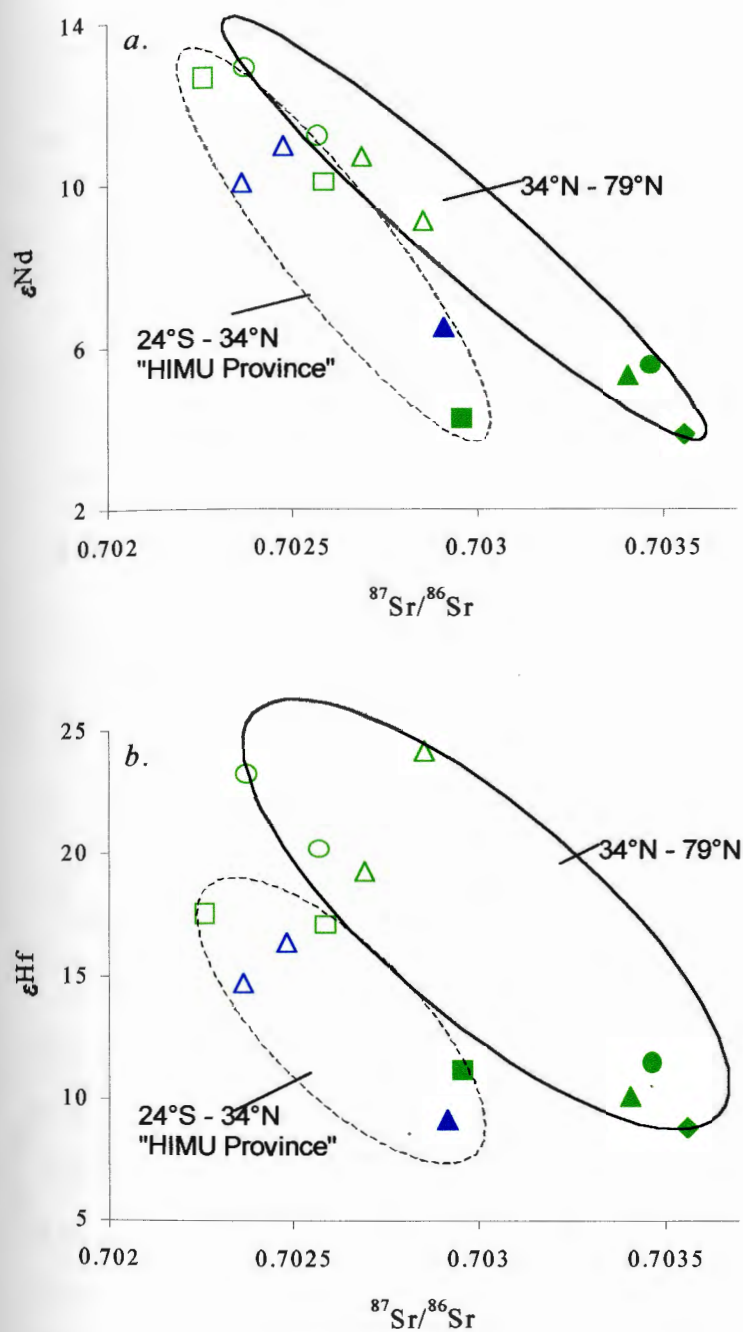


Figure 2.6. Atlantic MORB populations from 24°S to 79°N. *Dashed oval*, southern region (24°S - 34°N). This includes basalts influenced by Sierra Leone, Circe and St. Helena plume and the 14°N anomaly. This is the "HIMU region". *Solid oval*, northern region (34°N - 79°N). This includes basalts influenced by Jan Mayen, Azores and Great Meteor plumes. *Open symbols* are NMORB. *Closed symbols* are EMORB. *Green triangles*- Jan Mayen; *green circles*- Azores; *green diamond*- Great Meteor; *green squares*- Sierra Leone; *blue triangles*- St. Helena.

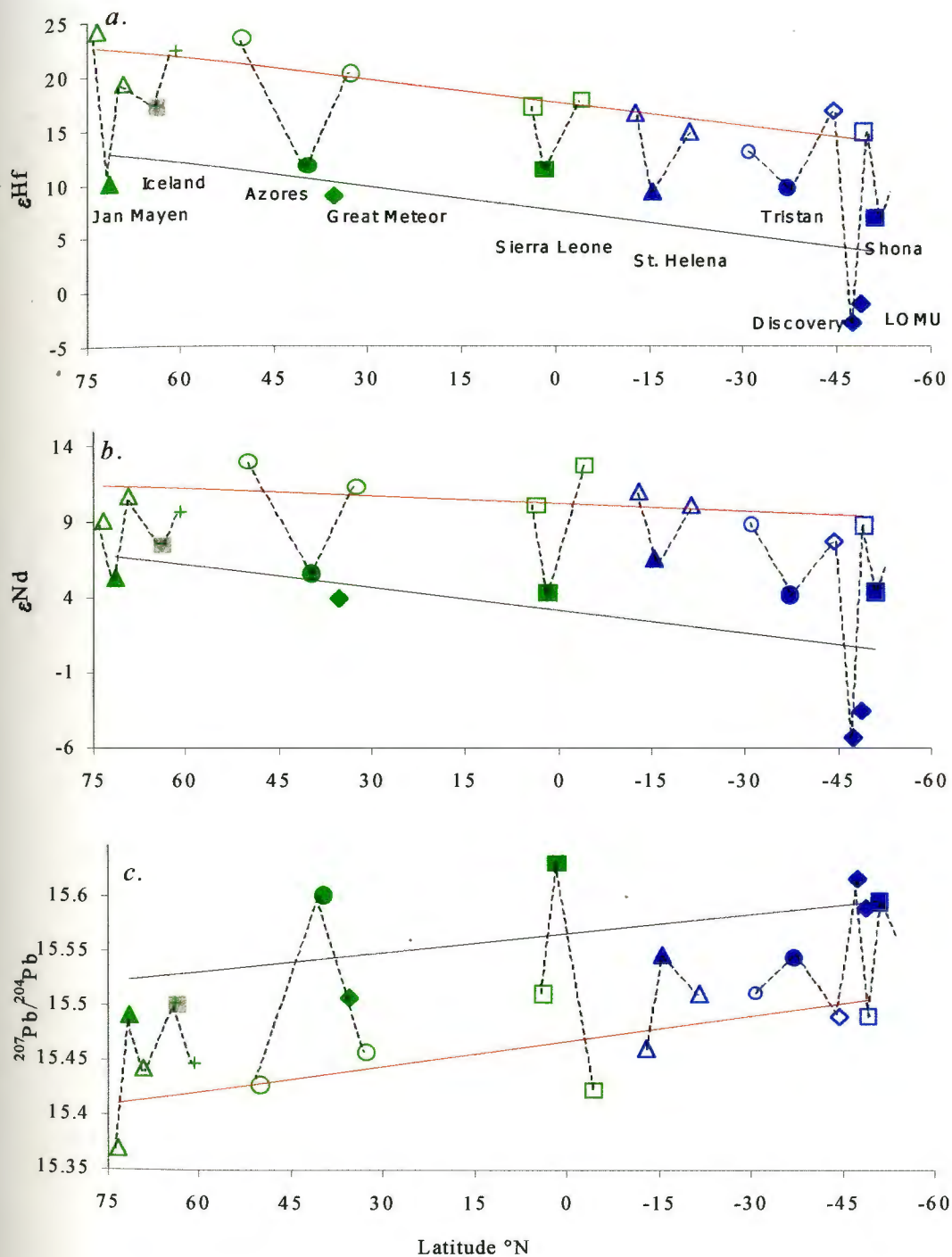


Figure 2.7. Atlantic MORB isotope profiles. *Filled symbols*, plume-influenced Atlantic MORB (EMORB); *open symbols*, Atlantic MORB not influenced by plumes (NMORB). *Red line*, regression line through the NMORB population. *Black line*, regression line through EMORB population.

Figure and caption continued on next page .

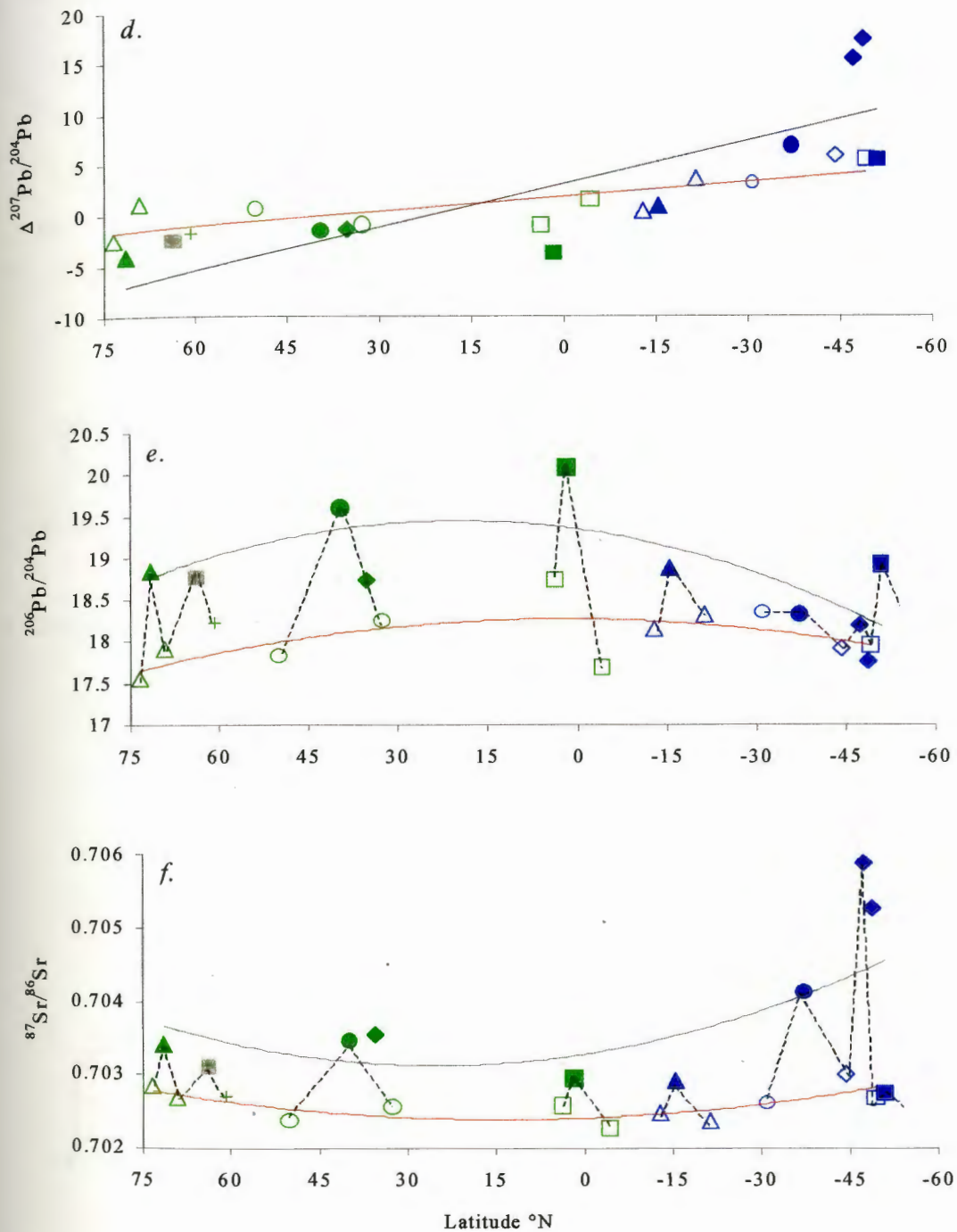
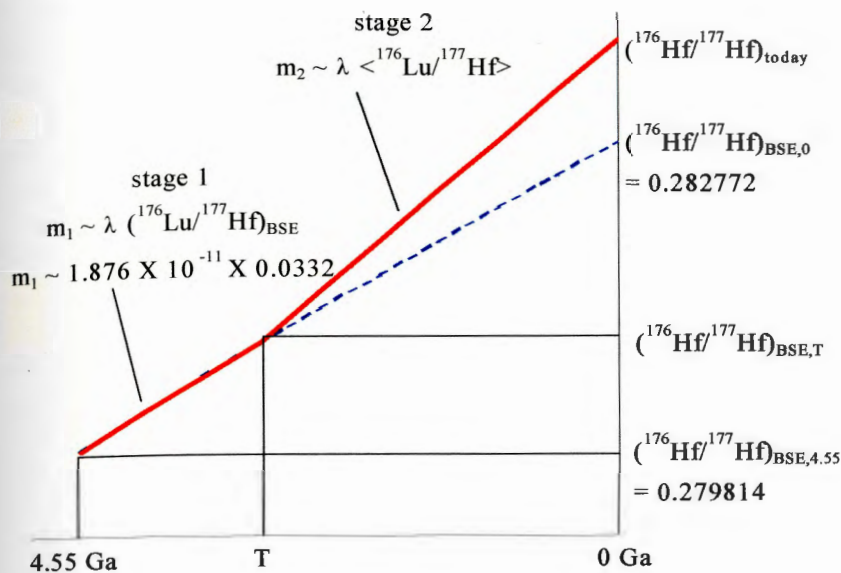


Figure 2.7. Continued from previous page.

Work around Iceland is still in progress at URI. In order to include MORB near all major Atlantic plumes in the Atlantic profile, an Iceland EMORB (grey square with green cross) and NMORB (green cross) from the literature are included. For these two MORB Hf data is from Patchett 1980, corrected to the current JMC 475 value and Pb isotope data is from Sun et al. 1975.

a. Discrete melting



b. Continuous melting

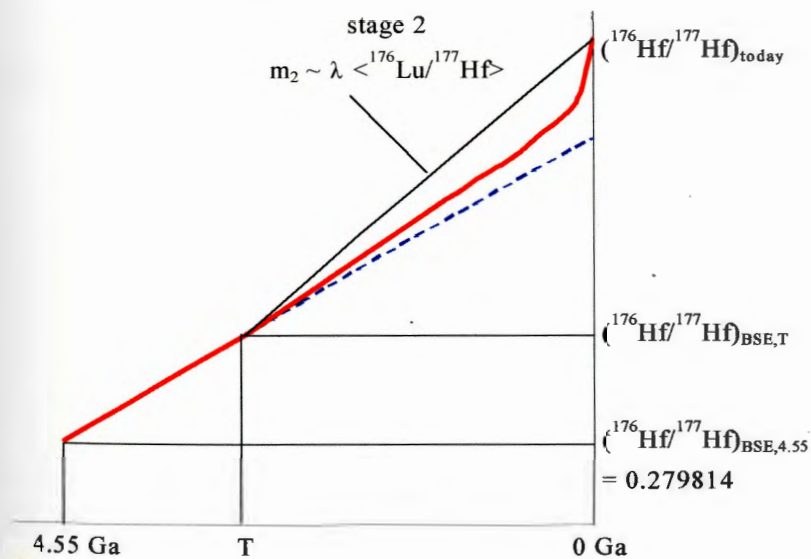


Figure 2.8. Two-stage ${}^{176}\text{Hf}/{}^{177}\text{Hf}$ evolution of the upper mantle. 2.8a. shows a discrete melting event at time T while 2.8b. shows continuous melting beginning at time T. The red lines show the isotopic evolution of the upper mantle. In both cases $\langle {}^{176}\text{Lu}/{}^{177}\text{Hf} \rangle$ for stage two is proportional to the slope of the line connecting $({}^{176}\text{Hf}/{}^{177}\text{Hf})_{\text{BSE},T}$ to $({}^{176}\text{Hf}/{}^{177}\text{Hf})_{\text{today}}$. Dashed line shows the evolution of a reservoir with Bulk Silicate Earth ${}^{176}\text{Lu}/{}^{177}\text{Hf}$ (0.0332) for comparison.

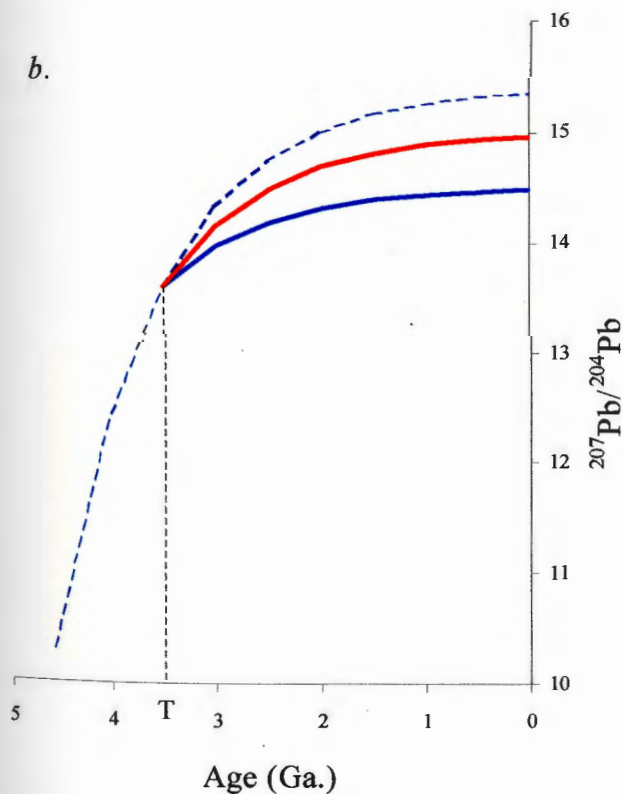
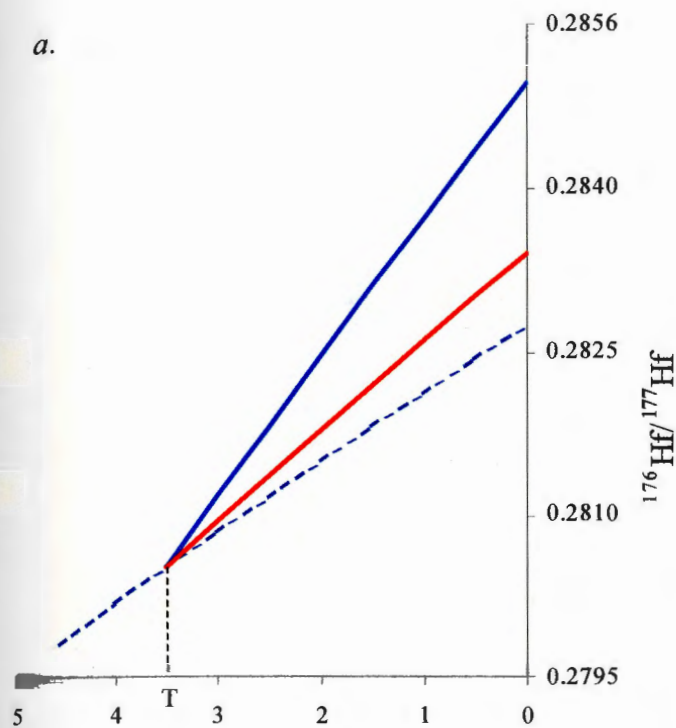


Figure 2.9. Model 1a: decrease in $\langle F \rangle$ from north to south for a constant T . *Blue lines* represent evolution of the Atlantic upper mantle in the north. *Red lines* show evolution of the Atlantic upper mantle in the south. *Dashed lines* show evolution of a reservoir with Bulk Silicate Earth parent-daughter ratios.

A decrease in the average, time-weighted, mean degree of melting, $\langle F \rangle$, from north to south causes a decrease in $\langle ^{176}\text{Lu}/^{177}\text{Hf} \rangle$ from north to south and thus a decrease in $^{176}\text{Hf}/^{177}\text{Hf}$ from north to south (figure 2.9a). The same applies to the Sm-Nd system.

This decrease in $\langle F \rangle$ from north to south leads to an increase in $^{207}\text{Pb}/^{204}\text{Pb}$ from north to south (figure 2.9b).

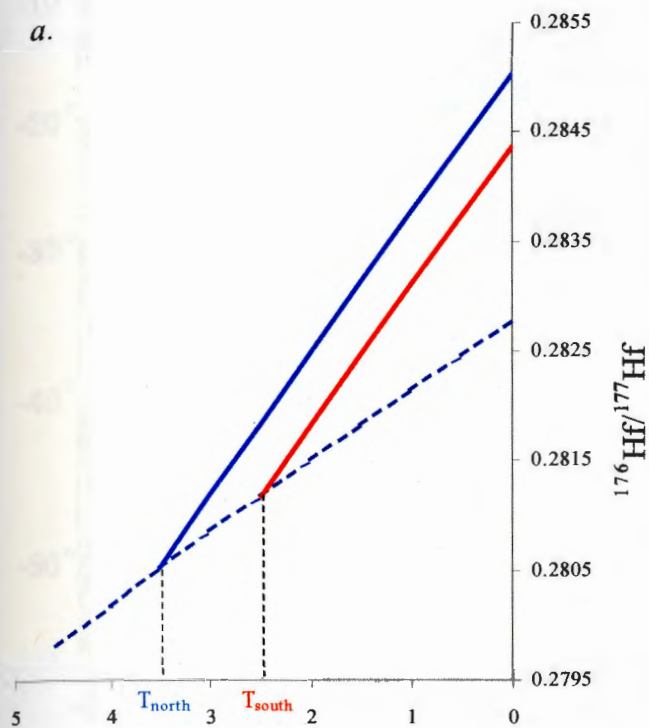
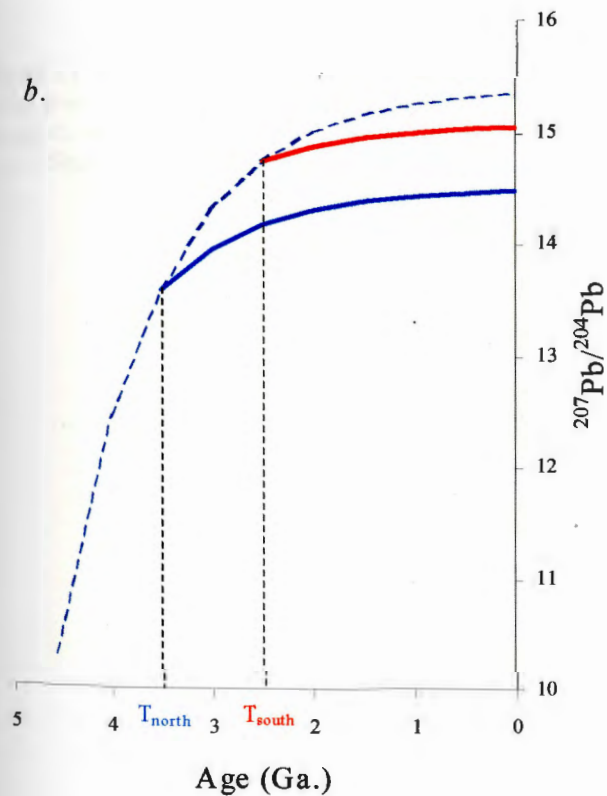


Figure 2.10. Model 1b: decrease in age of melting, T , from north to south. *Blue lines* represent evolution of the Atlantic upper mantle in the north. *Red lines* show evolution of the Atlantic upper mantle in the south. *Dashed lines* show evolution of a reservoir with Bulk Silicate Earth parent-daughter ratios.

Melting which begins earlier in the north than in the south leads to a decrease in $^{176}\text{Hf}/^{177}\text{Hf}$ (and $^{143}\text{Nd}/^{144}\text{Nd}$) from north to south (figure 2.10a). This decrease in T , also leads to and increase of $^{207}\text{Pb}/^{204}\text{Pb}$ from north to south (figure 2.10b).



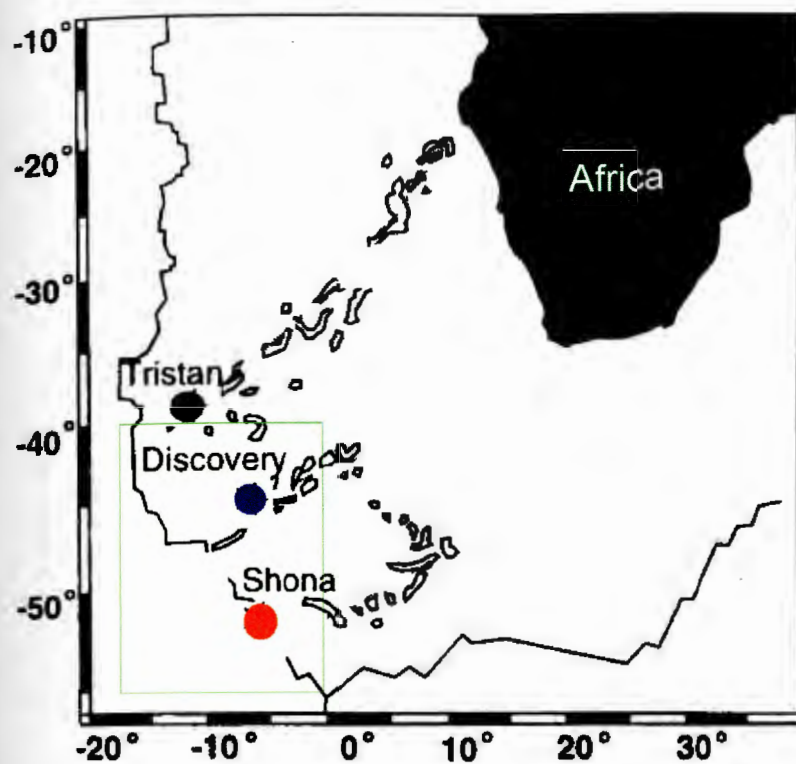


Figure 3.1. South Atlantic map. Map shows the South Atlantic study area (40°S - 55°S along the MAR) in the green rectangle. The Bouvet triple junction (where the MAR, SWIR and AAR come together) is just south of the study area. Black circle, Tristan da Cunha hotspot; blue circle, Discovery hotspot; red circle, Shona hotspot. Hotspot tracks are also shown. Based on figure 10 of Douglass et al. (1999).

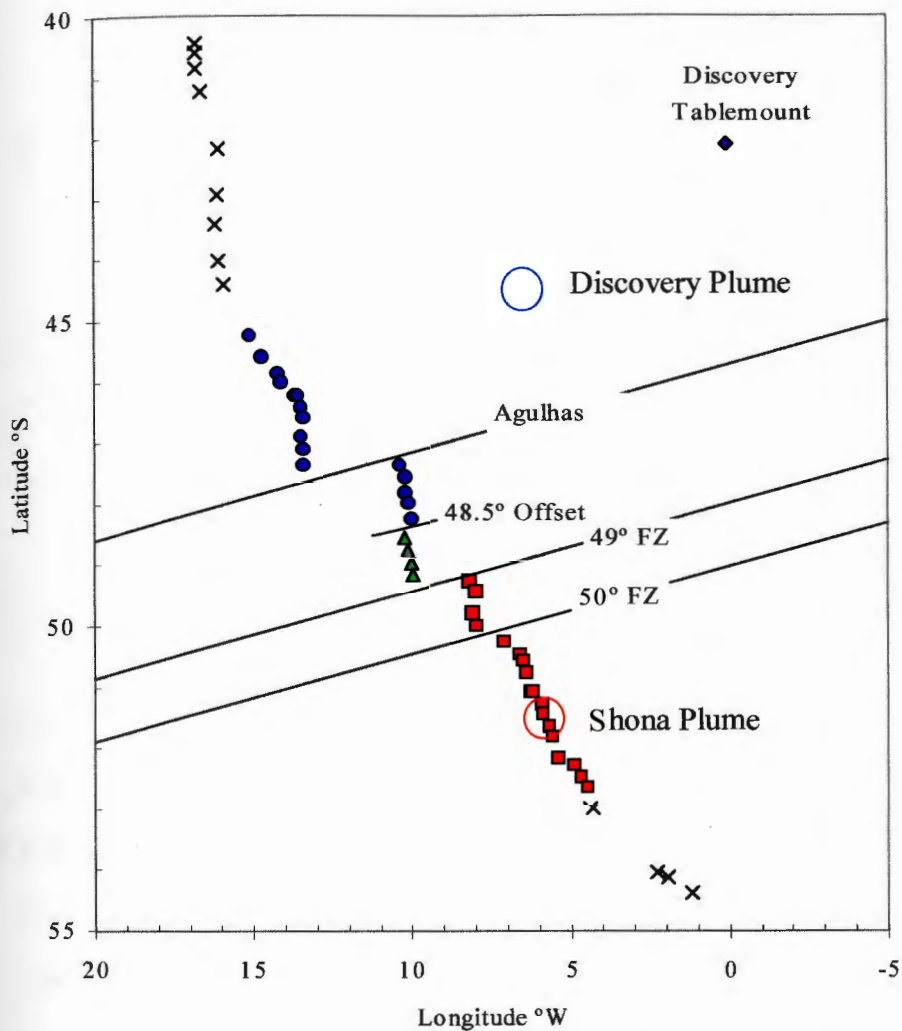


Figure 3.2. Dredge station locations in the South Atlantic. *Blue circles*, Discovery anomaly basalts; *blue diamond*, Discovery Tablemount; *green triangles*, LOMU section basalts; *red squares*, Shona anomaly basalts; *black Xs*, all other basalts included in study, *open blue circle*, Discovery plume, *open red circle*, Shona plume.

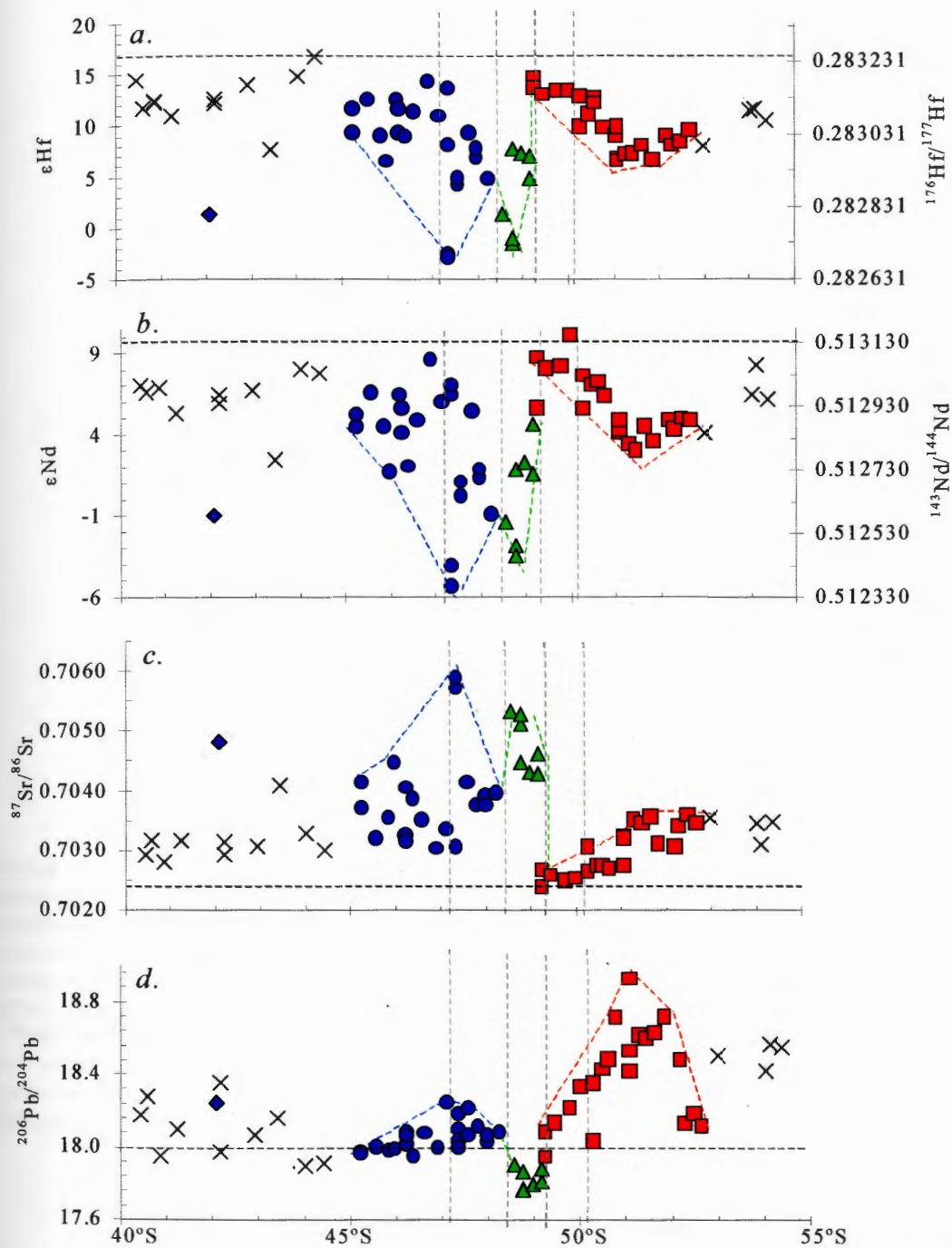


Figure 3.3. Isotope profiles for South Atlantic basalts. *a*, ϵ_{Hf} - latitude; *b*, ϵ_{Nd} - latitude; *c*, $^{87}\text{Sr}/^{86}\text{Sr}$ - latitude; *d*, $^{206}\text{Pb}/^{204}\text{Pb}$ - latitude. Baseline isotope values for ambient South Atlantic mantle are shown with horizontal black dashed lines. Blue circles, Discovery anomaly basalts; blue diamond, Discovery Tablemount; green triangles, LOMU section basalts; red squares, Shona anomaly basalts; black Xs, all other basalts included in study. Grey dashed lines, fracture zones: Agulhas FZ, 48.5° Offset, 49° FZ and 50° FZ. ϵ_{Hf} errors in *a* are smaller than symbols.

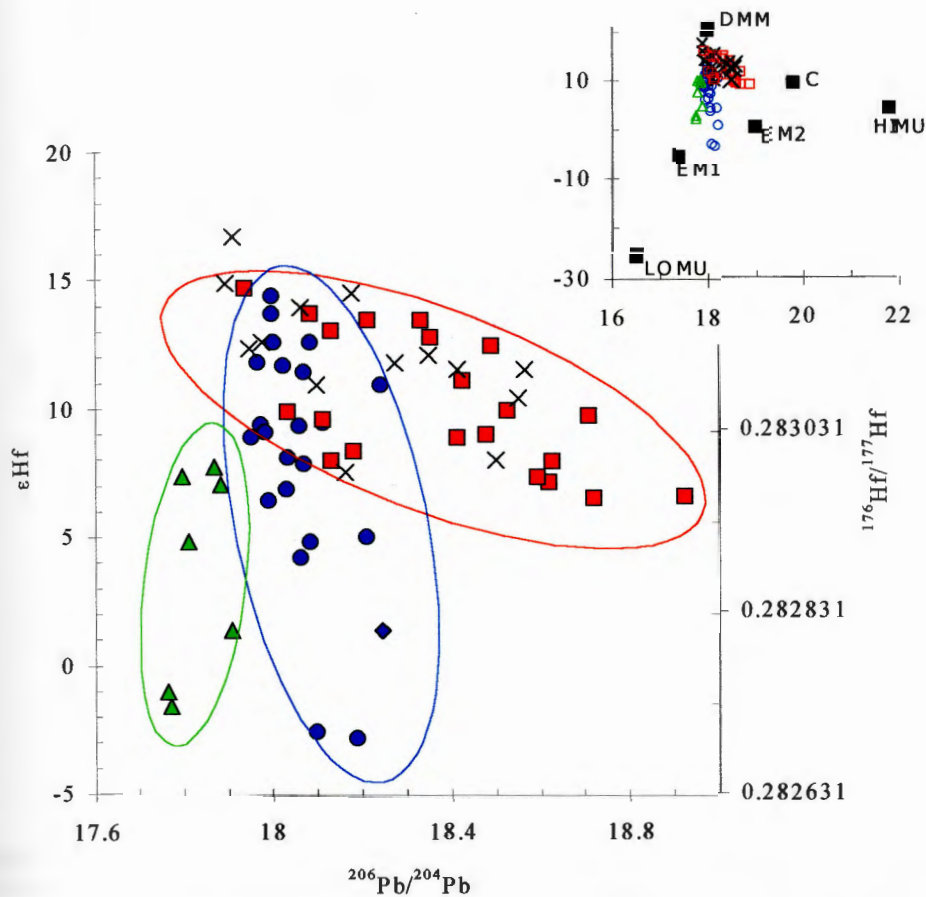


Figure 3.4. $\epsilon_{\text{Hf}} - {}^{206}\text{Pb}/{}^{204}\text{Pb}$ for South Atlantic basalts. *Blue circles*, Discovery anomaly basalts; *blue diamond*, Discovery Tablemount; *green triangles*, LOMU section basalts; *red squares*, Shona anomaly basalts; *black Xs*, all other basalts included in study. Ellipses are to group the data. Inset shows data relative to mantle end-members discussed in chapter 2. C composition is based on Hanan and Graham (1996) with ϵ_{Hf} calculated from their ϵ_{Nd} and the equation for the mantle array. For EM1, EM2, HIMU and DMM ${}^{206}\text{Pb}/{}^{204}\text{Pb}$, ${}^{87}\text{Sr}/{}^{86}\text{Sr}$ and ϵ_{Nd} are from Hart et al (1992) and ${}^{207}\text{Pb}/{}^{204}\text{Pb}$ and ${}^{208}\text{Pb}/{}^{204}\text{Pb}$ are from Hart (personal communication). For EM1, EM2 and HIMU ϵ_{Hf} is from Salters and White (1998). For DMM ϵ_{Hf} is from ϵ_{Nd} and the equation of the mantle array (Blichert-Toft personal communication). LOMU composition is from basalt S18-60/1 reported in Kamenetsky et al. (2001) except for ϵ_{Hf} which is from Kamenetsky (personal communication).

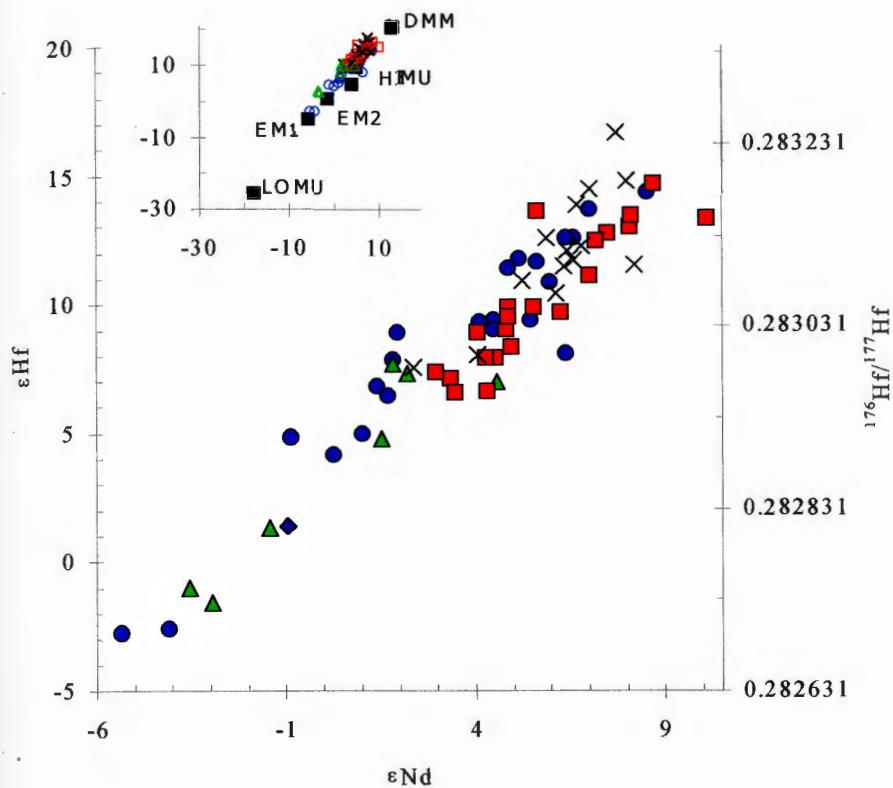


Figure 3.5. $\epsilon_{\text{Hf}} - \epsilon_{\text{Nd}}$ for South Atlantic basalts. *Blue circles*, Discovery anomaly basalts; *blue diamond*, Discovery Tablemount; *green triangles*, LOMU section basalts; *red squares*, Shona anomaly basalts; *black Xs*, all other basalts included in study. Inset shows data relative to mantle end-members discussed in chapter 2. See caption in figure 3.4 for sources.

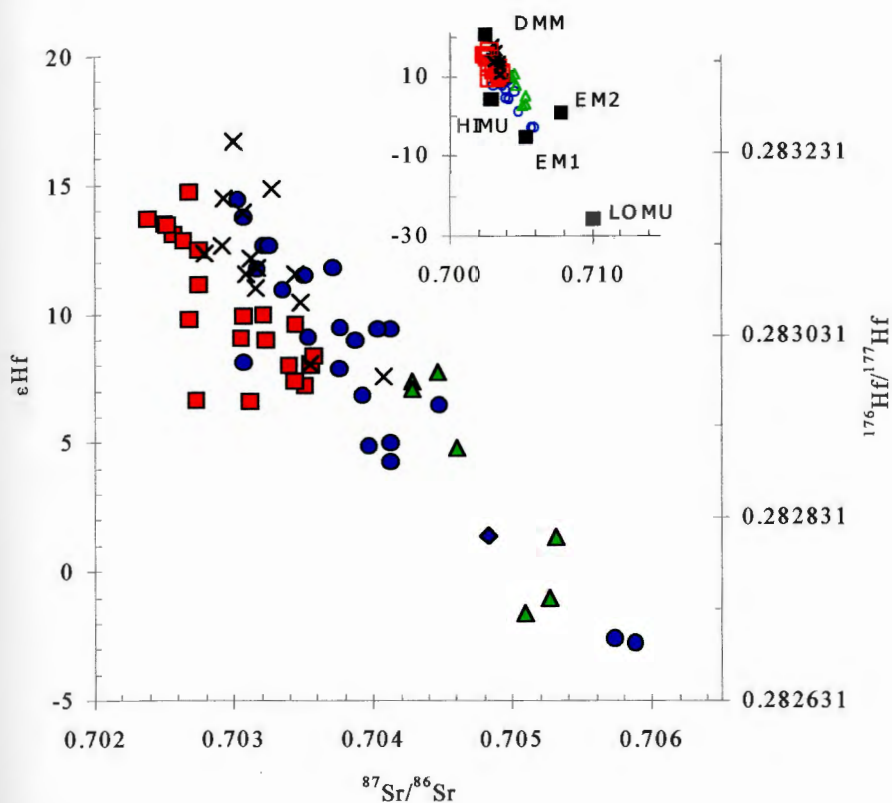


Figure 3.6. $\epsilon_{\text{Hf}} - {}^{87}\text{Sr}/{}^{86}\text{Sr}$ for South Atlantic basalts. *Blue circles*, Discovery anomaly basalts; *blue diamond*, Discovery Tablemount; *green triangles*, LOMU section basalts; *red squares*, Shona anomaly basalts; *black Xs*, all other basalts included in study. Inset shows data relative to mantle end-members discussed in chapter 2. See caption in figure 3.4 for sources.

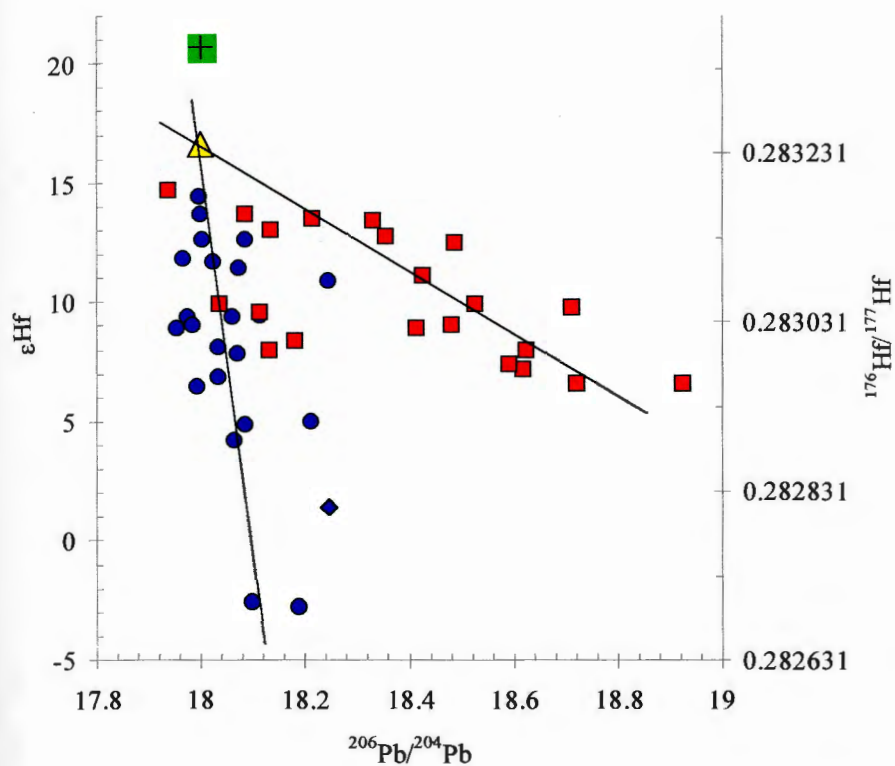


Figure 3.7. ϵ_{Hf} of South Atlantic ambient upper mantle. *Yellow triangle*, ambient upper mantle composition (ADM) determined from the intersection of Shona and Discovery trends. *Blue circles*, Discovery anomaly basalts; *blue diamond*, Discovery Tablemount; *red squares*, Shona anomaly basalts; *green square with +*, normal upper mantle composition (DM). ϵ_{Hf} of normal upper mantle is calculated from the equation of mantle array: $\epsilon_{\text{Hf}} = 1.37\epsilon_{\text{Nd}} + 2.72$ (Janne Blichert-Toft, personal communication) using ϵ_{Nd} for normal upper mantle from Hart et al. (1992).

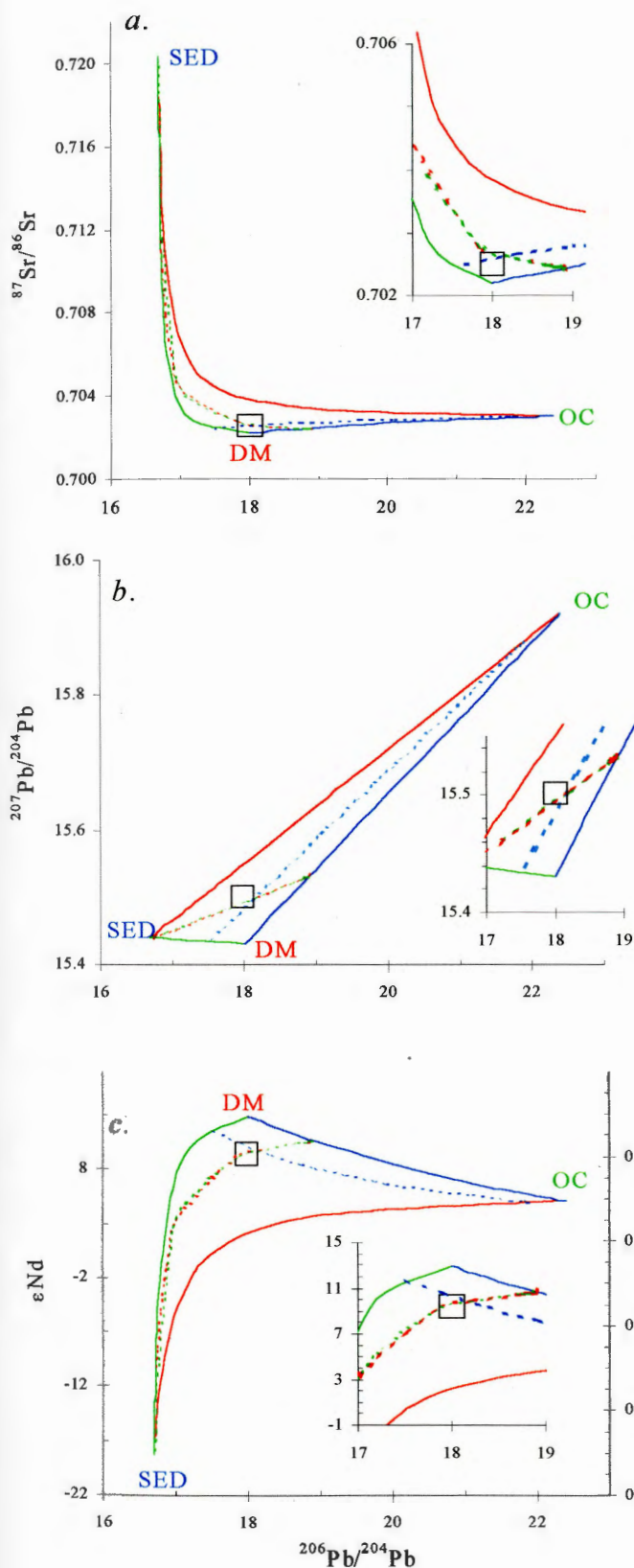


Figure 3.8. DM-OC-SED mixtures to generate ADM. DM is normal upper mantle. OC is altered subducted 1.5Ga. oceanic crust. SED is 1.5 Ga. subducted pelagic sediment. See table 3.3 for component compositions. *Blue solid line*, DM-OC binary; *red solid line*, OC-SED binary; *green solid line*, DM-SED binary. These three binaries bound the area of allowable 3 component mixtures. *Open square*, observed composition of ambient upper mantle (ADM) from Douglass et al. (1999) and this study. See table 3.2. for composition of ADM. Dashed lines show compositions of mixtures where the proportion of one end-member is held constant as the proportions of the other two end-members vary. *Red dashed line*, constant proportion of DM = 96%; *green dashed line*, constant proportion of OC = 3.94%; *blue dashed line*, constant proportion of SED = 0.06%. These lines intersect at the composition of ADM and thus successfully reproduce observed ADM composition.

Figure continued on next page.

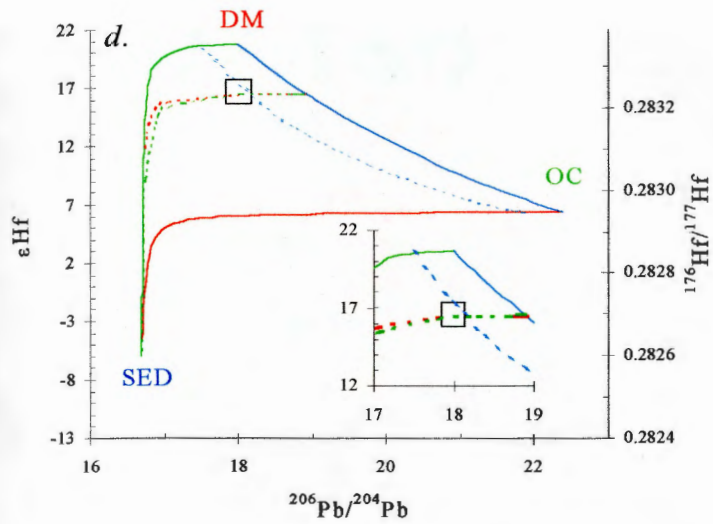


Figure 3.8. Continued from previous page.

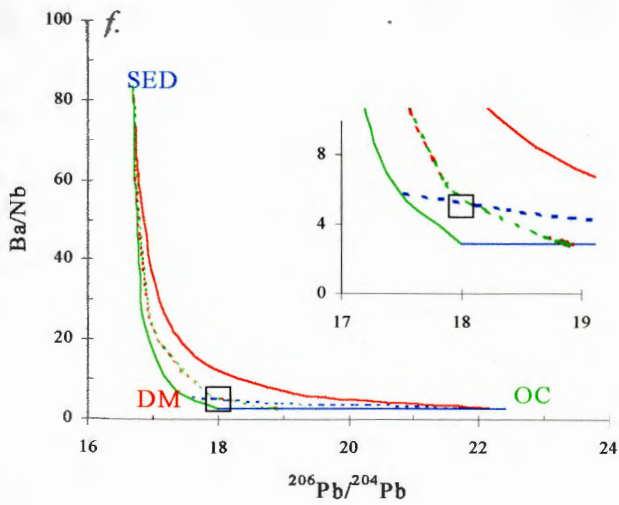
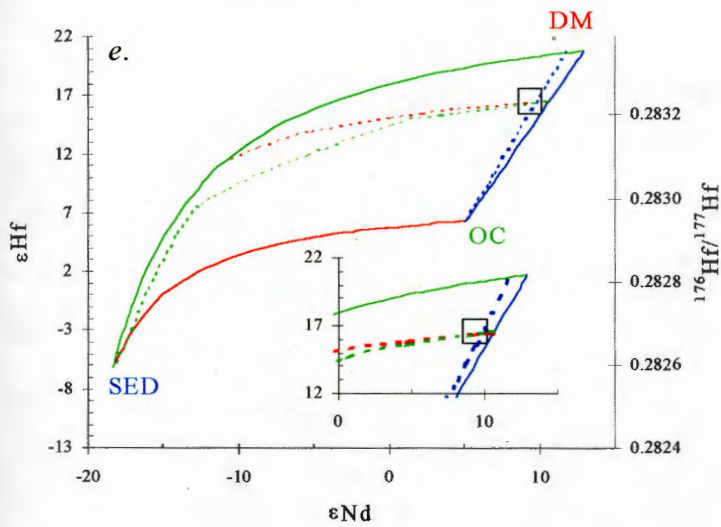




Figure 3.9. Plume - upper mantle mixing models. Figure shows views along ridge axis. *a*, homogeneous plume (*red*) mixing with upper mantle (*grey*) that contains passive heterogeneities (*yellow*) embedded in it. MORB are produced by 3 component mixing of plume, ambient upper mantle and embedded heterogeneities. As pictured here, the proportion of heterogeneities involved in mixing to produce MORB increases to the right. *b* heterogeneous plume (*red, orange and yellow*) mixing with homogeneous ambient upper mantle (*grey*). MORB are produced by binary mixing of sections of the heterogeneous plume with the upper mantle.

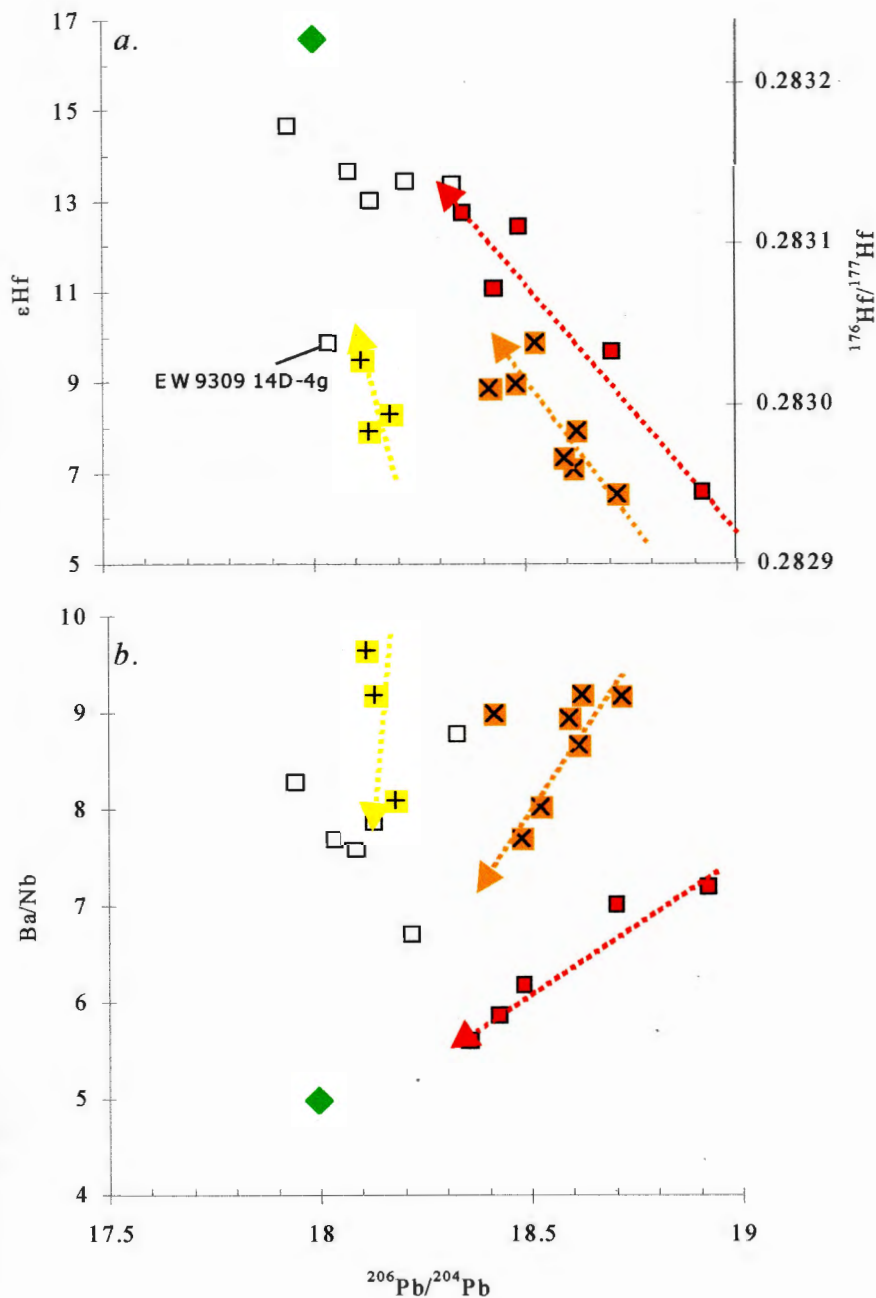


Figure 3.10. ϵ_{Hf} and Ba/Nb - $^{206}\text{Pb}/^{204}\text{Pb}$ for Shona segmentation. *Open squares*, segment 1; *red squares*, segment 2; *orange squares with Xs*, segment 3; *yellow squares with +s*, segment 4; *green diamond*, ambient upper mantle. Arrows show that the isotope trends converge on the ambient upper mantle composition. Segment 1 basalts lie along same trend as segment 2 basalts in *a* but not in *b*. This indicates a recent decoupling of isotope ratios and trace element concentrations, possibly due to melting of the Shona plume as it flows along the MAR. EW9309 14D-4g is discussed in the appendix.

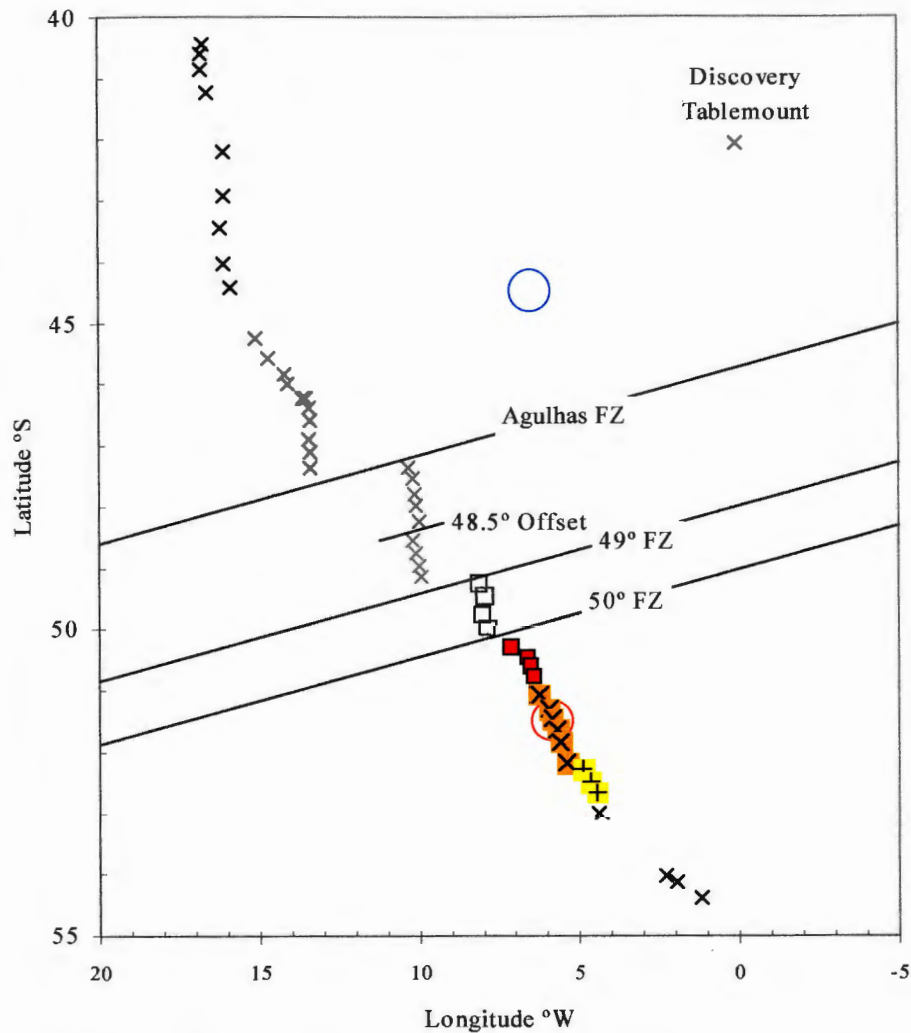


Figure 3.11. Map of Shona anomaly segmentation: . *Open squares*, segment 1 (49.25°S - 49.99°S); *red squares*, segment 2 (50.27°S - 51.06°S); *orange squares with Xs*, segment 3 (51.05°S - 52.16°S); *yellow squares with +'s*, segment 4 (52.27°S - 52.65°S); *grey Xs*, all other South Atlantic samples.

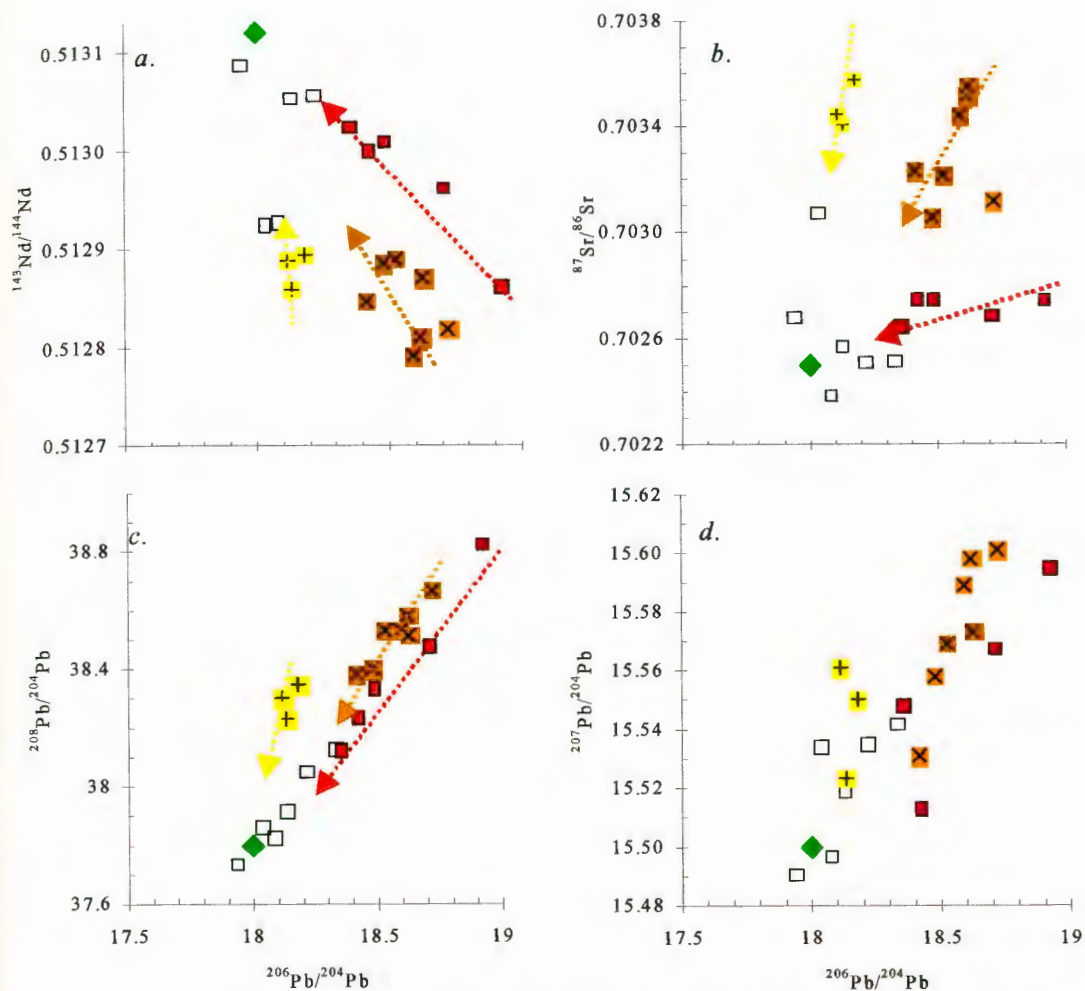


Figure 3.12. Isotope-isotope plots for Shona segmentation. *Open squares*, segment 1; *red squares*, segment 2; *orange squares with Xs*, segment 3; *yellow squares with +'s*, segment 4; *green diamond*, ambient upper mantle. Arrows show that the isotope trends converge on the ambient upper mantle composition except in *d* where different trends are not discernable.

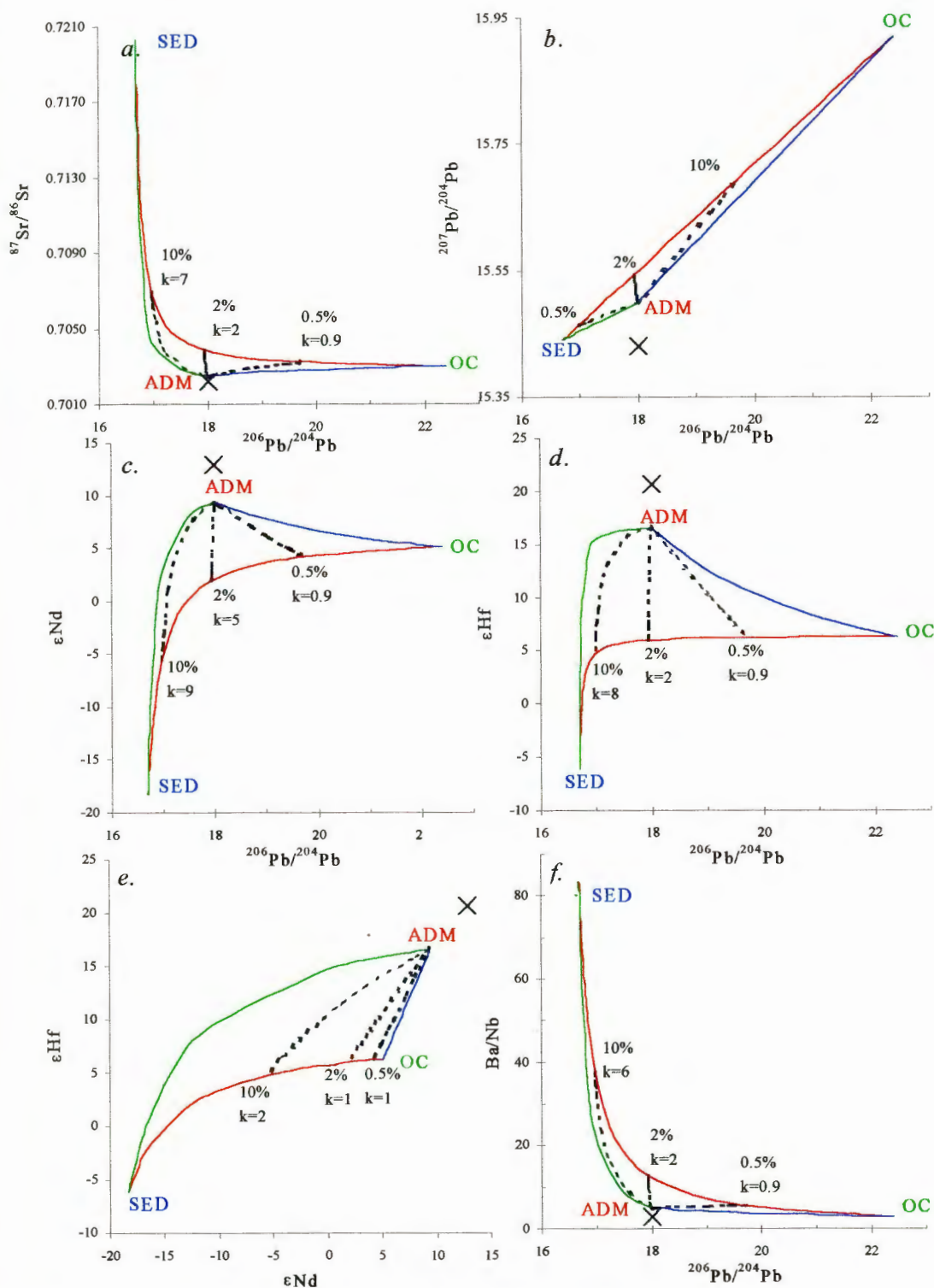


Figure 3.13. ADM-OC-SED mixtures. ADM is ambient upper mantle. OC is altered subducted 1.5Ga. oceanic crust. SED is 1.5 Ga. subducted pelagic sediment. See table 3.4 for component compositions. Blue solid line, ADM-OC binary; red solid line, OC-SED binary; green solid line, ADM-SED binary.

These three binaries bound the area of allowable 3 component mixtures. *Black X*, normal upper mantle composition shown for reference. *Dashed lines* each represent compositions of mixtures of ADM with a different recycled component (REC). REC consists of SED and OC where the SED-OC ratio is constant in a given recycled component. The recycled components shown in the graphs contain 0.5% SED, 2% SED and 10% SED respectively. k values are listed for the ADM-REC mixtures. k is a function of the trace element concentrations in the end-members (e.g. for plot *a*, $k = (\text{Sr/Pb})_{\text{DM}}/(\text{Sr/Pb})_{\text{REC}}$ and $(\text{Sr/Pb})_{\text{REC}}$ is a function of the amount of SED in the recycled component). The closer k is to 1, the smaller the degree of curvature of the ADM-REC mixing line is.

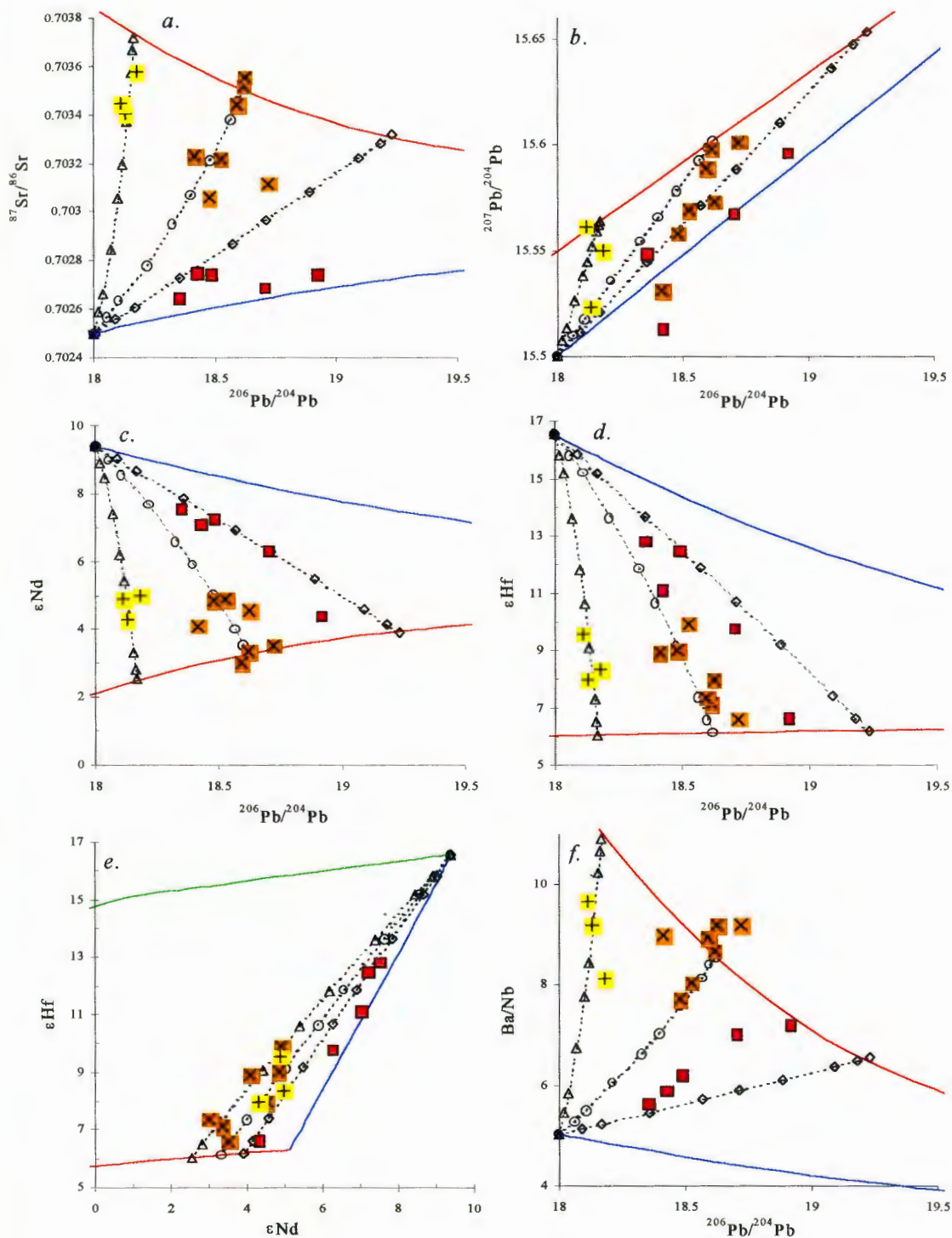


Figure 3.14. Modeling Shona segmentation with ADM-OC-SED mixtures. *Blue solid line*, ADM-OC binary; *red solid line*, OC-SED binary; *green solid line* (only visible in e), ADM-SED binary; *red squares*, segment 2 basalts; *orange squares with Xes*, segment 3 basalts; *yellow squares with +es*,

segment 4 basalts. *Dashed lines*, compositions of 3 different ADM-REC mixtures with tick marks at 1%, 2%, 5%, 10%, 15%, 25%, 50%, 75% and 100% REC. *Open diamonds*, REC contains 0.7% SED; *open circles*, REC contains 1.1% SED; *open triangles* REC contains 1.6% SED. Mixtures of these three REC compositions with ADM successfully reproduce the observed isotope and Ba/Nb trends of the Shona anomaly.

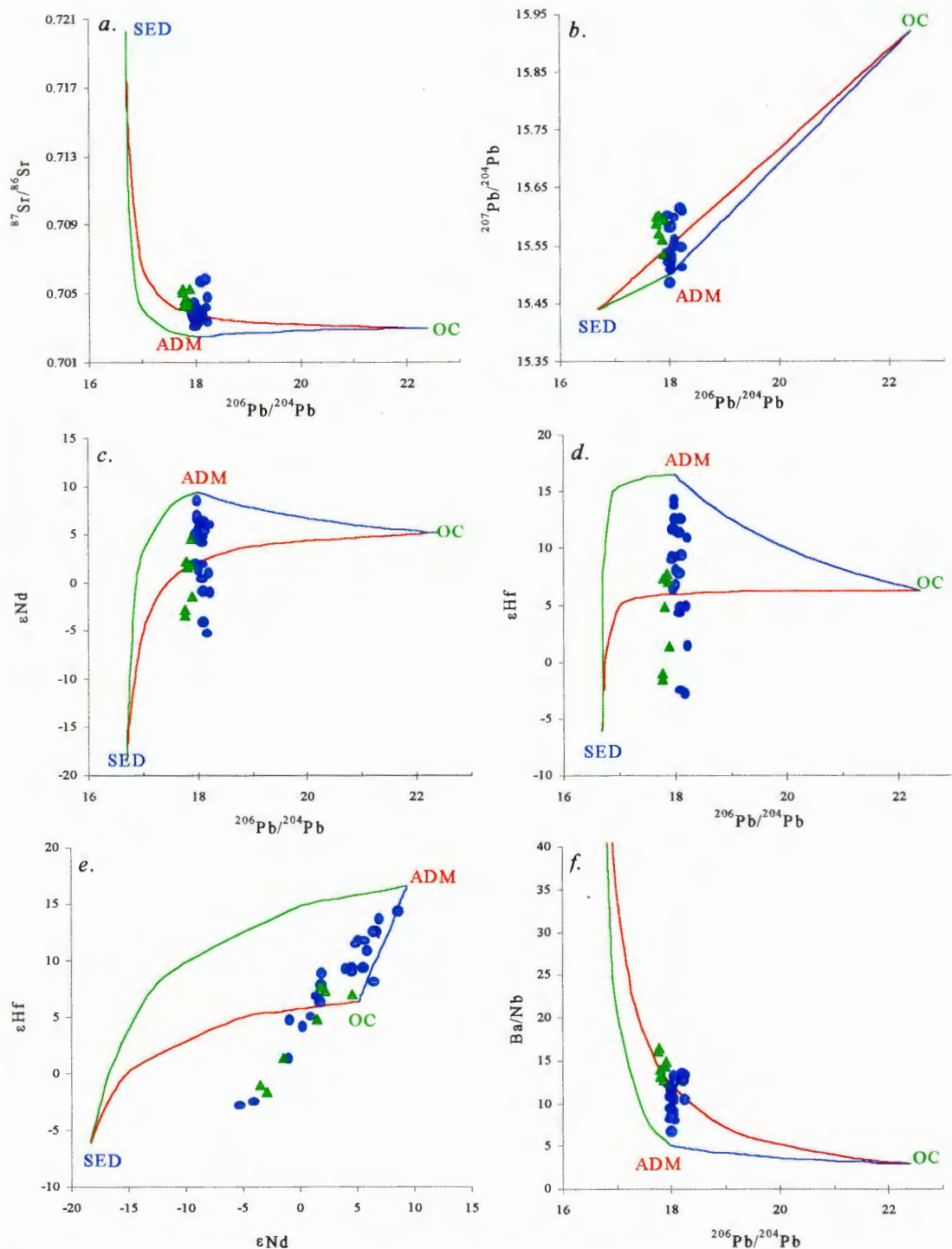


Figure 3.15. Discovery and LOMU anomalies relative to ADM-OC-SED. *Blue solid line*, ADM-OC binary; *red solid line*, OC-SED binary; *green solid line*, ADM-SED binary. These three binaries bound the area of allowable 3 component mixtures. *Blue circles*, Discovery anomaly basalts; *green triangles*, LOMU segment basalts. Many basalts from these two regions fall outside of the area of possible ADM-OC-SED compositions.

APPENDIX

APPENDIX

3-component mixtures: DM-OC-SED

The following mass balance equations are used to model the ambient upper mantle (ADM) as a three component mixture of normal upper mantle (DM), 1.5Ga. subducted oceanic crust (OC) and 1.5 Ga. pelagic sediment (SED).

$$({}^{176}\text{Hf}/{}^{177}\text{Hf})_{\text{ADM}} = \frac{z_{\text{DM}}\text{Hf}_{\text{DM}}({}^{176}\text{Hf}/{}^{177}\text{Hf})_{\text{DM}} + z_{\text{OC}}\text{Hf}_{\text{OC}}({}^{176}\text{Hf}/{}^{177}\text{Hf})_{\text{OC}} + z_{\text{SED}}\text{Hf}_{\text{SED}}({}^{176}\text{Hf}/{}^{177}\text{Hf})_{\text{SED}}}{z_{\text{DM}}\text{Hf}_{\text{DM}} + z_{\text{OC}}\text{Hf}_{\text{OC}} + z_{\text{SED}}\text{Hf}_{\text{SED}}}$$

$$({}^{143}\text{Nd}/{}^{144}\text{Nd})_{\text{ADM}} = \frac{z_{\text{DM}}\text{Nd}_{\text{DM}}({}^{143}\text{Nd}/{}^{144}\text{Nd})_{\text{DM}} + z_{\text{OC}}\text{Nd}_{\text{OC}}({}^{143}\text{Nd}/{}^{144}\text{Nd})_{\text{OC}} + z_{\text{SED}}\text{Nd}_{\text{SED}}({}^{143}\text{Nd}/{}^{144}\text{Nd})_{\text{SED}}}{z_{\text{DM}}\text{Nd}_{\text{DM}} + z_{\text{OC}}\text{Nd}_{\text{OC}} + z_{\text{SED}}\text{Nd}_{\text{SED}}}$$

$$1 = z_{\text{DM}} + z_{\text{OC}} + z_{\text{SED}}$$

z is the mass fraction of each component (DM, OC or SED) in the mixture.

Nd and Hf are the concentrations of these elements in each component (DM, OC or SED).

Since the isotope ratios of DM, OC, SED and ADM are known and the trace element concentrations in DM, OC and SED are known, there are 3 unknowns (z_{DM} , z_{OC} , z_{SED}) in the above equations. Thus the equations have a unique solution.

Since identical sets of equations can be written for each isotope ratio pair, (e.g. for ${}^{206}\text{Pb}/{}^{204}\text{Pb}$ and ${}^{87}\text{Sr}/{}^{86}\text{Sr}$) the problem is over-determined. The values of z reported in the text were chosen so as to minimize the errors in the calculated and observed ADM isotope ratios.

The following table shows the discrepancy between the observed and the calculated ambient depleted mantle (ADM) composition which results from $z_{\text{DM}} = 96\%$, $z_{\text{OC}} = 3.94\%$ and $z_{\text{SED}} = 0.06\%$.

Table A.1. Errors in the calculated composition of ADM

	Observed ADM composition	Calculated ADM composition	Difference
$^{206}\text{Pb}/^{204}\text{Pb}$	18.0	18.1	0.1
$^{207}\text{Pb}/^{204}\text{Pb}$	15.5	15.5	0
$^{208}\text{Pb}/^{204}\text{Pb}$	37.8	37.6	- 0.2
$^{87}\text{Sr}/^{86}\text{Sr}$	0.7025	0.7026	0.0001
$^{143}\text{Nd}/^{144}\text{Nd}$	0.51312	0.51314	0.0002
$^{176}\text{Hf}/^{177}\text{Hf}$	0.28324	0.28324	0

In light of the uncertainty regarding the input parameters to the mixing model (isotope ratios and element concentrations in the 3 components and isotope ratios observed in the ambient mantle), these errors are negligible.

The same mixing equations apply to calculations of ADM-OC-SED mixtures which reproduce the Shona anomaly basalts.

Sample EW 9309 14D-4g

This basalt is excluded from the discussion regarding the Shona anomaly segmentation because its isotopic composition is anomalous in comparison to other basalts in the region. This can be seen clearly from the isotope profiles (figure A.1). In comparison to basalts from the same dredge haul and from neighboring dredge stations, this basalt has very low $^{206}\text{Pb}/^{204}\text{Pb}$ as well as slightly high ϵHf and ϵNd and slightly low $^{87}\text{Sr}/^{86}\text{Sr}$. The source of this basalt is unclear. It may be a very small heterogeneity in the upper mantle or in the Shona plume, but since it is an individual sample, this is not explored further.

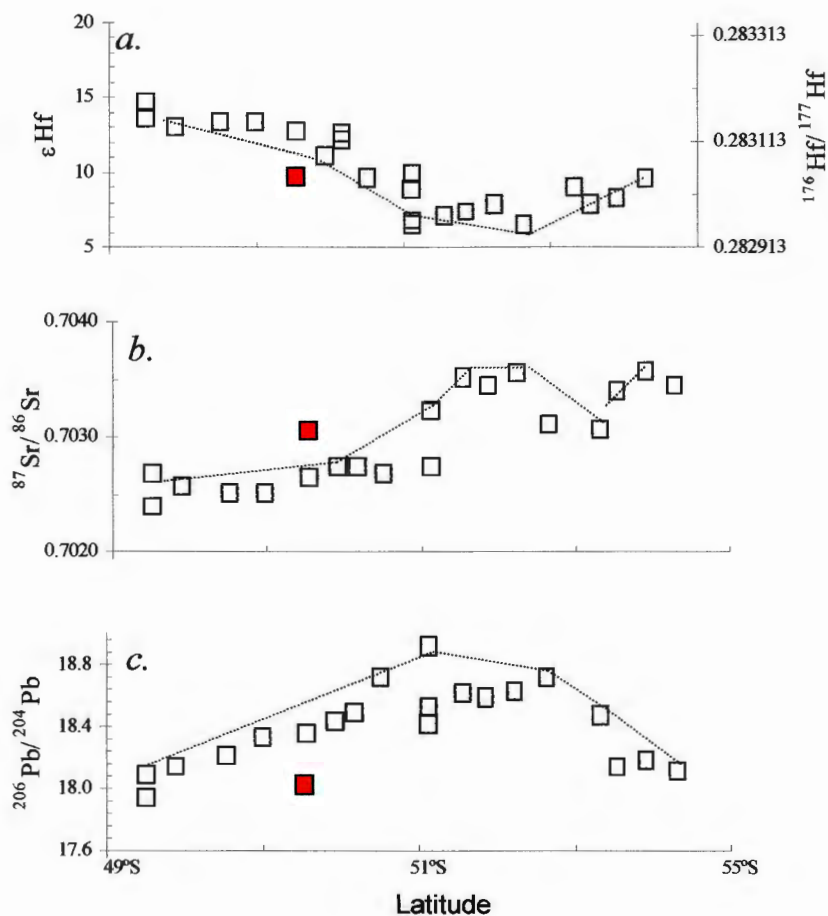


Figure A.1. Anomalous Shona basalt. EW9309 14D-4g is shown in red in the isotope profiles. *Open grey squares* are all other basalts from the Shona anomaly. This basalt has more plume-like ϵ_{Hf} , ϵ_{Nd} (not shown) and $^{87}\text{Sr}/^{86}\text{Sr}$ but less plume-like $^{206}\text{Pb}/^{204}\text{Pb}$ than EW9309 14D-1g from the same dredge haul.

BIBLIOGRPAHY

BIBLIOGRAPHY

- Allègre, C. J., S. R. Hart, and J.-F. Minster, Chemical structure and evolution of the mantle and continents determined by inversion of Nd and Sr isotopic data, II, Numerical experiments and discussion, *Earth and Planetary Science Letters*, 66, 191-213, 1983.
- Allègre, C. J., and E. Lewin, Chemical structure and history of the Earth: Evidence from the global non-linear inversion of isotopic data in a three-box model, *Earth and Planetary Science Letters*, 96, 61-88, 1989.
- Allègre, C. J., E. Lewin, and B. Dupré, A coherent crust-mantle model for the uranium-thorium-lead isotopic system, *Chemical Geology*, 70, 211-234, 1988.
- Bau, M., Controls on the fractionation of isovalent trace elements in magmatic and aqueous systems: evidence from Y/Ho, Zr/Hf, and lanthanide tetrad effect, *Contributions to Mineralogy and Petrology*, 123, 323-333, 1996.
- Ben Othman, D., W. M. White, and P. J. Patchett, The geochemistry of marine sediments, island arc magma genesis, crust-mantle recycling, *Earth and Planetary Science Letters*, 94, 1-21, 1989.
- Blichert-Toft, J., and W. White, Hf Geochemistry of the Galapagos Islands, *Geochemistry, Geophysics, Geosystems*, submitted.
- Blichert-Toft, J., and F. Albarède, The Lu-Hf isotope geochemistry of chondrites and the evolution of the mantle-crust system, *Earth and Planetary Science Letters*, 148, 243-258, 1997.
- Blichert-Toft, J., C. Chauvel, and F. Albarède, Separation of Hf and Lu for high-precision isotope analysis of rock samples by magnetic sector-multiple collector ICP-MS, *Contributions to Mineralogy and Petrology*, 127, 248-260, 1997.
- Blichert-Toft, J., and F. Albarède, Hf isotopic compositions of the Hawaiian Scientific Drilling Project core and the source mineralogy of Hawaiian basalts, *Geophysical Research Letters*, 26(7), 935-938, 1999.
- Blichert-Toft, J., F. Frey, and F. Albarède, Hf isotope evidence for pelagic sediments in the source of Hawaiian basalts, *Science*, 285, 879-882, 1999.
- Castillo, P., The Dupal anomaly as a trace of the upwelling lower mantle, *Nature*, 336, 667-670, 1988.
- Chauvel, C., and H. C., Melting a complete section of recycled crust: trace element and Pb isotopic evidence from Iceland, *Geochemistry, Geophysics, Geosystems*, 1, 1999GC00002, 2000.
- Chauvel, C., A. W. Hofmann, and P. Vical, HIMU EM1: the French Polynesian connection, *Earth and Planetary Science Letters*, 110, 99-119, 1992.
- Dalmasso, J., G. Barci-Funel, and G. J. Ardisson, Reinvestigation of the decay of the long-lived odd-odd ^{176}Lu nucleus, *Applied Radiation and Isotopes*, 43, 69-76, 1992.
- Dosso, L., B. B. Hanan, H. Bougault, J.-G. Schilling, and J.-L. Joron, Sr-Nd-Pb geochemical morphology between 10° and 17° N on the Mid-Atlantic Ridge: A new MORB isotope signature, *Earth and Planetary Science Letters*, 106, 29-43, 1991.

- Douglass, J., Isotopic and trace element variations along the southern Mid-Atlantic Ridge (40° - 55°S): an evaluation of regional plume-ridge interaction and large scale mantle heterogeneities, in *Graduate School of Oceanography, Dissertation, University of Rhode Island, Kingston, 2000.*
- Douglass, J., and J.-G. Schilling, Plume-ridge interactions of the Discovery and Shona mantle plumes with the southern Mid-Atlantic Ridge (40°S-55°S), *Journal of Geophysical Research*, 104(B2), 2941-2962, 1999.
- Douglass, J., J.-G. Schilling, R. H. Kingsley, and C. Small, Influence of the Discovery and Shona mantle plumes on the southern Mid-Atlantic Ridge: Rare earth evidence, *Geophysical Research Letters*, 22(21), 2893-2896, 1995.
- Dupré, B., and C. J. Allègre, Pb-Sr isotope variation in Indian Ocean basalts and mixing phenomena, *Nature*, 303, 142-146, 1983.
- Eiler, J. M., P. Schiano, N. Kitchen, and E. M. Stolper, Oxygen-isotope evidence for recycled crust in the sources of mid-ocean-ridge basalts, *Nature*, 403, 530-534, 2000.
- Farley, K. A., and H. Craig, Mantle plumes and mantle sources, *Science*, 258, 821-822, 1992.
- Fontignie, D., and J.-G. Schilling, Mantle heterogeneities beneath the South Atlantic: a Nd-Sr-Pb isotope study along the Mid-Atlantic Ridge (3°S-46°S), *Earth and Planetary Science Letters*, 142, 209-221, 1996.
- Gasperini, D., J. Blichert-Toft, D. Bosch, A. D. Moro, P. Macera, P. Télouk, and F. Albarède, Evidence from Sardinian basalt geochemistry for recycling of plume heads into the Earth's mantle, *Nature*, 408, 701-704, 2000.
- Goldschmidt, V. M., *Geochemistry*, Oxford University Press, London, 1958.
- Graham, D. W., W. J. Jenkins, J.-G. Schilling, G. Thompson, M. D. Kurz, and S. E. Humphris, Helium isotope geochemistry of mid-ocean ridge basalts from the South Atlantic, *Earth and Planetary Science Letters*, 110, 133-147, 1992.
- Hamelin, B., and C. J. Allègre, Large-scale regional units in the depleted upper mantle revealed by an isotope study of the Southwest Indian Ridge, *Nature*, 315, 196-199, 1985.
- Hamelin, B., B. Dupré, and C. J. Allègre, Pb-Sr-Nd isotopic data of Indian Ocean Ridges: New evidence of large scale mapping of mantle heterogeneities. Indian Ocean Ridges, Amsterdam, Mauritius, *Earth and Planetary Science Letters*, 76, 288-299, 1986.
- Hanan, B. B., and D. W. Graham, Lead and helium isotope evidence from oceanic basalts for a common deep source of mantle plumes, *Science*, 272, 991-995, 1996.
- Hanan, B. B., R. H. Kingsley, and J.-G. Schilling, Pb isotope evidence in the South Atlantic for migrating ridge-hotspot interactions, *Nature*, 322, 137-144, 1986.
- Hart, S. R., A large-scale isotope anomaly in the Southern Hemisphere mantle, *Nature*, 309, 753-757, 1984.
- Hart, S. R., E. H. Hauri, L. A. Oschmann, and J. A. Whitehead, Mantle plumes and entrainment: Isotopic evidence, *Science*, 256, 517-520, 1992.
- Hart, S.R. and T. Dunn, Experimental cpx/melt partitioning of 24 trace elements, *Contributions to Mineralogy and Petrology*, 113, 1-8, 1993.

- Hauri, E. H., Major-element variability in the Hawaiian mantle plume, *Nature*, 382, 415-419, 1996.
- Hawkesworth, C. J., M. S. M. Mantovani, P. N. Taylor, and Z. Palacz, Evidence from the Paraná of south Brazil for a continental contribution to Dupal basalts, *Nature*, 322, 356-359, 1986.
- Hawkesworth, C. J., M. J. Norry, J. C. Roddick, and R. Vollmer, $^{143}\text{Nd}/^{144}\text{Nd}$ and $^{86}\text{Sr}/^{87}\text{Sr}$ ratios from the Azores and their significance in LIL-element enriched mantle, *Nature*, 280, 28-31, 1979.
- Hofmann, A. W., Chemical differentiation of the Earth: the relationship between mantle, continental crust, and oceanic crust, *Earth and Planet. Science Letters*, 90, 297-314, 1988.
- Hofmann, A. W., and W. M. White, Mantle plumes from ancient oceanic crust, *Earth and Planetary Science Letters*, 56, 421-436, 1982.
- Huang, Y.-M., P. v. Calsteren, and C. J. Hawkesworth, The evolution of the lithosphere in southern Africa: a perspective on the basic granulite xenoliths from kimberlites in South Africa, *Geochimica et Cosmochimica Acta*, 59, 4905-4920, 1995.
- Humphris, S. E., G. Thompson, J.-G. Schilling, and R. H. Kingsley, Petrological and geochemical variations along the Mid-Atlantic Ridge between 46°S and 32°S: Influence of the Tristan da Cunha mantle plume, *Geochimica et Cosmochimica Acta*, 49, 1445-1464, 1985.
- Johnson, C. M., and B. L. Beard, Evidence from hafnium isotopes for ancient sub-oceanic mantle beneath the Rio Grande Rift, *Nature*, 362, 441-444, 1993.
- Kamenetsky, V. S., R. Maas, N. Sushchevskaya, M. Norman, I. Cartwright, and A. A. Peyve, Remnants of Gondwanan continental lithosphere in oceanic upper mantle: Evidence from the South Atlantic Ridge, *Geology*, 29, 243-246, 2001.
- Kempe, D. R. C., and J.-G. Schilling, Discovery Tablemount Basalt: Petrology and geochemistry, *Contributions to Mineralogy and Petrology*, 44, 101-115, 1974.
- Kincaid, C., J.-G. Schilling, and C. Gable, The dynamics of off-axis plume-ridge interaction in the uppermost mantle, *Earth and Planetary Science Letters*, 137, 29-44, 1996.
- Kingsley, R. H., and J.-G. Schilling, Plume - ridge interaction in the Easter - Salas y Gomez seamount chain - Easter microplate system: Pb isotope evidence, *Journal of Geophysical Research*, 103, 24159-24177, 1998.
- Kurz, M.D., A.P. le Roex and H.J.B. Dick, Isotope geochemistry of the oceanic mantle near the Bouvet triple junction, *Geochimica et Cosmochimica Acta*, 62, 841-852, 1998.
- le Roex, A. P., H. J. B. Dick, L. Gulen, A. M. Reid, and A. J. Erlank, Local and regional heterogeneity in MORB from the Mid-Atlantic Ridge between 54.5°S and 51°S: Evidence for geochemical enrichment, *Geochimica et Cosmochimica Acta*, 51, 541-555, 1987.
- le Roex, A. P., H. J. B. Dick, A. J. Erlank, A. M. Reid, F. A. Frey, and S. R. Hart, Geochemistry, mineralogy and petrogenesis of lavas erupted along the Southwest Indian Ridge between the Bouvet triple junction and 11°E, *Journal of Petrology*, 24, 267-318, 1983.

- le Roux, P. J., A. P. LeRoex, and J.-G. Schilling, Crystallization processes beneath the southern Mid-Atlantic Ridge (40-55S): evidence for high pressure crystallization, *Contributions to Mineralogy and Petrology*, in press.
- le Roux, P. J., A. P. I. Roex, and J.-G. Schilling, MORB melting processes beneath the southern Mid-Atlantic Ridge (40-55S) a role for pyroxenite and residual garnet, *submitted*.
- le Roux, P. J., A. P. I. Roex, J.-G. Schilling, N. Shimizu, W. W. Perkins, and N. J. G. Pearce, Mantle heterogeneity beneath the southern Mid-Atlantic Ridge: trace element evidence for contamination of ambient asthenospheric mantle, in preparation.
- Mahoney, J. J., A. P. I. Roex, Z. Peng, R. L. Fisher, and J. H. Natland, Southwestern limits of Indian Ocean ridge mantle and the origin of low $^{206}\text{Pb}/^{204}\text{Pb}$ mid-ocean ridge basalt: isotope systematics of the central Southwest Indian Ridge (17°-50°E), *Journal of Geophysical Research*, 97, 19,771-19,790, 1992.
- Mahoney, J. J., W. M. White, B. G. J. Upton, C. R. Neal, and R. A. Scrutton, Beyond EM1: lavas from Afanasy Nikitin Rise and the Crozet Archipelago, Indian Ocean, *Geology*, 24, 615-618, 1996.
- McDonough, W. F., and S.-s. Sun, The composition of the earth, *Chemical Geology*, 120, 223-253, 1995.
- Moreira, M., P. J. Valbracht, T. Staudacher, and C. J. Allègre, Rare gas systematics in Red Sea ridge basalts, *Geophysical Research Letters*, 23, 2453-2456, 1996.
- Morgan, W. J., Rodriguez, Darwin, Amsterdam, A second type of hotspot island, *Journal of Geophysical Research*, 83, 5355-5360, 1978.
- Nir-El, Y., and N. Lavi, Measurement of half-life of ^{176}Lu , *Applied Radiation and Isotopes*, 49, 1653-1655, 1998.
- Patchett, J., Importance of the Lu-Hf isotopic system in studies of planetary chronology and chemical evolution, *Geochimica et Cosmochimica Acta*, 47, 81-91, 1983.
- Patchett, J., and T. M., A routine high-precision method for Lu-Hf isotope geochemistry and chronology, *Contributions to Mineralogy and Petrology*, 75, 263-267, 1980a.
- Patchett, P. J., and M. Tatsumoto, Hafnium isotope variations in oceanic basalts, *Geophysical Research Letters*, 7, 1077-1080, 1980b.
- Patchett, P. J., W. M. White, H. Feldmann, S. Kielinczuk, and A. W. Hofmann, Hafnium/rare earth element fractionation in the sedimentary system and crustal recycling into the Earth's mantle, *Earth and Planetary Science Letters*, 69, 365-378, 1984.
- Plank, T., and L. C.H., The chemical composition of subducting sediment and its consequences for the crust and mantle, *Chemical Geology*, 145, 235-394, 1998.
- Rehkämper, M., and A. W. Hormann, Recycled ocean crust and sediment in Indian Ocean MORB, *Earth and Planetary Science Letters*, 147, 93-106, 1997.
- Rideout, M., and S. J.-G., DSDP Leg 82: REE, $^{87}\text{Sr}/^{86}\text{Sr}$ and $^{143}\text{Nd}/^{144}\text{Nd}$ mantle source variations, *Initial Report DSDP 82*, 483-492, 1985.

- Rogers, N. W., and C. J. Hawkesworth, Proterozoic age and cumulate origin for granulite xenoliths, Lesotho, *Nature*, 299, 409-413, 1982.
- Rudnick, R. L., and D. M. Fountain, Nature and composition of the continental crust: a lower crustal perspective, *Reviews of Geophysics*, 33, 267-309, 1995.
- Rudnick, R. L., and S. L. Goldstein, The Pb isotopic compositions of lower crustal xenoliths and the evolution of lower crustal Pb, *Earth and Planetary Science Letters*, 98, 192-207, 1990.
- Salters, V. J. M., and W. White, Hf isotope constraints on mantle evolution, *Chemical Geology*, 145, 1998.
- Salters, V., and A. Zindler, Extreme $^{176}\text{Hf}/^{177}\text{Hf}$ in the sub-oceanic mantle, *Earth and Planetary Science Letters*, 129, 13-30, 1995.
- Salters, V. J. M., The generation of mid-ocean ridge basalts from the Hf and Nd isotope perspective, *Earth and Planetary Science Letters*, 141, 109-123, 1996.
- Salters, V. J. M., and S. R. Hart, The hafnium paradox and the role of garnet in the source of mid-ocean-ridge basalts, *Nature*, 342, 420-422, 1989.
- Salters, V. J. M., and S. R. Hart, The mantle sources of ocean ridges, islands and arcs: the Hf-isotope connection, *Earth and Planetary Science Letters*, 104, 364-380, 1991.
- Sarda, P., M. Moreira, and T. Staudacher, Rare gas systematics on the southernmost Mid-Atlantic Ridge: Constraints on the lower mantle and the Dupal source, *Journal of Geophysical Research*, 105(B3), 5973-5996, 2000.
- Schiano, P., J.-L. Birck, and C. J. Allègre, Osmium-strontium-neodymium-lead isotopic covariations in mid-ocean ridge basalt glasses and the heterogeneity of the upper mantle, *Earth and Planetary Science Letters*, 150, 363-379, 1997.
- Schilling, J.-G., Upper mantle heterogeneities and dynamics, *Nature*, 314, 62-67, 1985.
- Schilling, J.-G., R. H. Kingsley, and J. D. Devine, Galápagos Hotspot - Spreading Center System, 1, Spatial petrological and geochemical variations (83°W-101°W), *Journal of Geophysical Research*, 87, 5593-5610, 1982.
- Schilling, J.-G., B. B. Hanan, B. McCully, R. H. Kingsley, and D. Fontignie, Influence of the Sierra Leone mantle plume on the equatorial Mid-Atlantic Ridge: A Nd-Sr-Pb isotopic study, *Journal of Geophysical Research*, 99, 12,005-12,028, 1994.
- Schilling, J.-G., R. H. Kingsley, D. Fontignie, R. Poreda, and S. Xue, Dispersion of the Jan Mayen and Iceland mantle plumes in the Arctic: A He-Pb-Nd-Sr isotope tracer study of basalts from the Kolbeinsey, Mohns, and Knipovich Ridges, *Journal of Geophysical Research*, 104, 10,543-10,569, 1999.
- Schilling, J.-G., R. H. Kingsley, B. B. Hanan, and B. L. McCully, Nd-Sr-Pb isotopic variations along the Gulf of Aden: Evidence for Afar mantle plume-continental lithosphere interaction, *Journal of Geophysical Research*, 97(B7), 10,927-10,966, 1992.
- Schilling, J.-G., G. Thompson, R. Kingsley, and S. Humphris, Hotspot-migrating ridge interaction in the South Atlantic, *Nature*, 313, 187-191, 1985.

- Shirey, S. B., B. J.F., and C. H. Langmuir, Three-component isotopic heterogeneity near the Oceanographer transform, Mid-Atlantic Ridge, *Nature*, 325, 217-223, 1987.
- Small, C., Observations of ridge-hotspot interactions in the Southern Ocean, *Journal of Geophysical Research*, 100, 17,931-17,946, 1995.
- Stacey, J. S., and J. D. Kramers, Approximation of terrestrial lead isotope evolution by a two-stage model, *Earth and Planetary Science Letters*, 26, 207-221, 1975.
- Stille, P., U. D.M., and T. M., Pb, Sr, Nd and Hf isotopic evidence of multiple sources for Oahu, Hawaii basalts, *Nature*, 304, 25-29, 1983.
- Stille, P., U. D.M., and T. M., Pb, Sr, Nd and Hf constraints on the origin of Hawaiian basalts and evidence for a unique mantle source, *Geochimica et Cosmochimica Acta*, 50, 2303-2319, 1986.
- Storey, M., A. D. Saunders, J. Tarney, I. L. Gibson, M. J. Norry, M. F. Thirlwall, P. Leat, R. N. Thompson, and M. A. Menzies, Contamination of Indian Ocean asthenosphere by the Kerguelen-Heard mantle plume, *Nature*, 338, 574-576, 1989.
- Sun, S.-S., and W. F. McDonough, Chemical and isotopic systematics of oceanic basalts: Implications for mantle composition and processes, in *Magmatism in the Ocean Basins*, vol. Special Publication. No. 42, edited by A. D. Saunders and M. J. Norry, pp. 313-345, Geol. Soc., 1989.
- Sun, S.-S., M. Tatsumoto, and J.-G. Schilling, Mantle plume mixing along the Reykjanes Ridge axis: Lead isotopic evidence, *Science*, 190, 143-147, 1975.
- Tatsumoto, M., Isotopic composition of lead in oceanic basalt and its implication to mantle evolution, *Earth and Planetary Science Letters*, 38, 63-87, 1978.
- Tatsumoto, M., A. R. Basu, H. Wankang, W. Junwen, and X. Guanghong, Sr, Nd, and Pb isotopes of ultramafic xenoliths in volcanic rocks of eastern China: enriched components EM1 and EM2 in subcontinental lithosphere, *Earth and Planetary Science Letters*, 113, 107-128, 1992.
- van Westrenen, W., J. Blundy, and B. Wood, High field strength element/rare earth element fractionation during partial melting in the presence of garnet: Implications for identification of mantle heterogeneities, *Geochemistry Geophysics Geosystems*, 2, 2000GC000133, 2001.
- Verma, S. P., and J.-G. Schilling, Galápagos hotspot-spreading center system, 2. $^{87}\text{Sr}/^{86}\text{Sr}$ and large ion lithophile element variations (85°W - 101°W), *Journal of Geophysical Research*, 87, 10838-10856, 1982.
- Verma, S. P., J.-G. Schilling, and D. G. Waggoner, Neodymium isotopic evidence for Galápagos hotspot-spreading center system evolution, *Nature*, 306, 654-657, 1983.
- Vervoort, J., and J. Blichert-Toft, Evolution of the depleted mantle: Hf isotope evidence from juvenile rocks through time, *Geochimica et Cosmochimica Acta*, 63, 533-556, 1998.
- Vervoort, J. D., P. J. Patchett, J. Blichert-Toft, and F. Albarède, Relationships between Lu-Hf and Sm-Nd isotopic systems in the global sedimentary system, *Earth and Planetary Science Letters*, 168, 79-99, 1999.
- Walker, R. J., R. W. Carlson, S. B. Shirey, and F. R. Boyd, Os, Sr, Nd and Pb isotope systematics of southern African peridotite xenoliths: implications for the chemical evolution of subcontinental mantle, *Geochimica et Cosmochimica Acta*, 53, 1583-1595, 1989.

- Weaver, B. L., Trace element evidence for the origin of ocean-island basalts, *Geology*, 19, 123-126, 1991.
- Weaver, B. L., D. A. Wood, J. Tarney, and J. L. Joron, Role of subducted sediment in the genesis of ocean-island basalts: Geochemical evidence from South Atlantic Ocean islands, *Geology*, 14, 275-278, 1986.
- Wedepohl, K. H., Handbook of Geochemistry, vol. 2, Springer-Verlag, New York, 1978.
- White, W., and J.-G. Schilling, The nature and origin of geochemical variation in Mid-Atlantic Ridge basalts from the central North Atlantic, *Geochimica et Cosmochimica Acta*, 42, 1501-1516, 1978.
- White, W. M., Sources of oceanic basalts: Radiogenic isotopic evidence, *Geology*, 13, 115-118, 1985.
- White, W. M., A. R. McBirney, and R. A. Duncan, Petrology and geochemistry of the Galápagos Islands: Portrait of a pathological mantle plume, *Journal of Geophysical Research*, 98(B11), 19,533-19,563, 1993.
- Yu, D., D. Fontignie, and J.-G. Schilling, Mantle plume - ridge interactions in the Central North Atlantic: A Nd isotope study of Mid-Atlantic Ridge basalts from 30°N to 50°N, *Earth and Planetary Science Letters*, 146, 259-272, 1997.
- Zindler, A., and S. Hart, Chemical geodynamics, *Annual Review of Earth and Planetary Science*, 14, 493-571, 1986.